공학박사학위논문

Fluorescent Graphene Oxide-based Optical Biosensors for Detection of Disease-related Protease

질병 관련 단백질 분해 효소 검출을 위한

형광성 산화 그라핀 기반의

광학 바이오센서 개발에 관한 연구

2017년 2월

서울대학교 대학원

화학생물공학부

양 진 경

ABSTRACT

Fluorescent Graphene Oxide-based Optical Biosensors for Detection of Disease-related Protease

Jin-Kyoung Yang

School of Chemical and Biological Engineering

The Graduate School

Seoul National University

Graphene oxide (GO) have attracted considerable attention as a fluorescent probe for biosensors due to its unique and fascinating properties such as strong UV absorption, stable fluorescence in biological environment, and fluorescence quenching ability as well as preferential interaction with biomolecules. Although many attempts have shown promising results by using GO as a quencher for fluorescent dye in fluorescence resonance energy transfer (FRET) sensor, there are still several challenging issues including the use of unstable organic dyes. Therefore, various optical biosensors were designed by using GO as a fluorescent probe to enhance its performance for the detection of target biomolecule.

In the first part, GO PL-based optical biosensor consisting of a luminescent GO donor covalently linked with a peptide-quencher complex was described for a simple, rapid, and sensitive detection of proteases. To this end, the quenching efficiency of various candidate quenchers of GO fluorescence, such as metalloprotoporphyrins and QXL_{570}, were examined and QXL_{570} was found to be much more effective for quenching the intrinsic fluorescence of GO than other charge transfer-based quenchers. The designed GO-peptide-QXL system was able to sensitively detect specific proteases, chymotrypsin and matrix metalloproteinase-2, via "turn-on" response of quenched GO fluorescence after proteolytic cleavage of the quencher. Finally, the GO–peptide–QXL hybrid successfully detected MMP-2 secreted from living cells, human hepatocytes HepG2, with high sensitivity.

In the second part, a new type of GO optical 'turn-on' biosensor for the detection of MMP-2 was fabricated by means of of a peptide-induced assembly of fluorescent GO. Functionalization of GO with a peptide substrate for MMP-2 bearing a thiol group led to its self-assembly via disulfide bonding, accompanied by selfquenching of GO's fluorescence. This peptide-induced GO assembly was then disassembled by proteolytic cleavage in the presence of MMP-2, thereby restoring the level of self-quenched GO fluorescence. With this approach, we were able to detect MMP-2 and to investigate the kinetic parameters of MMP-2 activity. The GO–peptide assembly was successfully applied to the selective and sensitive detection of MMP-2 secreted by living

cells, human hepatocytes HepG2, at a concentration of 2 ng mL^{-1}.

In the third part, cysteine-modified GO (Cys-GO) doped with nitrogen and sulfur atoms was described. Cys-GO was simply synthesized by reacting with cysteine in the acidic water/dimethylformamide cosolvent system via ultra-sonication method under mild reaction conditions. The N and S contents in Cys-GO dramatically increased to 10.4 and 23.3 wt%. As-synthesized Cys-GO exhibited highly fluorescent properties compared to pristine GO, which could be attributed to the synergistic effective on radiative emission from heteroatoms of Cys-GO. Cys-GO was further found to be suitable as fluorescent probe for more sensitive detection of MMP-2.

These studies suggest that GO PL-based optical biosensors could be a promising platform for sensitive and selective biomolecule detection in the fields of medicine and pharmaceutical industry.

Keywords: Graphene oxide, fluorescence nanomaterials, fluorescence resonance energy transfer, optical biosensor, matrix metalloproteinase-2, molecule-induced assembly, self-quenching, N,S-doped GO

Student number: 2011-21046

TABLE OF CONTENTS

LIST OF TABLES

Chapter I. Introduction

Chapter III. Result and Discussion

LIST OF FIGURES

Chapter I. Introduction

Chapter III. Result and Discussion

LIST OF ABBREVIATIONS

AFM	Atomic force microscopy
BOP	Benzotriazole-1-yl-oxy tris(dimethyhlamino)phosphonium hexafluorophosphate
CD	Carbon dot
CM GO	Carboxymethylated graphene oxide
CNT	Carbon nanotube
CoPP	Cobalt protoporphyrin
CuPP	Copper protoporphyrin
CVD	Chemical vapor deposition
DBCO	Dibenzocyclooctyne-PEG_4-acid
DCM	Dichloromethane
DFT	Density functional theory
DIC	*N,N'*-diisopropylcarbodiimide
DIPEA	Diisopropylethylamine
DMAP	4-dimethylaminopyridine
DMF	Dimethylformamide
DMSO	Dimethyl sulfoxide
DODT	3,6-dioxa-1,8-octanedithiol
EDC	1-Ethyl-3-(3-dimethylaminopropyl)-carbodiimide
EDTA	Ethylenediaminetetraacetic acid
EELS	Electron energy loss spectroscopy
ELISA	Enzyme-linked immunosorbent assay
FBS	Fetal bovine serum
FePP	Protoporphyrin IX iron(II)
Fmoc	9-fluorenylmethoxycarbonyl
FT-IR	Fourier transform infrared
GO	Graphene oxide
GQD	Graphene quantum dot
HEPES	4-(2-hydroxyethyl)-1-piperazineethanesulfonic acid

HOBt	Hydroxybenzotriazole
HRP	Horseradish peroxidase
HR-TEM	High resolution transmission electron microscopy
MEM	Minimum essential medium
MePP	Metallo protoporphyrin
MMP-2	Matrix metalloproteinase-2
MS	Mass spectrometry
NHS	*N*-hydroxysuccinimide
NIR	Near-infrared
NMP	*N*-methyl-2-pyrrolidone
NP	Nanoparticle
PBS	Phosphate buffered saline
PL	Photoluminescenc
QD	Quantum dot
QY	Quantum yield
RPMI	Roswell park memorial institute medium
SEM	Scanning electron microsopy
TEM	Transmission electron microscopy
TFA	Trifluoroacetic acid
TIPS	Triisopropylsilane
TMB	3,3’,5,5’-tetramethylbenzidine
UV	Ultraviolet
XPS	X-ray photoelectron spectroscopy
ZnPP	Zinc protoporphyrin

Fluorescent Graphene Oxide-based Optical Biosensors for the Detection of Disease-related Protease

Chapter I.
Introduction

1. Fluorescent Nanomaterials in Biosensing

The highly sensitive detection of patholoigical biomolecules is in critical need in clinical diagnostic area. Many efforts have been made to elevate its sensitivity via signal amplification based on polymerase chain reaction and mass spectrometric techniques.[1-3] Although the development of comparable signal amplification method improved the assay sensitivity, these techniques often suffered from time-consuming operation, high-cost, and destructivity. Meanwhile, fluorescence or photoluminescence labelings have been the most popular methods in the field of biosensor technology due to various advantages such as high detection sensitivity enabling single molecule detection, rapid signal acquisition, and availability of multiple dyes with diverse spectral properties for multiplexed assays.[4] However, it is difficult to obtain low detection limit in fluorescence detection of the conventional organic dyes due to short lifetime, poor photostability, and the susceptibility to operating environment. Therefore, with recent achievement of nanotechnology, the combination of nanomaterials into diagnosis field has attracted rising interest in recent years and opened a new prospect in the signal amplification the biomolecule detection with unique optical

properties as well as sensitivity, selectivity, reliability, and rapid analysis.[5, 6]

Broadly studied luminescent nanomaterials are quantum dots (QDs), metal nanoparticles (NPs), upconversion NPs, and carbon-based NPs including graphene oxide (GO), carbon dots (CDs), carbon nanotubes (CNT), etc.. Especially, QDs have become an important class of fluorescent biomaterials in bio-sensing and bio-imaging due to several characteristic properties such as wide UV/Vis absorption, narrow emission, and tunable optical properties.[7-11] In addition, metal NPs[12-15] and upconversion NPs[16-20] are also significant fluorescent materials for biotechnology applications. On the other hand, carbon-based NPs have recently emerged as a new class of fluorescence imaging agents with nontoxic property and high performance.[21-32] This class of materials includes CNT[24-26], CDs[22, 23, 27, 31], graphene quantum dots (GQDs)[21, 33], and GO[28-30]. These carbon-based NPs have been studied as benign alternatives for QDs or other heavy metals, owing to their toxicity. Carbon-based materials showed no toxic effects, raising the prospect for *in vivo* biocompatibility. The optical properties and the use of carbon materials will be described in Section 2.

Three types of signal transduction mechanisms are dominant in biosensor development: fluorescence resonance energy transfer (FRET), electron transfer, and molecule-induced assembly or aggregation of fluorescent materials. One of the most widely used strategy for the fluorescence-based biodetection is FRET, a non-radiative energy transfer between excited luminescent donor and an acceptor.[34-36] As FRET process occurs when the emission spectrum of fluorescent dornor overlaps with the absorption spectrum of acceptor, donor and acceptor molecules should be in close proximity in the order of a few nanometers (Figure 1-1).[37] Therefore, fluorescence signal can be readily controlled through the change in distance between donor and acceptor. Various FRET sensors have been developed using QDs[38-42], upconversion NPs[18, 43, 44], and carbon-based NPs[45-47] as energy donors linked with biomolecules labeled with an acceptor quencher, which is commonly working through signal switching by biorecognition events leading to the association or dissociation of the acceptors (Figure 1-2). This strategy has enabled rapid, simple, sensitive, and selective detection of analytes.

Molecule-induced assembly of nanomaterials has emerged as an effective strategy for manipulating their sizes, shapes and interparticle

interactions, leading to change of their unique chemical and physical properties.[48, 49] Fluorescent nanomaterials have been widely used as building blocks for molecule-induced assembly to modulate their optical properties.[50, 51] Fluorescent nanomaterials, when assembled, often show changes in their emission intensities and/or wavelengths, which can be subsequently restored to their original state by disassembly.[52-55] In particular, self-quenching driven by self-assembly of the fluorescent nanomaterials can be utilized as a principle for designing fluorescence sensors to detect target molecules, because interactions with specific target molecules can trigger the restoration of self-quenched fluorescence of the nanomaterials (Figure 1-3).[54-56] The self-quenching approach does not require any quencher molecules that are essential in FRET sensors, and thus it allows simple and rapid detection with high signal-to-background ratio.[57-59]

Although there are considerable advances of fluorescent NPs in recent years, several challenging issues still remain to be solved, such as toxicity, photostability, and high quantum yields for providing detection sensitivity, assay simplicity, and low-cost assay methods.

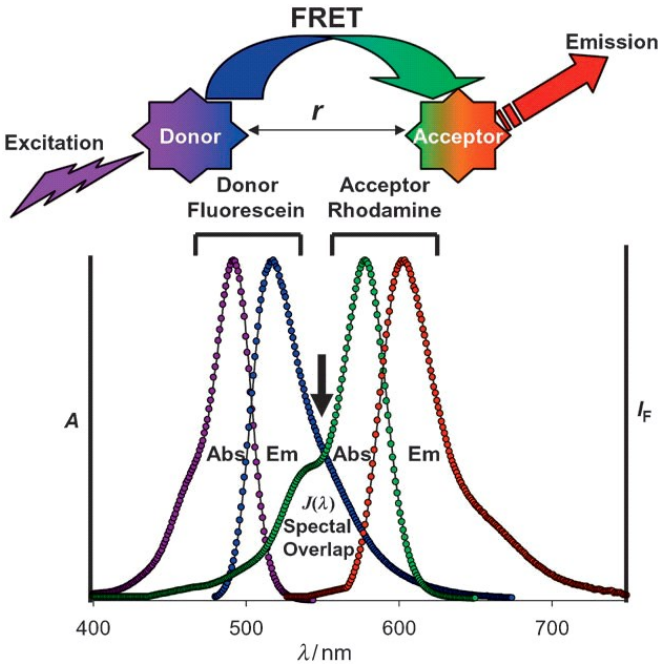

Figure 1-1. Schematics of FRET process. Upon excitation, the excited state donor molecule transfers energy non-radiatively to a proximal acceptor molecule located at close distance from the donor. The spectral overlap between the emission of donor and the absorbance of acceptor is necessary.[37]

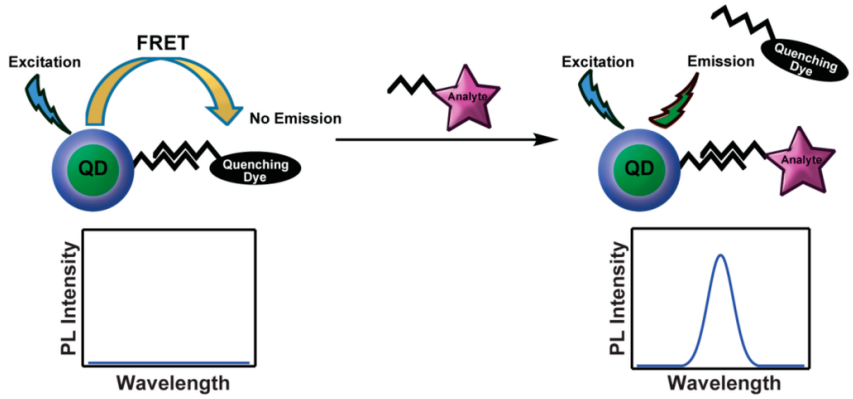

Figure 1-2. Schematics of common FRET strategy to detect target biomolecules.[42]

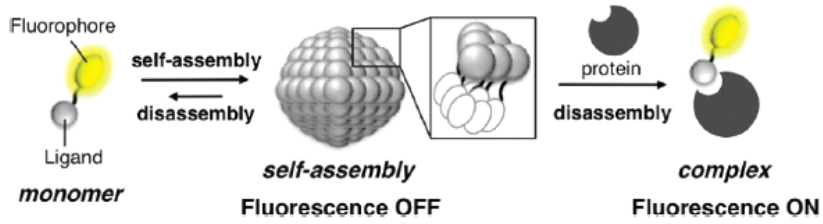

Figure 1-3. Fluorophore self-assembly strategy for specific protein detection via turn-on fluorescence.[54]

2. Photoluminescence Properties of Graphenes

Graphene oxide (GO), which is a single layer sheet of carbon material exfoliated by oxidation of graphite[60], is a new type of fluorophore that emits photoluminescence (PL) in the visible and NIR regions of the electromagnetic spectrum.[61-65] In GO, a large fraction (0.5-0.6) of carbon is sp^3 hybridized and covalently linked with oxygen in the form of epoxy and hydroxyl groups.[66, 67] The remaining fraction of carbon is sp^2 hybridized with neiboring oxygen in the form of carboxyl and carbonyl groups at the edges of the GO sheets. These sp^2 islands in GO contribute to PL emission in one of the two ways. The first one is confinement effect of π electrons within sp^2 clusters. The size of sp^2 clusters determines the local energy gap, and therfore, the wavelength of GO PL is controllable (Figure 1-4).[62-64, 68, 69] Typically, GO shows broad emission spectra because a broad range of sp^2 cluster size are present in GO. Therefore, much efforts have been tried to either shift or narrow the emission wavelength by controlling the size of sp^2 clusters through reduction.[62, 63, 68] The second one is the electronic transition between oxygen-containing functional groups at the edge of sp^2 clusters and non-oxidized carbon.[69-72] Although mechanistic details of these defect-derived

photoluminecence are not still clear, there have been many efforts to improve the GO PL via modification of functional groups (Figure 1-5).[63, 72]

On the other hand, there have been continuous efforts, including above-mentioned strategies, to enhance the quantum efficiency of GO, as photoluminescence of GO is inherently weak (QY 0.3 ~ 6%)[73, 74]. Among various approaches, CDs doped with heteroatoms, such as N[75-84], S[75, 79, 81, 85], and P[86, 87], have given outstanding results. CDs are synthesized via bottom-up method with a precursor comprising carbon source and heteroatom source such as citric acid and L-cysteine, respectively. The resulting CDs show high QY emission through the introduction of a new kind of surface state affording a high yield of radiative recombination. However, a common approach to synthesize CDs requires harsh reaction conditions including thermal annealing[75, 79-84, 87-90], plasma treatment[78], microwave[76, 77, 86], electrochemical process[85, 91], ion etching[92], and CVD process[93] (Figure 1-6). Therefore, it is still needed to develop a new strategy to make GO brighter while avoiding bottom-up method.

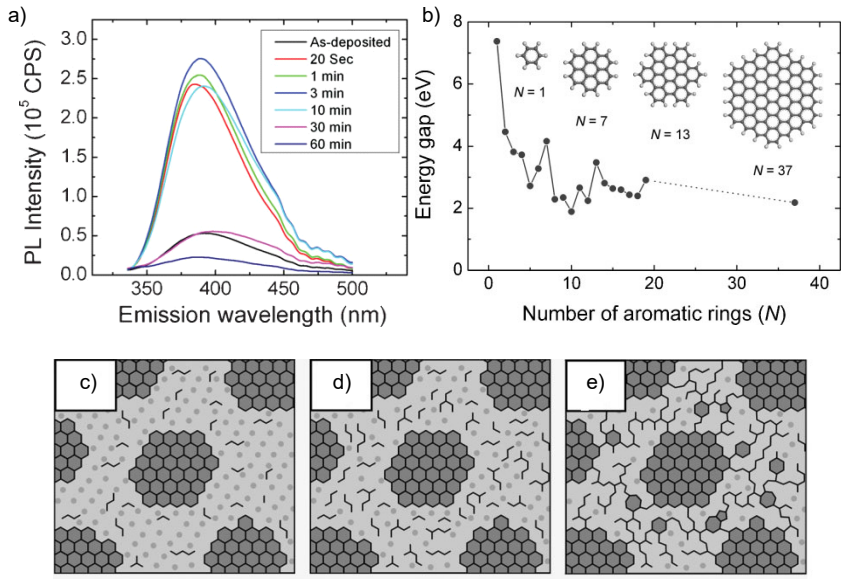

Figure 1-4. Bandgap fluorescence of GO. a) Fluorescence spectra of progressively reduced GO thin films. b) Energy gap of π-π* transitions calculated based on density functional theory (DFT) as a function of the number of fused aromatic ring. c) Structural models of GO at different stages of reduction.[62]

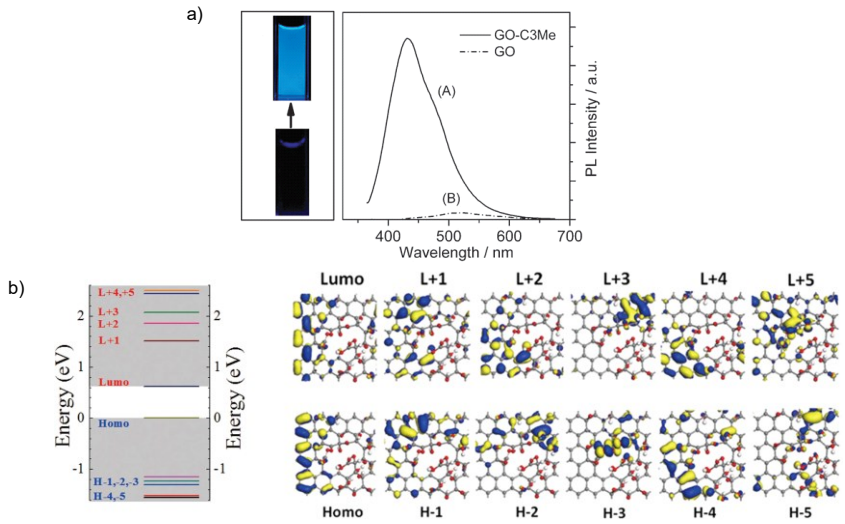

Figure 1-5. Defect-derived fluorescence of GO. a) Photographs of butylamine-modified GO (GO-C3Me) (up) and GO (down) and fluorescence spectra of (A) GO-C3Me and (B) GO in water.[61] b) Molecular orbital energy levels (left) and related orbital structure (right) of GO showing the electronic transition between oxygen-functional group related defect and neighboring carbon.[70]

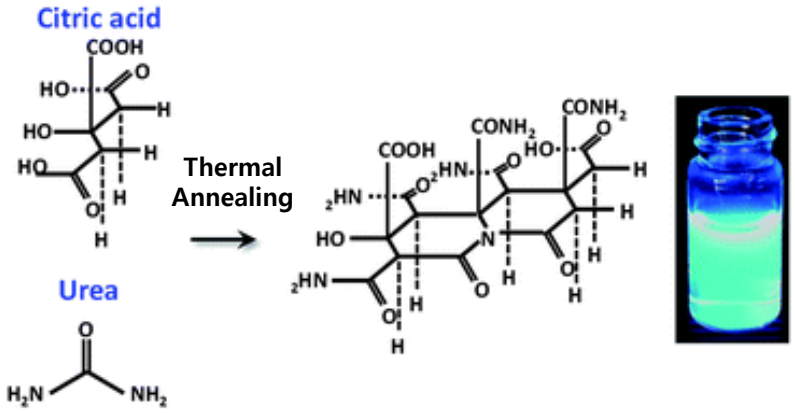

Figure 1-6. Formation of nitrogen-doped carbon dots (N-CDs) via thermal annealing of citric acid and urea, and the photograph of N-CDs showing bright fluorescence.[84]

3. Optical Biosensors based on Graphene Materials

GO has a number of beneficial characteristics such as biocompatibility, large surface area, easy preparation and chemical modification, and good stability when applied in the field of biotechnology and nanomedicine.[94-97] Very recently, GO has been utilized as a fluorescent label for cellular imaging due to its resistibility ro photobleaching under biological environment .[98-101] To date, however, GO has been extensively used as a universal quencher for organic fluorescent dyes rather than as a fluorophore in currently prevailing bioassay systems (Table 1).[28, 101-115] General principle of the previously reported systems relies on the preferential binding of GO to a target-binding molecule containing fluorescence organic dyes, thereby quenching the fluorescence of dyes by FRET. The quenched fluorescence could be recovered in the presence of target molecules by releasing the fluorescence dyes from GO quencher (Figure 1-7a). However, these type of sensor can be suffered from inherent drawbacks of organic dyes such as photo/chemical degradation, pH susceptibility, and narrow absorption overlapped with broad emission windows[36]. On the other hand, GO has been scarcely explored as an emitting fluorophore (donor) for signal transduction in

Table 1. Graphene Oxide in FRET Biosensing Applications

	Fluorescent lable or Quencher	Recognition probe	Analyte	Ref
GO as a FRET acceptor	Pyrene	Positively charged Pyrene derivatives	DNA	102
	FAM	Aptamer	Thrombin	30
	FAM	ssDNA	DNA	29
	FAM, Cy3, Cy5	dsDNA	Helicase	103, 112
	FAM, ROX, Cy5	PNA	microRNA	109
	FAM	ssDNA	Caspase-3	114
	FAM	ssDNA	Pb^{2+}	106
	FITC	ssDNA	PSA	108
	FITC	Peptide	MMP-2	121, 194
	FITC	Peptide	Thrombin	115
	Quantum dot	ssDNA	DNA	101
GO as a FRET donor	Au NPs	Antibody	Rotavirus	100
	Au NPs	ssDNA	DNA	98

FRET-based bioassay systems[98, 100], although it exhibits outstanding fluorescence properties. Therefore, it is of great interest to develop a pair of GO fluorescent donor and its quencher for a FRET-based bioassay platform to detect biomolecules, since GO PL with unique photophysical properties will be helpful to address some problems that the conventional organic fluorophores have shown in bioassay. In order to exploit GO as an emitting donor in FRET-based bioassay (Figure 1-7b), screening of effective quenchers for GO PL is required, and the quenching mechanism should be understood.

In addition, the self-quenching process accompanied by molecule-induced assembly has not yet been applied in designing GO fluorescence biosensors for selective detection of biological molecules. Therefore, it will be interesting to develop self-quenching-based biosensors operated by the assembly of fluorescent GO for selective recognition of proteins (Figure 1-7c).

Meanwhile, matrix metalloproteinases (MMPs) are of great interest as a target biomolecules because MMPs are endopeptidases capable of breaking down the extracellular matrix (ECM) to control cell behaviors in regular biological processes. MMPs are believed to be involved in

cancer biology[116], including cancer cell growth, differentiation, apoptosis, migration, invasion, and immune surveillance.[117] Among the MMPs, MMP-2 has been considered as a putative tumor marker for clinical applications, since it is known to be closely associated with the metastasis of malignant cells.[118, 119] To date, several studies have been reported for the detection of MMP-2, such as zymography,[120] enzyme-linked immunosorbent assay (ELISA),[121] and activity assays.[122] However, these methods often require multiple reaction steps, making them time-consuming, laborious, and complex.[123] Hence, simpler and more efficient approaches need to be explored for the selective detection of MMP-2.[124-129]

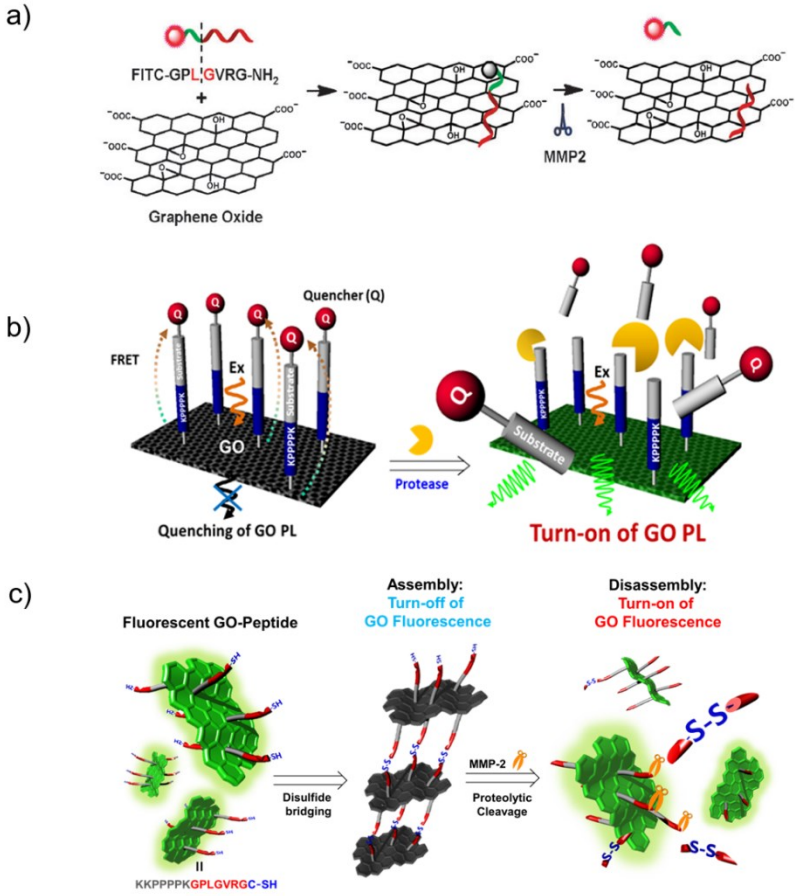

Figure 1-7. Schematic illustration of various type of protease sensor using GO. a) Conventional FRET sensor using GO as a FRET acceptor.[124] b) GO based optical sensor using GO as a FRET donor.[74] c) GO based optical sensor using self-assembly/self-quenching strategy.[130]

4. Research Objectives

In this thesis, fluorescent GO are described as a signal transduction tool for the detection of matrix metalloproteinase-2 (MMP-2).

In the first part, optical biosensor based on GO PL was designed as a biologically stable and sensitive fluorescent probe overcoming the disadvanteges of conventional FRET sensor. GO PL-based optical biosensor composed of a luminescent GO donor covalently linked with a peptide-quencher complex. To find the optimal quencher for GO PL, the quenching efficiency and the mechanism based on charge or energy transfer were explored. The designed GO-peptide-quencher revealed high selectivity for the detection of chymotrypsin and MMP-2 *in vitro* assay by turn-on response of inherent GO fluorescence. Also, GO-peptide-quencher sensor was applied to a real biosystem as a turn-on sensor for the detection of MMP-2 secreted from living cells with high sensitivity.

In the second part, peptide-induced assembly of fluorescent GO was described as more simple optical turn-on biosensor for the detection of MMP-2. Functionalization of GO with a peptide substrate for MMP-2 bearing a thiol group led to its self-assembly via disulfide bonding,

accompanied by self-quenching of GO's fluorescence. This GO-peptide assembly sensor was then disassembled by proteolytic cleavage in the presence of MMP-2, thereby restoring the level of self-quenched GO fluorescence. Furthermore, GO-peptide assembly sensor was successfully applied for the selective and sensitive detection of MMP-2 secreted by living cells.

In the third part, a simple and mild way to obtain heteroatom-doped GO was described to enhance the fluorescence of GO. GO was homogenized with cysteine (Cys) as a N and S source in acidic solvent cosolvent system, resulting in Cys-modified GO (Cys-GO). X-ray photoelectron spectroscopy (XPS) revealed that as made Cys-GO contained high percentage of N and S atoms. Fluorescence signal of Cys-GO was significantly enhanced via these high doping level. Finally, Cys-GO was used as a fluorescence turn-on sensor for the detection of MMP-2.

Chapter II.
Experiments

1. General

1.1 Chemicals and Materials

Graphite, potassium permanganate ($KMnO_4$), protoporphyrin IX cobalt chloride (CoPP), protoporphyrin IX Zinc (II) (ZnPP), protoporphyrin IX iron(II) (FePP), propagyl amine, 1-ethyl-3-(3-dimethylaminopropyl)-carbodiimide (EDC), *N*-hydroxysuccinimide (NHS), anisole, triisopropylsilane (TIPS), 3,6-dioxa-1,8-octanedithiol (DODT), α-chymotrypsin, phenylmethanesulfonyl fluoride, MMP-2 human (recombinant, expressed in E.coli), prinomastat hydrochloride, sodium ascorbic acid, Tris-HCl buffer were purchased from Sigma-Aldrich (St. Louis, MO, USA). Protoporphyrin IX copper (II) (CuPP) was purchased from Santa Cruz Biotech. (Delaware, CA, USA). Sulfuric acid (H_2SO_4,) *N,N'*-diisopropylethylamine (DIPEA), *N*-methyl-2-pyrrolidone (NMP), dimethyl sulfoxide (DMSO), ethanol, methanol, diethyl ether, dichloromethane (DCM), sodium hydroxide (NaOH), piperidine, and dimethylformamide (DMF) were purchased from Dae-Jung Chemicals (Korea). Trifluoroacetic acid (TFA) was bought from Acros Organics (Morris Plains, NJ, USA). Rink amide MBHA resin

(0.40 mmol g^{-1}), Fmoc-protected amino acids, benzotriazole-1-yl-oxy-tris(dimethylamino)phosphonium hexafluorophosphate (BOP), hydroxybenzotriazole (HOBt) and 4-hydroxymethylfuran-2(5*H*)-one, fritted polypropylene tube reactors (5 mL, Libra tube RT-5M) were obtained from BeadTech Inc. (Seoul, Korea). QXL_{570} C2 maleimide was bought from AnaSpec Inc. (Fremont, CA, USA), and 6-azido-hexanoic acid was purchased from Novabiochem (Darmstadt, Germany). Copper (II) sulfate pentahydrate ($CuSO_4 \cdot 5H_2O$) and potassium permanganate ($KMnO_4$) were purchased from Kanto Chemicals (Tokyo, Japan). Chloroacetic acid, disodium hydrogen phosphate, and sodium dihydrogen phosphate dihydrate were bought from Junsei Chemicals (Tokyo, Japan). HepG2 cells were kindly provided by research professor Mi Ran Seo from the Yonsei University, Collge of Medicine (Seoul, Korea), or purchased from the Korean Cell Line Bank (Seoul, Korea). Roswell Park Memorial Institute medium (RPMI) 1640, fetal bovine serum (FBS), 50 μg mL^{-1} streptomycin, and 50 U mL^{-1} penicillin, and 0.25% trypsin-0.53% mM EDTA (0.25% TE) were purchased from Gibco® (Carlsband, CA, USA). Human MMP-2 Enzyme liked immunosorbent assay (ELISA) kit was purchased from Abcam

(Cambridge, MA, USA). Dibenzocyclooctyne-PEG_4-acid (DBCO), 4-dimethylaminopyridine (DMAP), *N,N*'-diisopropylcarbodiimide (DIC) were purchased from Sigma-Aldrich (St. Louis, MO, USA). Sodium nitrate was purchased from Shimakyu Pure Chemicals (Osaka, Japan). Minimum essential medium (MEM) containing 4-(2-hydroxyethyl)-1-piperazineethanesulfonic acid (HEPES) and sodium bicarbonate ($NaHCO_3$) were purchased from Gibco (Carlsbad, CA, USA). L-Cysteine was purchased from Sigma-Aldrich (St. Louis, MO, USA). Hydrochloric acid (35%) was purchased from Dae-Jung Chemicals (Siheung, Korea).

1.2 Instruments

The UV absorption spectra were acquired by UV/Visible spectrophotometry (Optizen 2120 UV, Mecasys Co. Ltd., Korea). AFM images were acquired by Scanning Probe Microscope System (INNV-BASE, VEECO Inc., NY, USA). FT-IR spectra were obtained by FT-IR spectrometer (Cary 660, Agilent Technologies, CA, USA). Elemental analysis data to determinate carbon, hydrogen and nitrogen content were acquired by elemental analyzer (CHNS-932, LECO Inc. MI, USA). Peptide derivatives were purified using semi-preparative RP-HPLC (Thermo Scientific Spectra System AS3000; Thermo-Fisher, Waltham, MA, USA/YL HPLC system, Young Lin, Anyang, Korea). Mass spectrometry data were obtained by a QUATTRO triple quadrupole tandem mass spectrometer (Waters Micromass, MA, USA). Fluorescence spectra were acquired using a fluorescence spectrometer (LS-55, PerkinElmer, Waltham, MA, USA). Cells were incubated in CO_2 incubator (Sanyo, Osaka, Japan). Absorbance spectra of GO-Peptide-QXL were obtained using a UV spectrometer (Optizen 2120UV, Mecasys, Daejeon, Korea). Absorbance for ELISA was read using a microplate spectrophotometer (MQX200R, BioTek Inc., Winooski, VT,

USA). Atomic force microscopy (AFM) images were acquired using a scanning probe microscope system (MultiMode 8, Bruker AFM Probes, Camarillo, CA, USA). Fourier transform infrared (FT-IR) spectra were obtained using a FT-IR spectrometer (Nicolet 6700, Thermo Scientific, Waltham, MA, USA). Peptides were synthesized either using automatic peptide synthesizer (CS336X, CSBio, Menlo Park, CA, USA) or manually by a conventional solid phase peptide synthesis method. X-ray photoelectron spectroscopy (XPS) experiments were carried out using an AXIS His spectrometer (Kratos Analytical Ltd., Kyoto, Japan). High-resolution transmission electron microscopy (HR-TEM) images and electron energy loss spectroscopy (EELS) mapping images were collected on a Tecnai F20 microscope (FEI corp., Hillsboro, OR, USA). Cys-GO was synthesized via high-power sonication using probe sonicator (SONOPULS HD2070, Bandelin electronic GmbH & Co., Berlin, Germany).

2. Synthesis

2.1 Preparation of Peptides

Peptides were synthesized by conventional solid-phase synthesis method using Fmoc/tBu strategy on Rink amide MBHA resin (0.40 mmol g^{-1}). Various peptides containing a tetra-proline linker either including chymotrypsin or MMP-2 specific substrate, or non-specific substrate sequences were synthesized on Rink amide MBHA resin (0.41 mmol g^{-1}) using an automatic peptide synthesizer or manually. Each coupling reaction step was monitored by ninhydrin color test. Fmoc-amino acid (3 eqiv.), BOP (3 equiv.), and HOBt (3 equiv.) were dissolved in NMP and the mixture was added to the resin in the presence of DIPEA (6 equiv.). Each coupling reaction was continued for 2 h at RT, and Fmoc deprotection was carried out via reaching with 20 % piperidine/NMP for 30 min. And then, depending on the use, azidohexanoic acid (3 equiv.) or maleimidopropionic acid (3 equiv.) were coupled to *N*-terminal of peptide in the presence of BOP (3 equiv.), HOBt (3 equiv.), and DIPEA (6 equiv.) in NMP for 2 h at RT. The resulting azido- or maleimide-modified peptides (N_3-peptides or Mal-peptides) were cleaved from the

resin by treating with a cleavage cocktail containing TFA/anisole/DODT/TIPS (95.5/2/1.5/1%) for 2 h. The resin was filtered, and then washed with DCM (3×) and methanol (3×). The filtrate and washings were combined, concentrated under high vacuum, and then precipitated with cold diethyl ether to obtain the N_3-peptides or maleimide-peptide as a white powder. The precipitates were then centrifuged at 7,000 rpm for 3 min and washed with diethyl ether five times. The crude peptides were further purified using semi-preparative RP-HPLC (Thermo Scientific Spectra System AS3000; Thermo-Fisher, Waltham, MA) with A to B gradient (A: 0.1% TFA in water, B: 0.1% TFA in acetonitrile; from 10% to 90% B over 30 min, at a flow rate of 4.0 mL min^{-1}) and freeze-dried. The resulting N_3-peptides or maleimide-peptides were identified by a QUATTRO triple quadrupole tandem mass spectrometer (Waters Micromass, MA, USA).

2.2 Preparation of GO based Optical Sensors

Preparation of GO-Peptide-QXL

GO was synthesized from graphite flakes using a modified Hummers

method.[60] Graphite was oxidized in H_2SO_4 and $KMnO_4$, and subsequently sonicated for 1.5 h at 12 W in an ice bath. After centrifugation, GO was washed intensively with water. The GO was then dispersed in DMF via solvent exchange by means of centrifugation. Chloroacetic acid was reacted with GO to introduce more carboxylic groups on the GO surface. Five milliliters of GO solution (2.3 mg mL^{-1}) was dispersed in 5 mL of 6 M-NaOH solution. A 1.46 g portion of chloroacetic acid was added to the GO solution in an ice bath. The temperature was raised up to 60 °C, and then the reaction mixture was magnetically stirred for 1.5 h. After cooling down, carboxymethylated GO (CM GO) was centrifuged at 15,000 rpm for 40 min, and washed with water several times until the pH of the CM GO solution became 5.4. Then, propagyl amine (10 equiv.) was coupled to the carboxylic group of CM GO using EDC/NHS (10 equiv.) in phosphate buffer (0.1 M, pH 6.0) for 3 h at RT to introduce an alkyne group.

For preparation of GO-peptide-QXL hybrids as a chymotrypsin sensor, 'N_3-peptide 1' (1 equiv.), and 'N_3-peptide 2' (1 equiv.) were conjugated to alkyne-modified GO through triazole linkage by the Click chemistry with $CuSO_4.5H_2O$ (3 equiv.) and sodium ascorbic acid (8.5 equiv.) in

phosphate buffer (0.1 M, pH 7.0) for 18 h at RT. Then, the resulting GO-peptide-QXL hybrids were washed with water several times to remove the unreacted peptides. Then, QXL_{570} C2 maleimide (1 equiv.) was coupled to the thiol group at the *C*-terminal of GO-peptide conjugates in DMSO for 2 h. The resulting GO-peptide-QXL hybrids were then washed with DMSO and water several times. For the preparation of the GO-peptide 3-QXL hybrid for MMP-2, the MMP-2 substrate peptide (N_3-peptide 3, 1 equiv.) was first reacted with QXL_{570} C2 maleimide (1 equiv.) in a mixture of phosphate buffer (0.1 M, pH 7.0) and DMSO for 2 h. N_3-peptide 3-QXL (1 equiv.) was then coupled to alkyne-modified GO in the presence of $CuSO_4$-$5H_2O$ (3 equiv.) and sodium ascorbic acid (8.5 equiv.) in phosphate buffer (0.1 M, pH 7.0) for 18 h at RT. GO-peptide 3-QXL hybrid was washed with water several times.

Preparation of GO-Peptide Assembly

GO was reacted with ethanolamine to introduce more hydroxyl groups. GO was premixed with EDC (20 equiv.) and NHS (20 equiv.) in PBS (50 mM, pH 6.0) for 30 min, followed by the addition of ethanolamine (40 equiv.), and the coupling reaction was allowed to proceed for 3 h at RT.

The resulting hydroxyl group-rich ethanolamine-GO (GO-OH) solution was washed with water by centrifugation (13,000 rpm for 10 min) more than three times, and then dialyzed overnight. For use in further reactions, the solvent of the GO-OH solution was exchanged to DMF by centrifugation (15,000 rpm for 40 min) more than three times. DBCO (1.1 equiv.) was dissolved in anhydrous DCM, and DIC (1.1 equiv.) was then added and premixed for 30 min. DBCO activated by DIC was added to GO-OH in DMF solution (2 mg mL^{-1}) with DMAP (0.1 equiv.). The reaction was allowed to proceed for 6 h with vigorous shaking at RT. The DBCO conjugated GO (GO-DBCO) was washed with DMF and water by centrifugation (15,000 rpm for 15 min) multiple times. One and a half milliliters of GO-DBCO aqueous solution (1 mg mL^{-1}) was reacted with 0.5 mL of N_3-peptide (1.1 equiv.) in PBS (50 mM, pH 7.0) for 2 h with vigorous stirring at RT. The resulting GO–peptide hybrid was washed with water and then dialyzed overnight. Finally, the GO–peptide hybrid was suspended in a mixture of DMSO and water (1:1) with vigorous shaking (1400 rpm) overnight to form disulfide bonds. The suspension was then dialyzed overnight.

Preparation of Cys-GO

One milliliter of GO solution (1 mg mL^{-1}) was mixed with 1 mL of L-Cysteine (30 equiv.) dissolved in 1% HCl/water. Final solvent system was 1% HCl in water : DMF = 1 : 1 (0.5% HCl/DW-DMF). The resulting mixture was sonicated with a probe sonicator pulsed at a 0.5 s on/0.5 s off interval under 10.5 W power. After 1 h reaction, cysteine-modified GO (Cys-GO) was washed with water by centrifugation (17000 rpm for 30 min) multiple times, and suspended in water at a concentration of 1 mg mL^{-1}.

Preparation of Cys-GO-Peptide Assembly

Cys-GO and maleimide-peptides were conjugated through the specific reaction between thiol groups in Cys-GO and maleimide groups in Mal-Peptide. One milliliter of Cys-GO aqueous solution (1 mg mL^{-1}) was reacted with 1 mL of Mal-peptides (1.1 equiv.) in PBS (20 mM, pH 6.8) for overnight with vigirous shaking at 4 °C. The resulting Cys-GO-Peptide hybrid was washed with water, and then, suspended in a mixture of DMSO and water (1 : 1) with vigorous shaking (1400 rpm) overnight

to form disulfide bonds. The resulting Cys-GO-Peptide assembly was then washed with water several times.

2.3 Screening of Effective Quencher for GO

GO aqueous solution (2.3 mg mL^{-1}) was diluted with phosphate buffer (0.1 M, pH 7.0) to 0.1 mg mL^{-1}. MePPs and QXL_{570} were dissolved in DMSO and added to the GO solution. The final concentration of the quencher molecules was varied from 10 to 50 μM. After gentle mixing, the fluorescence of GO was measured by a fluorescence spectrometer (LS-55, PerkinElmer, MA, USA) using 400 nm-excitation and 1.0 sec integration time.

2.4 Detection of Chymotrypsin and MMP-2

Chymotrypsin was added to GO-peptide-QXL or GO-peptide assembly sensor (0.1 mg mL^{-1}) in Tris-HCl buffer (0.1 M, pH 7.8), and the reaction mixture was incubated for 10 min or 2 h at RT for GO-peptide-QXL sensor or GO-peptide assembly sensor, respectively. The final concentration of chymotrypsin was varied from 0 to 500 mU mL^{-1}. Then, the fluorescence response was measured with 400 nm-excitation and 1.0 sec integration time. To find out the effect of an inhibitor, the inhibitor was pre-incubated with chymotrypsin (50 mU mL^{-1}) in Tris-HCl buffer (0.1 M, pH 7.8) for 10 min at 25 °C, and then added to the GO sensor solution (0.1 mg mL^{-1}). For testing with MMP-2, MMP-2 was added to GO-peptide-QXL, GO-peptide assembly, or Cys-GO-peptide assembly (0.1 mg mL^{-1}) in Tris-HCl buffer (50mM, pH 7.6), and the reaction mixture was incubated at 37 °C for 30 min (GO-peptide-QXL sensor) or 2 h (GO/Cys-GO-peptide assembled sensor). The final concentration of MMP-2 was varied from 0 to 10 μg mL^{-1}. To find out the effect of an inhibitor, the inhibitor was pre-incubated with MMP-2 (5 μg mL^{-1}) for 10 min at 37 °C, and then added to the GO sensor solution

(0.1 mg mL^{-1}). For the specificity test of GO sensors, a different protease, chymotrypsin (0.05 U mL^{-1}) was added into GO sensor (0.1 mg mL^{-1}) in Tris-HCl buffer (0.1 M, pH 7.8) for 1 h at 25 °C. The relative PL intensity at 560 nm was obtained with 400 nm excitation and 1.0 sec integration time.

2.5 Kinetic Measurement of Chymotrypsin Activity

GO-peptide 1-QXL was diluted with Tris-HCl buffer (0.1M, pH 7.8) to various concentrations of 0.01, 0.05, and 0.1 mg mL^{-1}, and subsequently sonicated for 1 min at 2 W in an ice-bath. Soon after the addition of chymotrypsin (50 mU mL^{-1}), the fluorescence of GO was measured and repeated with time interval till PL response reached plateau. The fluorescence response was measured by a fluorescence spectrometer (LS-55, PerkinElmer, MA, USA) using 400 nm-excitation and 0.05 sec integration time. Then, the rates of fluorescence increase of the GO-peptide-QXL sensors were measured and plotted over the concentrations of peptide substrates on the sensors, which gave the values of K_m and v_{max} for proteolytic activity via *x*- and *y*-intercepts after linear regression to the data of Lineweaver-Burk plot.

2.6 Kinetic Mearurement of MMP-2 Activity

GO-Peptide 3-QXL or GO-P1 assembly was diluted with Tris-HCl buffer (50 mM, pH 7.6) to prepare samples with concentrations of 10, 50, and 100 μg mL^{-1}, and subsequently MMP-2 (5 μg mL^{-1}) was added to these solutions. During the initial reaction, the reaction was stopped after various intervals, and then fluorescence response was measured under 400 nm excitation. The rates of increase in fluorescence of GO sensors were measured and plotted versus the concentrations of the peptide substrates on the sensors, giving values of K_m and V_{max} for proteolytic activity from the slope and y-intercept of a linear regression to the data of Lineweaver-Burk plot.

2.7 Detection of MMP-2 Secreted from Living Cells

HepG2 cells were seeded in 10-cm dishes at a density of 2 x 10^6 cells per dish and cultured in RPMI 1640 containing 10% FBS and 1% penicillin-streptomycin until the cell confluence reached 60%. After replacing with a fresh medium, the cells were incubated for specific time intervals of 12, 24, and 48 h. Then, the cell culture supernatant was taken out at each interval to mix with the GO-peptide 3-QXL sensor or GO-P1 assembly sensor (0.1 mg mL^{-1}) for 30 min or 2 h at 37 ºC with gentle shaking (approximately 100 rpm). The fluorescence response of the sensor was measured by a fluorescence spectrometer (NanoLog, HORIBA Co. Ltd., Kyoto, Japan) with 400 nm excitation and 0.01 sec exposure time. In addition, the concentration of MMP-2 secreted from the cells was determined by a MMP-2 Human ELISA kit (Abcam®, Cambridge, UK). A 100 μL portion of each standard and sample were added into human MMP-2 specific antibody coated wells. After incubation for 2.5 h at 25 ºC with gentle shaking, the solution was completely removed. A 100 μL portion of biotinylated MMP-2 detection antibody was added to each well, and incubated for 1 h at 25 ºC with gentle shaking. The solution was discarded, then a 100 μL of HRP-

streptavidin solution was added to each well for 45 min at 25 ºC with gentle shaking. The washing step was repeated, and then a 100 µL of TMB one-step substrate reagent was added to each well, and incubated for 30 min at 25 ºC in the dark with gentle shaking. Absorbance was measured at 450 nm by a microplate spectrophotometer (MQX200R, BioTek Instruments, Inc., VT, USA) immediately after adding 50 µL of stop solution. A new standard curve was generated for each assay, and each sample was assayed in triplicates. In addition, control experiments were carried out for MMP-2 sensor. MMP-2 inhibitor (50 µM) was added to HepG2 cells culture media, and pre-incubated at 37 ˚C for 30 min. GO sensors (0.1 mg mL^{-1}) was treated and further incubated at 37 ˚C for 30 min for enzyme reaction. GO-peptide 1-QXL sensor, GO-P2, and GO-P3 assembly (0.1 mg mL^{-1}) was incubated with the same HepG2 cell culture media for 30 min at 37 ºC with gentle shaking. Control experiment was performed in triplicate.

Chapter III.
Results and Discussion

1. Fabrication of Luminescent GO with Peptide-Quencher Hybrids for MMP-2 Detection

1.1 Strategy for GO Based Protease Sensing

To develop GO-based sensing platform using inherent fluorescence of GO as a signal transduction tool in FRET bioassay systems, a pair of GO fluorescent donor and its quencher as a FRET platform was designed. GO and the quencher were linked with a target specific peptide substrate. GO-peptide-quencher hybrids can selectively detect target proteases through a turn-on response of inherent GO PL upon proteolytic cleavage of the quencher (Figure 3-1). To find out the most effective pair in the GO-based FRET system, various quencher candidates for GO PL such as metalloprotophophyrin derivatives (MePPs) and QXL_{570} were screened to evaluate their quenching efficiency, and the quenching mechanism was investigated. The designed GO-peptide-quencher hybrids were applied to selectively and specifically detect chymotrypsin and matrix metalloproteinase-2 (MMP-2) by the recovery of quenched GO PL arising from the cleavage of the peptide-quencher complex. Furthermore, cell secreted MMP-2 detection capability of GO-peptide-

quencher hybrids was also evaluated.

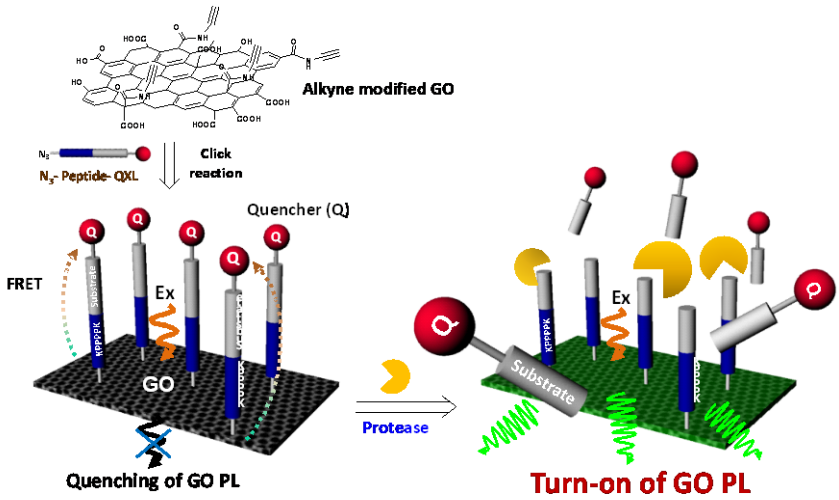

Figure 3-1. Schematic illustration of GO based optical sensor consisting of a luminescent GO donor and a peptide-quencher complex, and the optical detection of protease by the turn-on response of GO fluorescence.

1.2 Study on Quenching of GO PL

As-prepared GO showed unique optical properties as shown in Figure 3-2. In UV absorption spectra, GO had two characteristic peaks at 230 and 300 nm originating from π-π* transition of the C=C bond and n-π* transition of the C=O bond.[99] Also, an intense fluorescence emission peak at 543 nm was observed under 400 nm excitation, which results from the recombination of electron-hole pairs localized within a diminutive sp^2 domain embedded in a sp^3 matrix.[131] This emission property allows for the use of GO as a fluorescent donor in the FRET-based detection of proteases.

To find out an effective quencher for GO fluorescence, were selected, considering several metallo protoporphyrin derivatives (MePPs) and QXL_{570} in terms of two possible quenching mechanisms: charge transfer and FRET from GO to a quencher, respectively. Initially, we assumed that several MePPs such as zinc (Zn^{2+}) protoporphyrin (ZnPP), iron (Fe^{2+}) protoporphyrin (FePP), copper (Cu^{2+}) protoporphyrin (CuPP), and cobalt (Co^{3+}) protoporphyrin chlorides (CoPP) could quench GO fluorescence via charge transfer from GO to the metal ions. The protoporphyrin

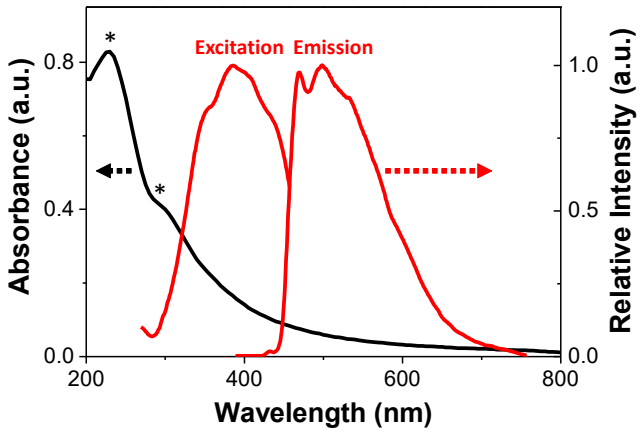

Figure 3-2. UV/Vis absorption spectrum of GO solution (black line, 0.1 mg mL^{-1}), and excitation and emission profiles (red lines), showing that the GO has an excitation maximum at 400 nm and an emission maximum at 543 nm.

structure was considered to enhance their quenching efficiency by putting them in a close proximity to the GO surface through π-π interaction. Moreover, we expected that QXL_{570} could play a role as a dark quencher since its absorption was largely overlapped with the maximum position of GO fluorescence (543 nm at 400 nm excitation).

As shown in Figure 3-3a, the addition of MePPs and QXL_{570} to the GO solution induced an instantaneous decrease in GO fluorescence at 400 nm excitation. GO fluorescence gradually decreased with increasing the concentration of the quenchers from 10 to 50 μM (Figure 3-4). Their quenching efficiency ($\Delta I_{543\ nm}$) linearly increased at this range of quencher concentrations, which is in good agreement with the Stern-Volmer equation (Figure 3-3b):

$$I_0/I = K_{SV}[Q] + 1 \qquad (1)$$

where I_0 is the intensity of GO fluorescence in the absence of a quencher, I is the intensity of GO fluorescence in the presence of a quencher, [Q] is the quencher concentration, K_{sv} is the Stern-Volmer quenching constant, $K_{sv} = k_q\tau_0$, k_q is the quenching rate constant, and τ_0 is the lifetime of GO fluorescence.

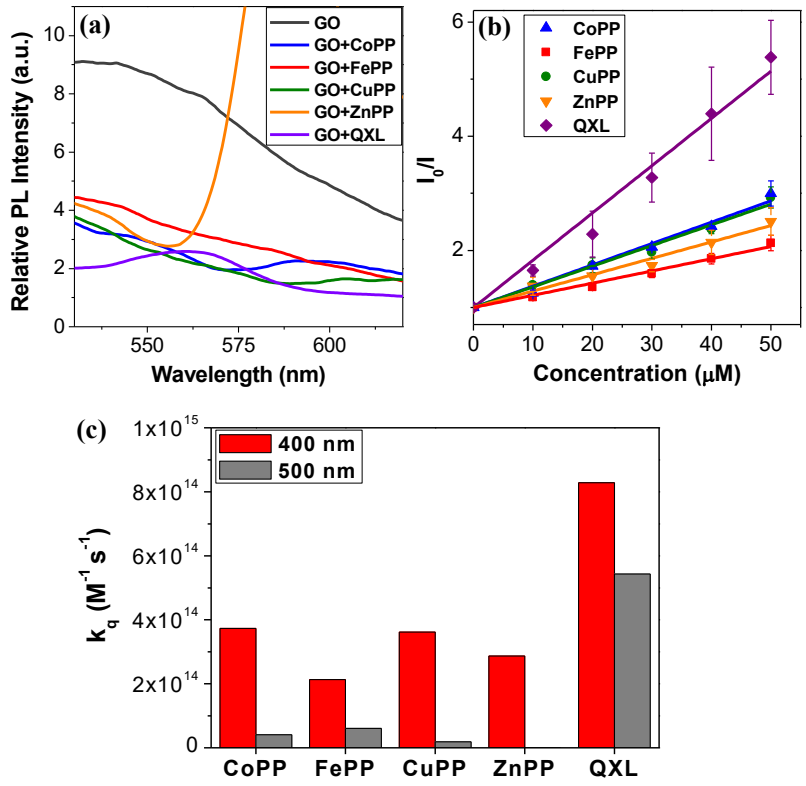

Figure 3-3. Screening of effective quencher for GO PL. (a) Fluorescence spectra of GO solution (0.1 mg mL^{-1}) in the presence of MePPs and QXL (50 μM) under excitation at 400 nm. (b) Stern-Volmer plot for GO fluorescence quenching by MePPs and QXL measured under excitation at 400 nm, showing linear fit to the Stern-Volmer equation. (c) Quenching rate constants of MePPs and QXL570 for GO fluorescence measured under excitation at 400 and 500 nm.

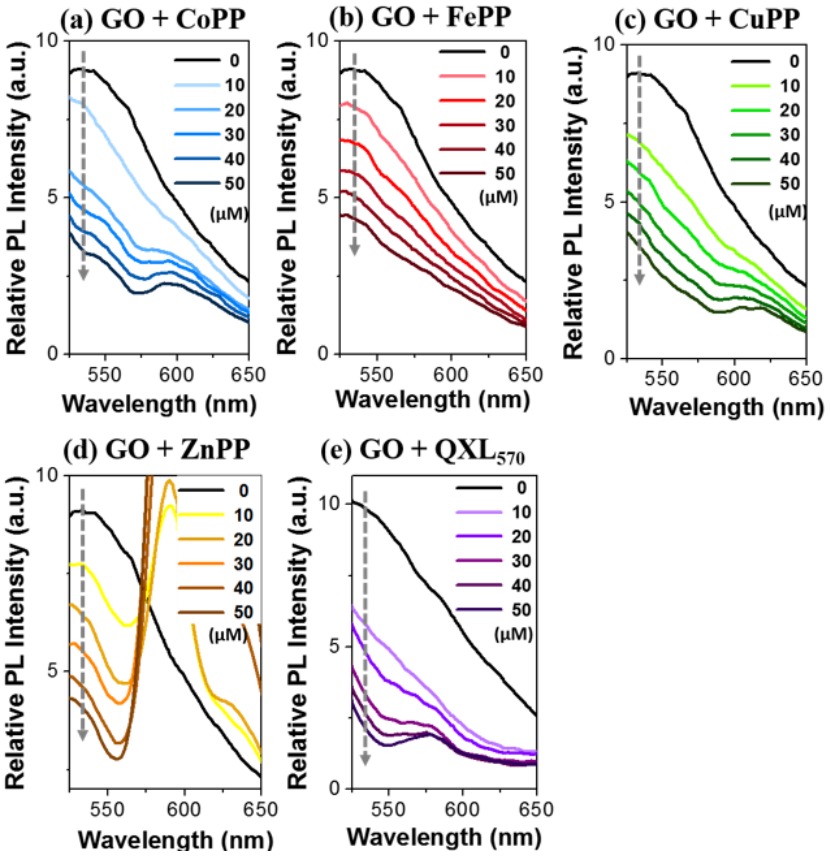

Figure 3-4. Fluorescence spectra of GO in the presence of (a) CoPP, (b) FePP, (c) CuPP, (d) ZnPP, and (e) QXL570 at various concentrations (0, 10, 20, 30, 40, and 50 μM). MePPs and QXL were dissolved in DMSO and added to GO solution (0.1 mg mL^{-1}) in phosphate buffer (0.1 M, pH 7.0). Fluorescence was measured at the excitation of 400 nm.

Moreover, the quenching rate constants for the quenchers were calculated. As shown in Figure 3-3c, QXL_{570} showed the highest quenching constant, twice higher than other MePP quenchers at 400 nm excitation (red bars). This effective quenching by QXL_{570} is clearly ascribed to FRET from the GO fluorescent donor to the QXL acceptor. As shown in Figure 3-5, the absorption spectrum of QXL_{570} was largely overlapped with the emission fluorescence of GO. MePP derivatives also showed good quenching efficiency. Being different from our assumption, the quenching of GO PL by MePPs mainly arose from their absorption of incident photons, not from charge transfer, since their absorption wavelength exactly matches with an excitation wavelength of 400 nm (Figure 3-5), which results in a significant decrease in the number of photons going to GO. Therefore, we changed the excitation wavelength from 400 nm to 500 nm and calculated the quenching rate constant for all the quenchers as well. As shown in Figure 3-3c (grey bars), the quenching efficiency of MePP derivatives significantly decreased, but still showed a moderate quenching effect through charge transfer from GO to metal ions.[132, 133] In contrast, QXL_{570} maintained effective quenching efficiency for GO fluorescence even at 500 nm excitation.

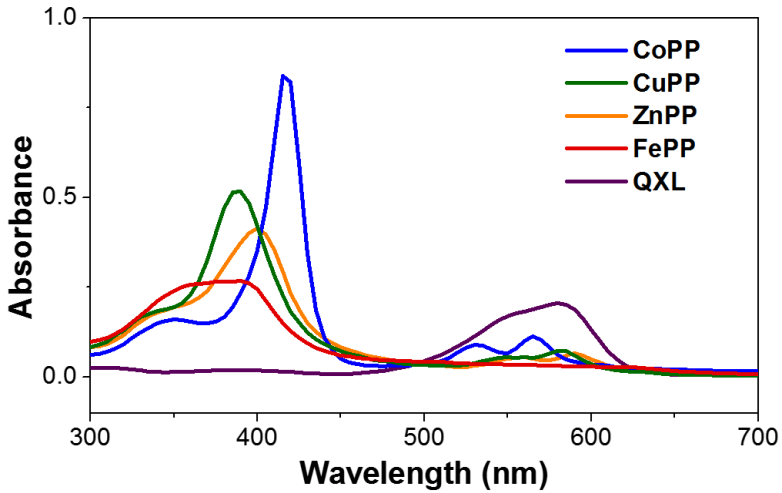

Figure 3-5. UV/Vis absorption spectra of quencher solutions. Quenchers were dissolved in DMSO and diluted to 5 μM with 0.1 M PBS (pH 7.0).

The small decrease in its quenching constant is attributed to the higher extinction coefficient of QXL_{570} at 500 nm. This result obviously indicates that the quenching of GO fluorescence by FRET is much more effective than by charge transfer. From this quenching study, we concluded that QXL_{570} was the most efficient quencher for GO fluorescence with the highest quenching constants regardless of excitation wavelength. Therefore, QXL_{570} was chosen as a quencher for further studies on a GO-based optical sensor for protease detection.

1.3 Peptide Design for Chymotrypsin and MMP-2 Detection

The peptide substrates for chymotrypsin and MMP-2 were rationally designed to impart several functions. The tetra-proline (PPPP) sequence was included as a stretchable rigid spacer for the peptide substrates to provide clear exposure to a protease cleavage site. In addition, two lysines (K, K) were introduced to make GO-peptide-QXL hybrids more hydrophilic and well-dispersible in aqueous solution to avoid aggregation. Cysteine was included at the *C*-terminal of peptides to attach QXL_{570} through the reaction of thiol with maleimide. Then, an azide group was coupled to the *N*-terminal of peptides to functionalize the GO bearing an alkyne group through the Click chemistry, which gives rise to the formation of GO-peptide-QXL hybrids. Finally, the active amino acid residues for specific protease recognition such as chymotrypsin and MMP-2 were introduced in the middle of the peptides.

We chose chymotrypsin and MMP-2 as model enzymes since chymostrypsin is a well-characterized protease and MMP-2 is one of the most important pharmaceutical target enzymes. Chymotrypsin is a serine protease that hydrolyzes peptide bonds at the *C*-terminal containing

hydrophobic or aromatic side chains such as phenylalanine. We designed two different peptides: one is Ala-Ala-Pro-Phe (AAPF), which has a chymotrypsin cleavage site, and the other is a control sequence, Gly-Gly-Gly-Gly (GGGG), which cannot be cleaved by chymotrypsin to prove the specificity of our optical sensor. MMP-2 is often overexpressed in tumors and deeply involved in cancer metastasis by allowing extravasate and invade normal tissues.[134-136] MMP-2 specifically cleaves the *N*-terminal of Gly at the center of Gly-Pro-Leu-Gly-Val-Arg-Gly[137] (GPLGVRG). Therefore, these peptide sequences were introduced to the peptide-QXL hybrids.

1.4 GO-Peptide-QXL Hybrids for Optical Detection of Proteases

To synthesize GO-peptide-QXL hybrids for the detection of chymotrypsin and MMP-2, GO was first functionalized with chloroacetic acid (CM GO) to increase the number of carboxylic acid groups on its surface.[99, 138] Then, propagyl amine was coupled to the carboxylic acid groups of CM GO to introduce alkyne groups on its surface (alkyne GO). Then, N_3-peptide was conjugated to the alkyne groups on GO through Click chemistry to obtain GO-peptide hybrids (GO-peptide). QXL_{570}-maleimide was then simply reacted with the thiol group of cysteine on the GO-peptide (GO-peptide-QXL). The resulting GO-peptide-QXL hybrids were characterized by atomic force microscopy (AFM), Fourier transform infrared (FT-IR) spectroscopy, and elemental analysis. The AFM images and the height profiles revealed that GO had a height of ~2 nm (Figure 3-6a), whereas GO-peptide-QXL hybrids had a height of around 15 nm (Figure 3-6b), which indicates that the peptide-QXL were successfully coupled to GO. We also analyzed the structure of GO-peptide-QXL hybrids using FT-IR spectroscopy.

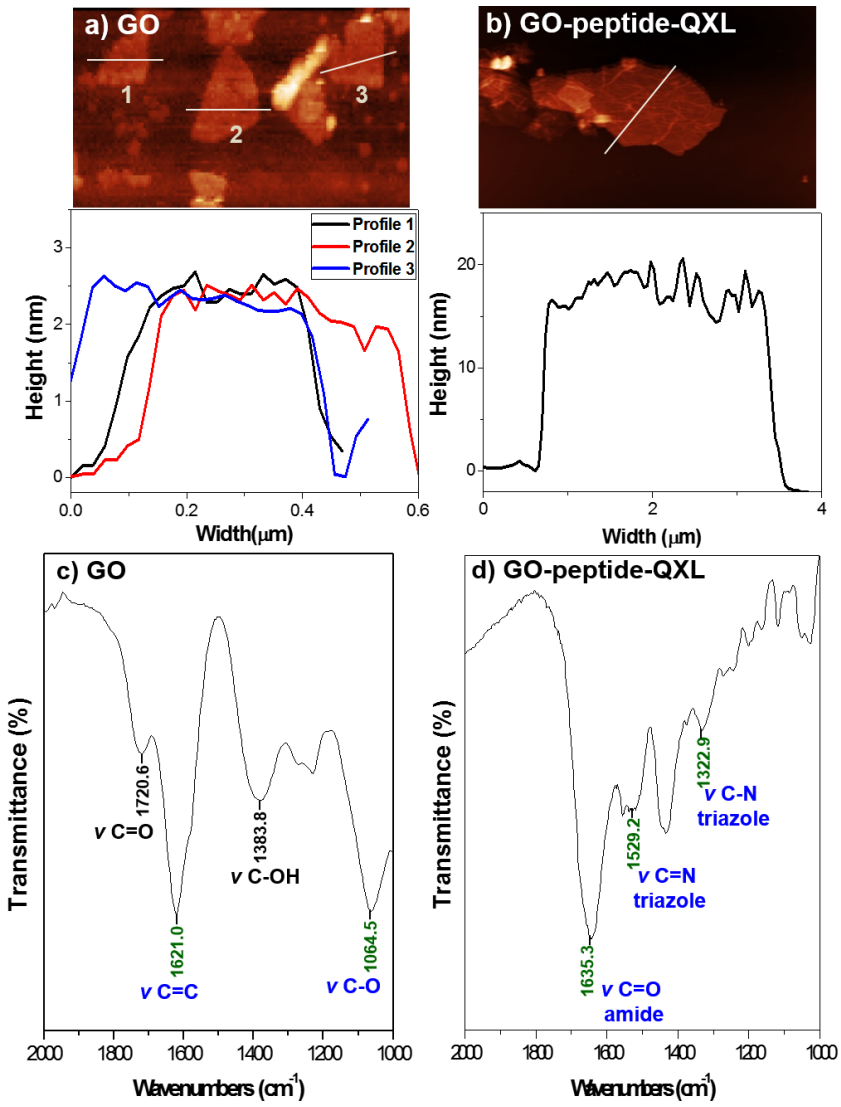

Figure 3-6. Characterization of GO-peptide-QXL hybrid. (a) AFM image and height profiles of GO and (b) GO-peptide 1-QXL. (c) FT-IR spectra of GO and (d) GO-peptide 1-QXL.

As shown in Figure 3-6d, the vibrational modes for an amide carbonyl group (C=O 1635 cm^{-1}) and a triazole group (C=N 1529 cm^{-1}, C-N 1323 cm^{-1}) in GO-peptide-QXL were distinctly observed, different from GO (Figure 3-6c) and CM GO (Figure 3-7a). In addition, the elemental analysis of GO-peptide-QXL hybrids showed an increase in nitrogen contents (11.5 wt%) compared to GO, CM GO, and alkyne-GO, as shown in Figure 3-7b. Lastly, we measured the fluorescence of GO-peptide-QXL. The fluorescence of GO decreased after coupling QXL_{570} to the peptides on GO (Figure 3-7c). These results clearly demonstrate the successful construction of GO-peptide-QXL hybrid sensors.

We then investigated the performance of GO-peptide-QXL hybrids for detecting chymotrypsin and MMP-2. First, the performance of GO-peptide-QXL hybrid sensors for chymotrypsin were evaluated. Figure 3-8 shows the structures of two sensors: GO-peptide 1-QXL bearing a specific peptide substrate sequence (AAPF) and GO-peptide 2-QXL bearing a control peptide sequence (GGGG). As shown in Figure 3-9a, the original fluorescence intensity of GO-peptide 1-QXL was very low due to the quenching by QXL_{570} via FRET. The quenched fluorescence of GO-peptide 1-QXL was restored only when chymotrypsin was added.

a)

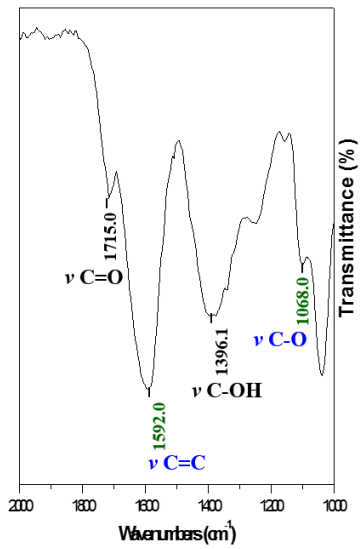

c)

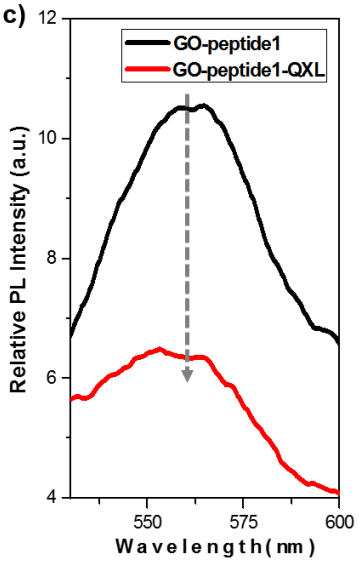

b)

	Carbon (wt %)	Hydrogen (wt %)	Nitrogen (wt %)
GO	49	2.7	0.2
CM GO	50	4.7	0.9
Alkyne GO	49	4.8	1.6
GO-peptide1	46	5.5	11.5

Figure 3-7. Characterization of various GO derivatives. (a) FT-IR (KBr) spectrum of CM GO. (b) Elemental analysis of GO, CM GO, propagyl GO and GO-peptide 1. (c) Fluorescence intensity of GO-peptide 1 and GO-peptide 1-QXL, showing a substantial decrease in the intensity (0.1 mg mL^{-1}).

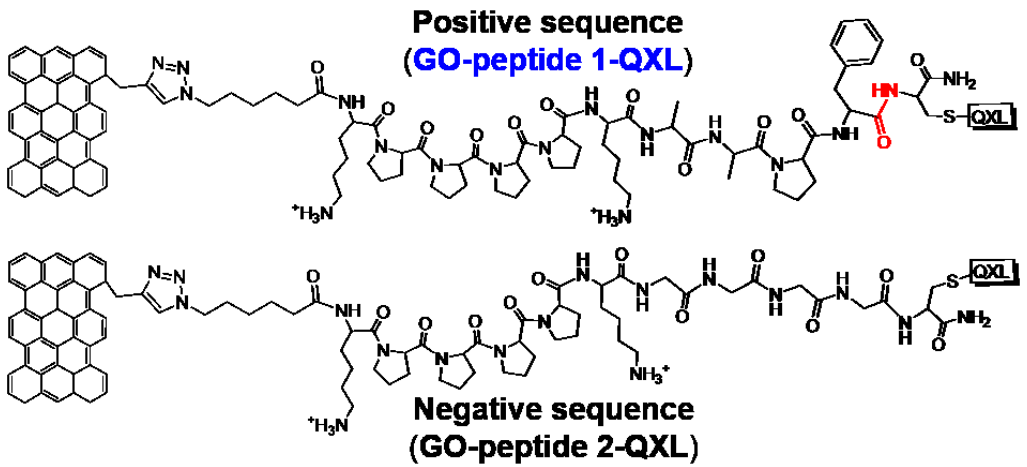

Figure 3-8. Chemical strucure of GO-peptide 1-QXL for chymotrypsin detection and GO-peptide 2-QXL as a negative control. The red color indicates the cleavage site by chymotrypsin.

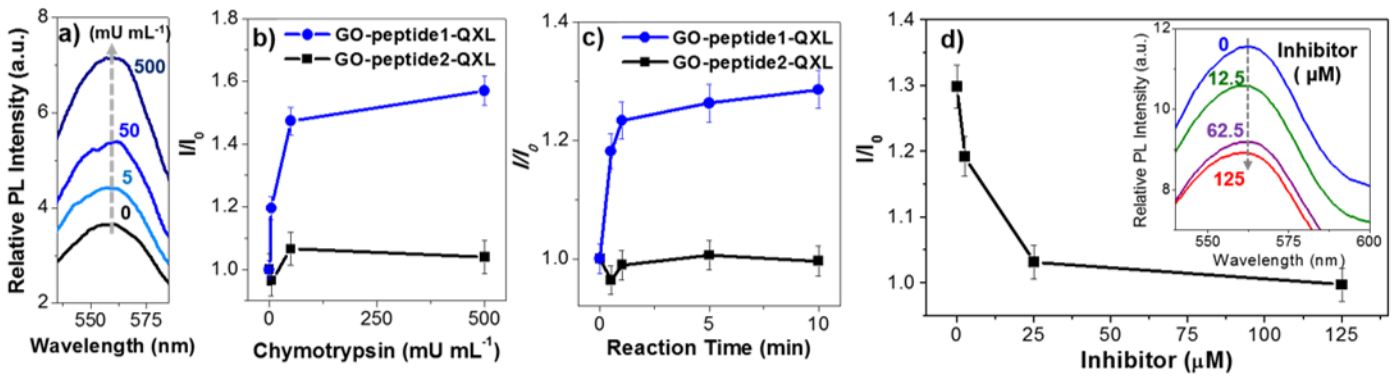

Figure 3-9. Optical detection of chymotrypsin with GO-peptide-QXL hybrid. a) Fluorescence response of GO-peptide 1-QXL to chymotrypsin at various concentrations. b) Fluorescence recovery from GO-peptide 1-QXL and GO-peptide 2-QXL as a function of chymotrypsin concentrations. c) Fluorescence recovery from GO-peptide 1-QXL and GO-peptide 2-QXL as a function of reaction time in the presence of chymotrypsin (50 mU mL^{-1}). d) Effect of chymotrypsin inhibitor on the fluorescence recovery of GO-peptide 1-QXL in the presence of chymotrypsin (50 mU mL^{-1}): the concentration of inhibitor (PMSF) was varied from 0 to 125 μM, and the inset presents the fluorescence spectra of GO-peptide 1-QXL at each inhibitor concentration. I_0 and I are the fluorescence intensity at 560 nm without and with chymotrypsin.

The fluorescence intensity gradually increased with increasing the concentration of the protease from 5 to 500 mU mL^{-1}. However, GO-peptide 2-QXL, which contains no specific peptide substrate sequence of chymotrypsin, did not restore its quenched fluorescence even after chymotrypsin was added (Figure 3-9b). These results clearly suggest that the designed GO-peptide 1-QXL was able to selectively recognize the presence of chymotrypsin. In addition, its response kinetics was so fast that the sensor recognized the target within 10 min (Figure 3-9c). For more rigorous study on the kinetics of enzyme detection, we measured the rates for the increase of fluorescence of the GO-peptide 1-QXL by chymotrypsin to obtain the Michaelis constant (K_m) and the maximum rate (V_{max}). From the Lineweaver-Burk plot, K_m and V_{max} were obtained as 0.16 μM and 0.15 min^{-1}, respectively, which suggest that the detection kinetics of GO-peptide 1-QXL sensor for chymotrypsin was very fast and efficient (Figure 3-10).

We further confirmed whether or not the restoration of the quenched fluorescence in GO-peptide 1-QXL was due to the cleavage of the peptide-QXL through mass spectrometry (MS) analysis. As shown in Figure 3-11a, after the addition of chymotrypsin to GO-peptide 1-QXL,

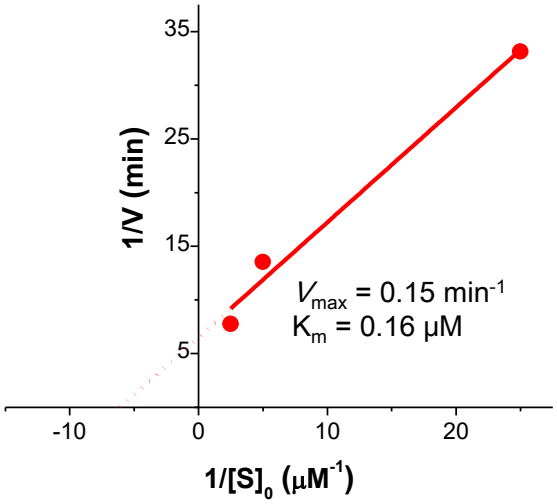

Figure 3-10. Lineweaver-Burk plot for the 'turn-on' response of GO-peptide 1-QXL hybrird by chymotrypsin. ($[S]_0$, concentrations of peptide substrates in GO-peptide 1-QXL sensor.)

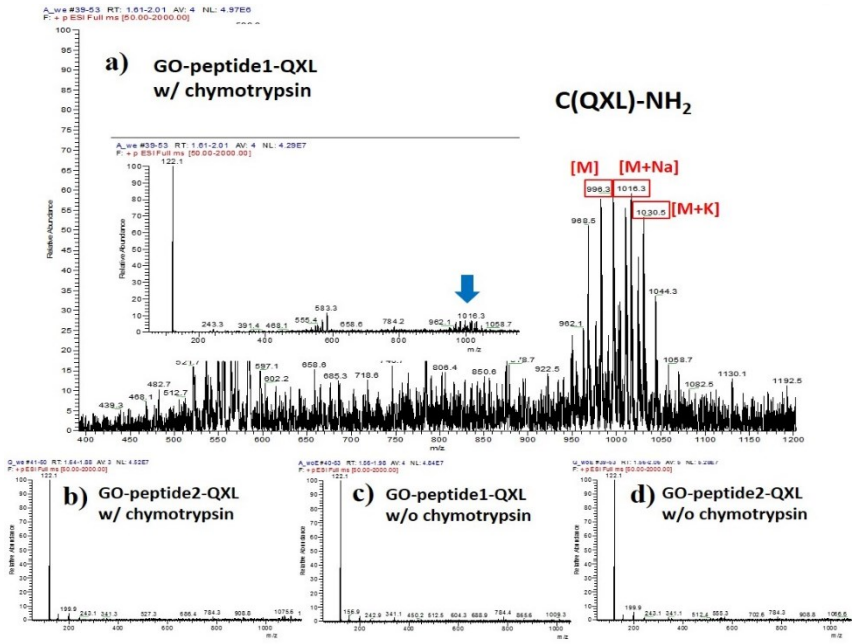

Figure 3-11. Mass spectroscopic analysis of proteolytic cleavage product of GO-peptide-QXL by chymotrypsin. a) MS spectrum of GO-peptide 1-QXL bearing specific peptide substrate sequence after chymotrypsin treatment for 30 min at 25 °C. b) MS spectrum of GO-peptide 2-QXL bearing control peptide substrate sequence after chymotrypsin treatment for 30 min at 25 °C. c) MS spectrum of GO-peptide 1-QXL without chymotrypsin treatment. d) GO-peptide 2-QXL without chymotrypsin treatment.

the hydrolyzed peptide-QXL fragment (C(QXL)-NH_2) with consistent mass (996.3) was detected in the mass spectra, while no other fragments were detected from GO-peptide 2-QXL (negative control) after chymotrypsin treatment (Figure 3-11b). Other cases of GO-peptide 1-QXL or GO-peptide 2-QXL without adding chymotrypsin, no extra mass fragment was detected (Figure 3-11c, d). These MS analysis results exhibit that the fluorescence turn-on in the GO-peptide 1-QXL sensor was caused by the cleavage of the peptide-QXL by chymotrypsin. Next, we investigated the effect of a chymotrypsin inhibitor on the fluorescence restoration of the sensor. As the chymotrypsin inhibitor, phenylmethanesulfonyl fluoride (PMSF), was added with the enzyme to the solution of GO-peptide 1-QXL. As expected, the degree of fluorescence restoration substantially decreased depending on the concentration of the inhibitor from 10 to 125 μM (Figure 3-9d). This result also supports that the sensor could be used for the screening of inhibitors to other proteolytic enzymes.

Then, we evaluated the performance of GO-peptide 3-QXL designed for sensing MMP-2. Figure 3-12 shows the structure of the sensor platform.

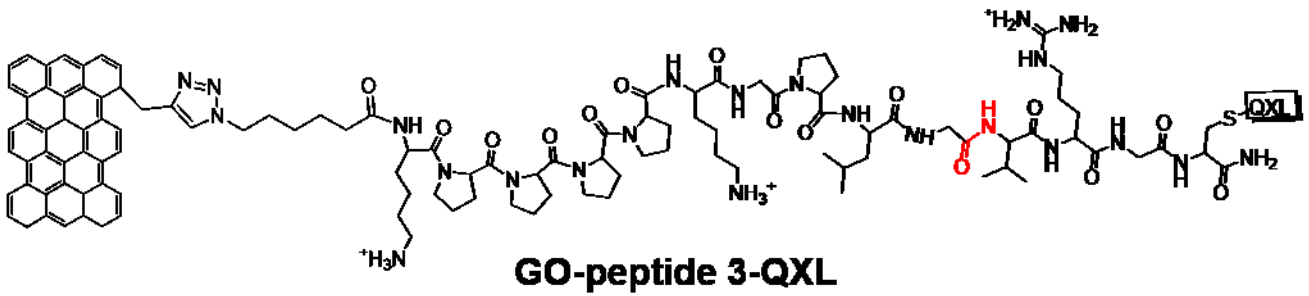

Figure 3-12. Chemical structure of of GO-peptide 3-QXL hybrid for detection of MMP-2. The red color indicates the cleavage site by MMP-2.

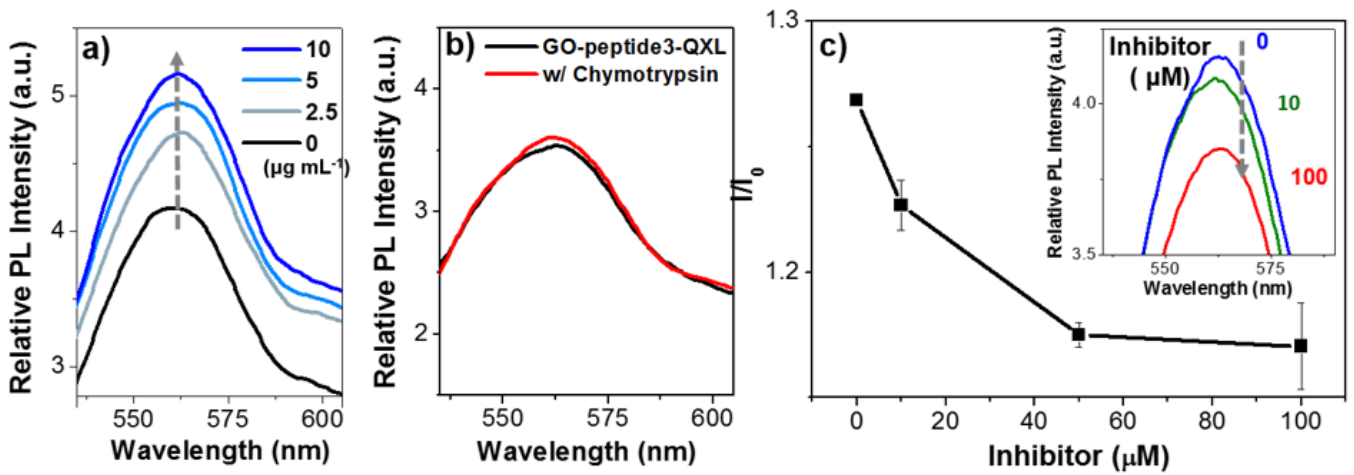

Figure 3-13. Optical detection of MMP-2 with GO-peptide-QXL hybrid. a) Fluorescence response of GO-peptide 3-QXL to MMP-2 at various concentrations (0, 2.5, 5, and 10 μg mL^{-1}). b) Fluorescence response of GO-peptide 3-QXL to chymotrypsin (50 mU mL^{-1}). c) Effect of MMP-2 inhibitor on the fluorescence recovery of GO-peptide 3-QXL at 560 nm in the presence of MMP-2 (5 μg·mL^{-1}): the concentration of MMP-2 inhibitor (Prinomastat hydrochloride) was varied from 0, 10, to 100 μM, and the inset presents the fluorescence spectra of GO-peptide 3-QXL at each inhibitor concentration. I_0 and I are the fluorescence intensity without and with MMP-2.

The quenched fluorescence of the GO-peptide 3-QXL sensor was restored after the addition of MMP-2 and the fluorescence recovery increased with increasing the concentration of the protease (Figure 3-13a). However, no fluorescence recovery was observed in the control experiment where GO-peptide 3-QXL was treated with chymotrypsin (Figure 3-13b). These results obviously suggest that the GO-peptide 3-QXL sensor was able to detect the specific protease MMP-2 through the turn-on response of the quenched fluorescence. We then measured the rates for the fluorescence response of the GO-peptide 3-QXL sensor to MMP-2 to obtain the values of K_m and V_{max}. After the linear regression of the Lineweaver-Burk plot (Figure 3-14), 0.76 μM for K_m and 0.49 min^{-1} for V_{max} were obtained, which suggest that the sensing kinetics of the GO-peptide 3-QXL sensor for MMP-2 was very fast as well. In addition, mass analysis data confirmed that the restoration of the quenched fluorescence in GO-peptide 3-QXL was caused by the proteolytic cleavage of the peptide-QXL by MMP-2. The hydrolyzed peptide fragment, H-VRGC(QXL)-NH_2, was detected in the mass data (Figure 3-15). Next, we investigated the effect of the MMP-2 inhibitor, prinomastat hydrochloride, on the fluorescence response of the sensor.

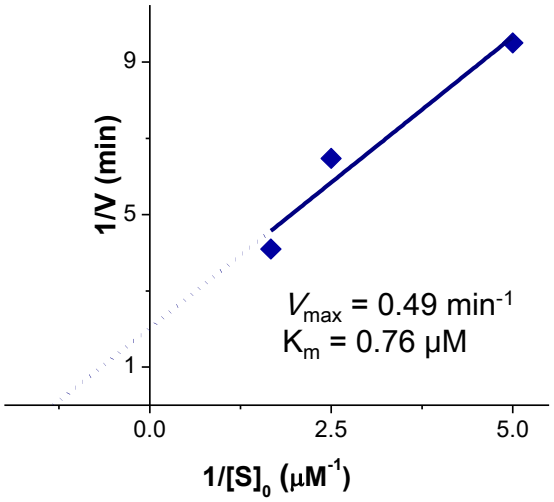

Figure 3-14. Lineweaver-Burk plot for the 'turn-on' response of GO-peptide 3-QXL hybrird by MMP-2. ($[S]_0$, concentrations of peptide substrates in GO-peptide 3-QXL sensor.)

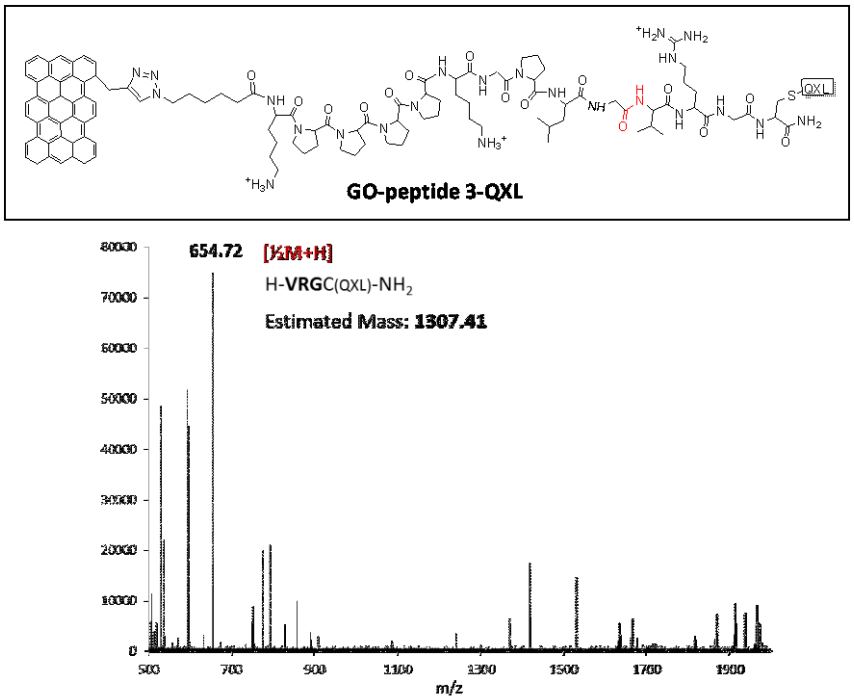

Figure 3-15. Mass analysis data of proteolytic cleavage product of GO-peptide 3-QXL by MMP-2.

When the MMP-2 inhibitor was added together with the protease into the solution of GO-peptide 3-QXL, the restoration rate of the quenched fluorescence significantly decreased depending on the inhibitor concentration from 10 to 100 μM (Figure 3-13c).

GO-peptide-QXL hybrids for the detection of the proteases exhibited superior stability for long-term storage. We found that GO-peptide-QXL hybrids perfectly maintained the quenching activity of fluorescence for 30 days at 25 ºC in water, and GO fluorescence was successfully recovered by the proteolytic cleavage of the quencher even after 30 days (Figure 3-16). We speculate that the stability may arise from covalent bonding between GO and QXL which prevents the peptide probes from being released from the GO surface during storage. Thus, the GO-peptide-QXL hybrid proved to be a more suitable biosensor for various biomedical applications, compared to other biosensors based on the physical adsorption of probe ligands and organic fluorescent dyes.

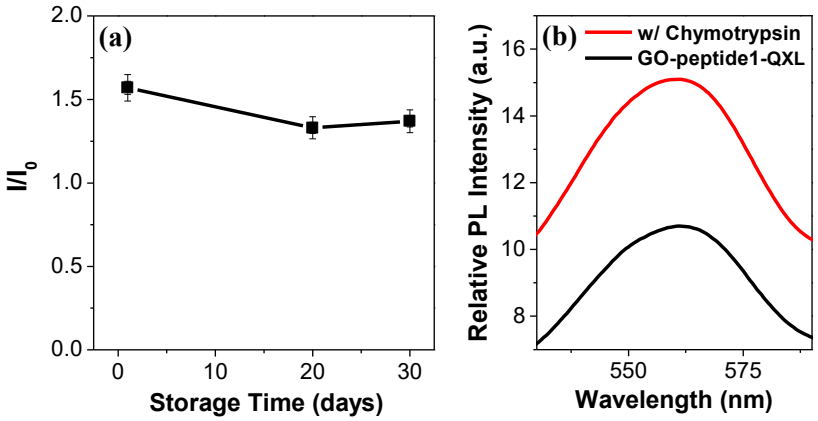

Figure 3-16. Long-term stability of GO-peptide 1-QXL sensor for detection of chymotrypsin. (a) Fluorescence recovery of GO-peptide 1-QXL after chymotrypsin treatment. I_0 and I are the fluorescence intensity before and after chymotrypsin treatment, respectively. (b) Fluorescence response of GO-peptide 1-QXL sensor to chymotrypsin after 30 days storage at 25 ºC.

1.5 Detection of MMP-2 Secreted from Living Cells

GO-peptide 3-QXL sensor was applied for the detection of MMP-2 secreted from living cells. MMP-2 detection in a biological environment is important for the diagnosis and therapy of cancers at an early stage. We could detect MMP-2 secreted from human liver hepatocellular carcinoma cells, HepG2 (Figure 3-17a), using GO-peptide 3-QXL. The recovery of fluorescence intensity was calculated by the following equation:

$$\text{Recovery of PL} = {}^{I}/_{I_0} - 1$$

where I is the fluorescence intensity after incubation of GO-peptide 3-QXL in a HepG2 cell-cultured media for 30 min, and I_0 is the fluorescence intensity after incubation of GO-peptide 3-QXL in cell-free media for 30 min. As expected, MMP-2 was secreted in the HepG2 cell-cultured media, while there was no MMP-2 secretion in the cell-free media. First, we quantified the amount of MMP-2 secreted from the cells using a standard enzyme-linked immunosorbent assay (ELISA) method. The amount of human MMP-2 secreted from HepG2 cells increased as a function of cell culture time (Figure 3-17b, green line). After incubation

for 48 h, 3.7 ng mL^{-1} of MMP-2 was secreted from the cells. At the same time intervals with an ELISA test, the fluorescence response of GO-peptide 3-QXL was measured. The quenched fluorescence of the sensors was gradually restored with increasing the incubation time (Figure 3-17b, blue line), indicating that the amount of secreted MMP-2 from the cell increased. This turn-on response of GO fluorescence was well correlated with the concentration of MMP-2 measured by ELISA, and the detection limit of the GO-peptide 3-QXL sensor was 2.0 ng mL^{-1}, which is lower than the previously reported one with MMP-2 FRET sensors.[124, 139, 140] To confirm that this turn-on response was caused by MMP-2 secreted from the cells, the cell-cultured media was pre-incubated with 50 μM of MMP-2 inhibitor, followed by addition of the GO-peptide 3-QXL sensor. As shown in Figure 3-17c (orange bar), a substantially decreased response was observed, which verifies that the turn-on response was caused by MMP-2 secreted from HepG2 cells. Finally, we conducted one more control experiment to demonstrate the specificity of the GO-peptide 3-QXL sensor for MMP-2. GO-peptide 1-QXL (0.1 mg mL^{-1}) bearing a peptide sequence which is not cleaved by MMP-2, was treated with HepG2 cell culture media under the same conditions. As shown in

Figure 3-17c, no valid fluorescence turn-on response was observed (purple bar), verifying that the GO-peptide 3-QXL specifically responded to MMP-2. These results clearly confirmed that the cell-secreted MMP-2 was successfully detected by the turn-on response of the GO-peptide-QXL system.

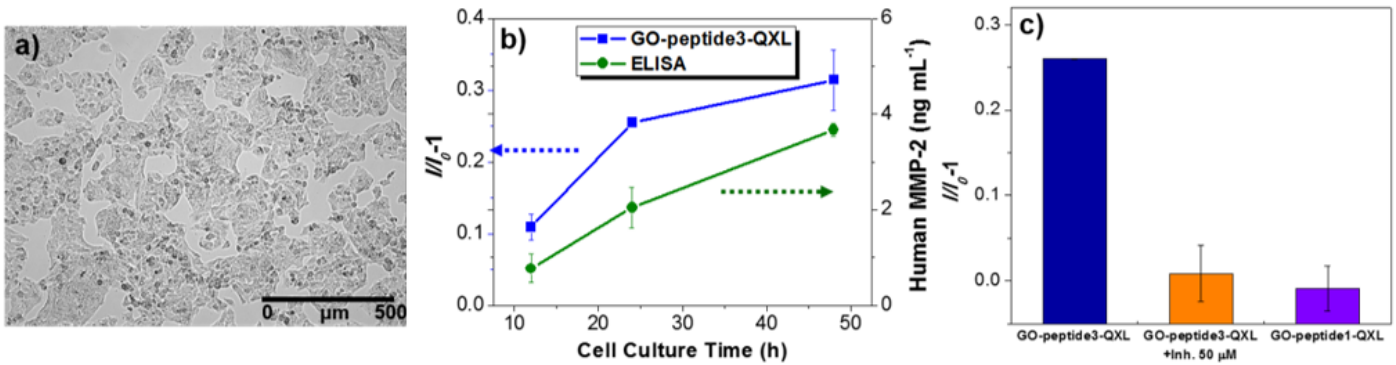

Figure 3-17. *In-vitro* detection of MMP-2 secreted from living cells with GO-peptide 3-QXL. (a) Optical image of HepG2 cells. (b) Fluorescence response (blue line) of GO-peptide 3-QXL to MMP-2 secreted from HepG2 as a function of cell culture time (12, 24, and 48 h): the concentration of MMP-2 secreted from HepG2 was measured by ELISA (green line). (c) Normalized fluorescence responses of GO-peptide-QXL hybrid: GO-peptide 3-QXL with HepG2 cell-cultured media with or without MMP-2 inhibitor (50µM) (blue and orange column, respectively); GO-peptide 1-QXL with HepG2 cell-cultured media (purple column). GO-peptide-QXL (0.1 mg mL^{-1}) were incubated with media for 30 min at 37 ºC with gentle shaking. I_0 and I present the fluorescence intensity after addition of the pristine cell media without HepG2 and after addition of HepG2 cell-cultured media, respectively.

1.6 Summary

A new type of GO-based optical biosensor consisting of luminescent GO and covalently linked peptide-quencher was constructed for the detection of protease with high sensitivity and specificity. In this FRET-based sensing system, GO was used as both an emitting fluorophore and a scaffold for attaching peptide-quencher complexes. Based on the quenching efficiency of MePPs and QXL_{570} on GO PL, GO-peptide-quencher hybrids were designed and their quenching mechanism was investigated depending on charge or energy transfer. The designed GO-peptide-QXL hybrids revealed their selectivity for the detection of chymotrypsin and MMP-2 *in vitro* assay by the "turn-on" response of inherent GO fluorescence. Eventually, the GO-peptide-QXL sensor was applied to a real biosystem as a "turn-on" sensor for the detection of MMP-2 secreted from HepG2 cells with high sensitivity. This GO-based FRET sensing platform has a great potential for the detection of various biological molecules in various fields including clinical diagnostics, pharmaceutical screening, and medical research.

2. Fabrication of Peptide-mediated GO Assemblies for Turn-on Fluorescence Sensing of MMP-2

2.1 Design of GO Assembly for MMP-2 Detection

FRET based sensors have enabled simple and efficient detection of MMP-2.[129, 141, 142] However, these sensing platforms have been suffered from poor photostability of fluorophore and lower sensitivity. Therefore, to address above-mentioned drawbacks, we have developed novel FRET platform using GO fluorescence which show exceptional stability against photobleaching.[74] Despite the successful proof of principle to detect MMP-2, preparation of the sensor was not easy task due to some limitations including complexity of synthesis and high cost caused by integration of expensive quencher molecules. To cirnumvent these restrictions, we have designed a concept of molecule-induced assembly of fluorescent nanomaterials which does not require quencher molecules. Fluorescent nanomaterials, when assembled, often show changes in their emission intensities and/or wavelengths, which can be subsequently restored to their original state by disassembly.[52-55] In particular, self-quenching driven by self-assembly of the fluorescent nanomaterials can

be utilized as an effective principle for designing fluorescence sensors to detect target molecules, because interaction with the specific target molecules triggers the restoration of self-quenched fluorescence of the nanomaterials.[54-56]

In a new sensing strategy for the selective detection of MMP-2, GO fluorophore was functionalized with a MMP-2 specific peptide substrate bearing a thiol group at the C-terminus to lead to self-assembly of GO via disulfide-bond formation, resulting in a significant amount of self-quenching of GO fluorescence. (Figure 3-18). Three different peptides were rationally designed for GO functionalization as well as for MMP-2 detection (Table 3-1). Peptide 1 contained an azide group at the *N*-terminus to allow its introduction to GO via the click chemistry, a hydrophilic and stretchable spacer (KKPPPPK), a MMP-2 substrate sequence (GPLGVRGC)[137], and a sulfhydryl group at the C-terminus for disulfide bond formation. Two additional peptides were synthesized for control experiments to demonstrate the necessity of disulfide bonding-induced assembly of GO and its specificity for MMP-2 detection. Peptide 2 had the same MMP-2 substrate sequence as that of the peptide 1, but contained no cysteine at the C-terminus. Due to the absence of cysteine,

peptide 2 was not expected to induce assembly of GO sheets via disulfide bond formation, and thus, would not induce self-quenching of GO fluorescence. Peptide 3 contained a non-specific substrate sequence for MMP-2 with cysteine at the C-terminus, and is consequently expected to induce GO assembly, but not disassembly by MMP-2. These three peptides were covalently introduced to GO by means of copper-free Click chemistry.

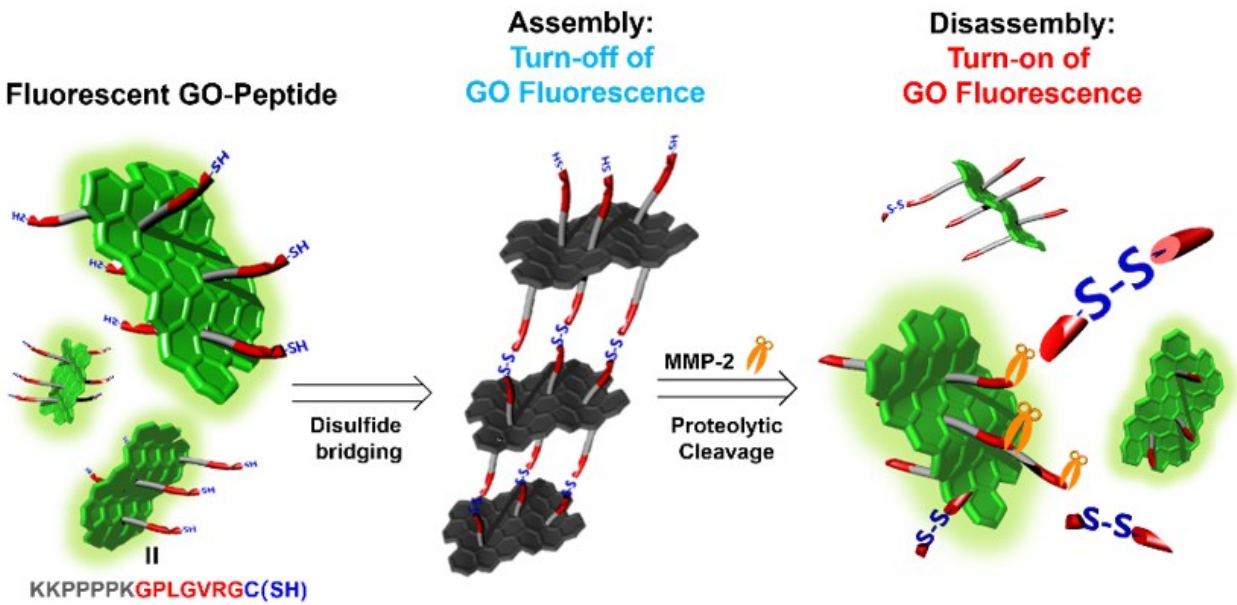

Figure 3-18. Schematic illustration of peptide-mediated GO assembly and its disassembly triggered by proteolytic cleavage for the turn-on fluorescence detection of MMP-2.

Table 3-1. Peptide Sequences Coupled onto the Surface of GO for MMP-2 Detection

Entry	Target Enzyme	Sequence
Peptide1	MMP-2	N_3-Lys-Lys-$(Pro)_4$-Lys-Gly-Pro-Leu-Gly[c]-Val-Arg-Gly-Cys[b]-$CONH_2$
Peptide2	MMP-2	N_3-Lys-Lys-$(Pro)_4$-Lys-Gly-Pro-Leu-Gly[c]-Val-Arg-Gly-Ala-$CONH_2$
Peptide3	Chymotrypsin[a]	N_3-Lys-Lys-$(Pro)_4$-Lys-Ala-Ala-Pro-Phe[d]-Cys[b]-$CONH_2$

[a]Negative control.

[b]Cystein residue responsible for disulfide bonding.

[c]MMP-2 recognition site.

[d]Chymotrypsin recognition site.

2.2 GO-Peptide Assembly for Optical Detection of MMP-2

The GO functionalized with peptide 1 (GO-P1) was characterized as below. The atomic force microscopy (AFM) images and height profiles of GO-P1 revealed that the pristine GO increased in its height from 2 nm to 7 nm after peptide conjugation, indicating the successful conjugation of the peptide 1 onto the GO surface (Figures 3-19a and c). The structure of GO-P1 was further analyzed by FT-IR spectroscopy. Vibrational peaks of an amide carbonyl group (C=O 1628 cm^{-1}) and a triazole group (C=N 1539 cm^{-1}, C−N 1278 cm^{-1}) were distinctly detected in the IR spectra of GO-P1 (Figure 3-20b) but not in that of pristine GO nor GO-OH and GO-DBCO (Figures 3-20a and 3-21a-b), indicating the successful covalent bonding of peptide 1 to GO. Additionally, the nitrogen content of GO-P1 significantly increased compared to that of pristine GO and to that of DBCO-functionalized GO (Table 3-2), indicating successful conjugation of peptide1 to GO. Functionalization of GO with the other peptides was also confirmed by the same method used for GO-P1.

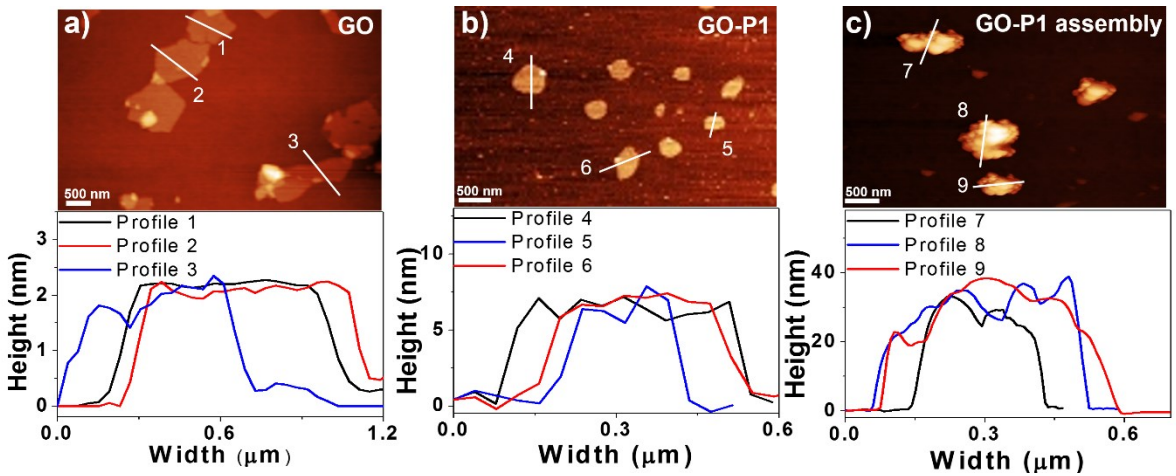

Figure 3-19. Thickness of GO, GO-P1 and its assembly. a) AFM image and height profile of GO, showing a single sheet of GO of uniform thickness (ca. 2 nm). b) AFM image and height profile of GO-P1 hybrids, showing individually dispersed GO sheets and an increase in their height to 7 nm. c) AFM image and height profile of GO-P1 assembly, showing five or six sheets of GO aggregates and an increase in its height to ca. 37 nm.

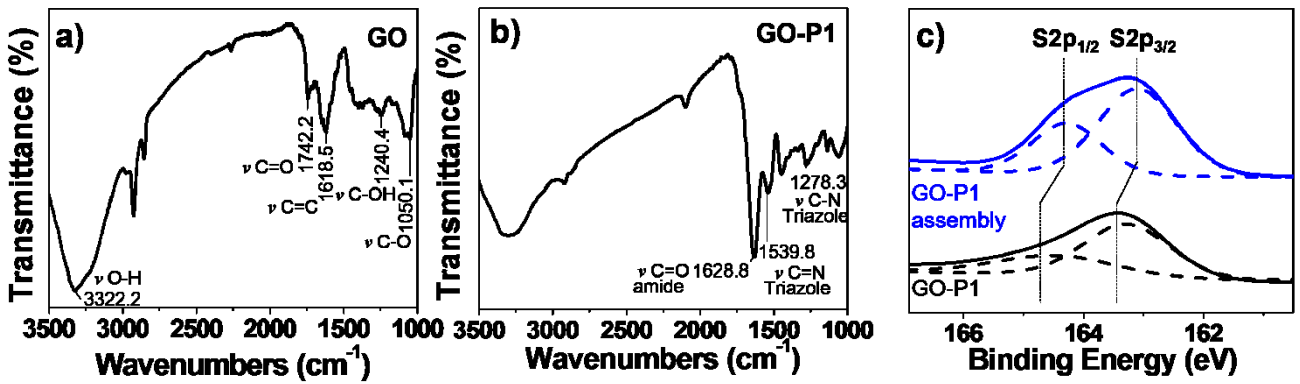

Figure 3-20. FR-IR spectra of a) GO and b) GO-P1 hybrids. c) XPS spectra of GO-P1 hybrids (black line) and GO-P1 assembly (blue line), indicating the formation of disulfide bonds.

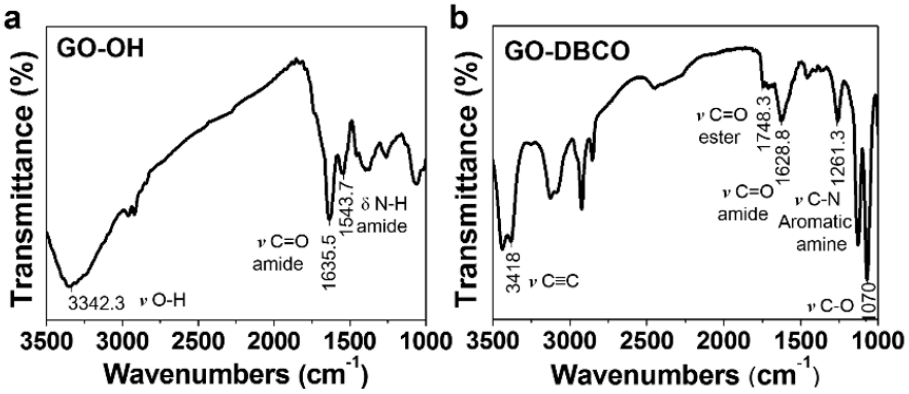

Figure 3-21. Characterization of functionalized GO. FT-IR (KBr) spectra of (a) GO-OH, and (b) GO-DBCO.

Table 3-2. Elemental Analysis of GO, GO-OH, GO-DBCO, and GO-P1

	C (wt %)	H (wt %)	N (wt %)
GO	56	2.3	0.3
GO-OH	51	2.8	3.4
GO-DBCO	50	1.1	1.8
GO-P1	45	7.9	5.5

GO-P1 sheets were assembled spontaneously when the GO-P1 dispersion was dissolved in DMSO (1 mg mL^{-1}) at RT. The resulting GO-P1 assembly was analyzed by AFM (Figure 3-19c), which clearly showed that an aggregated form of GO-P1 assembly increased its height and lateral size noticeably to c.a. 37 nm and c.a. 500 nm, respectively. This results indicate that each grain was comprised of 5 to 7 sheets of GO-P1. The GO-P1 assembly was characterized by XPS (Figure 3-20c) to investigate whether the assembly process was mediated by disulfide bonding. The S2p spectrum of GO-P1 before the assembly showed a doublet peak at 163.27 and 164.45 eV with a 2:1 peak area ratio, attributed to $S2p_{3/2}$ and $S2p_{1/2}$ peaks, respectively. The S2p peaks were shifted to a lower binding energy, 163.10 and 164.28 eV, respectively, after formation of GO-P1 assembly, which indicates that the disulfide bonds were formed in GO-P1 sheets.[143, 144] This clearly confirms that GO-P1 assembly was induced by the formation of disulfide bonds among the peptides on GO-P1.

Next, we investigated the optical properties of the GO-P1 assembly. The GO-P1 assembly was settled down to the bottom of a solution container, which led the solution optically visible (Figure 3-22a).

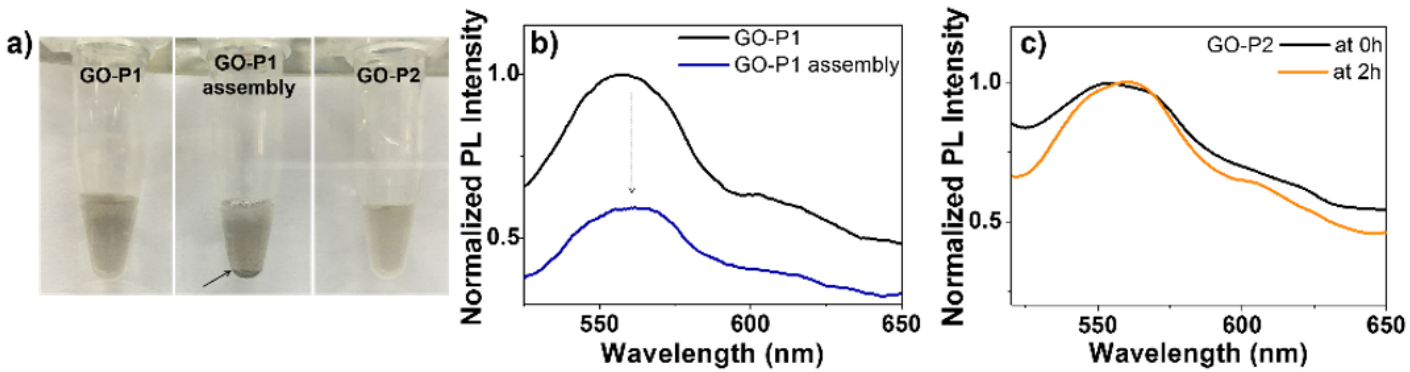

Figure 3-22. Fluorescence properties of GO-peptide and GO-peptide assemblies. (a) Optical photographs of GO-P1, GO-P1 assembly, and GO-P2 hybrid. A black arrow indicates a precipitated GO-P1 assembly. (b) Fluorescence spectra of GO-P1 (black line) and GO-P1 assembly (blue line), showing the significant fluorescence quenching after assembly. (c) Fluorescence spectra of GO-P2 hybrid at 0 h (black line) and in 2 h (orange line), showing no change in its fluorescence intensity. Fluorescence spectra were normalized by the maximum intensity (560 nm) of GO-P1; all spectra were obtained under excitation at 400 nm.

On the contraty, GO functionalized with peptide 2 (GO-P2) without cysteine did not form assembly, and showed stable dispersion in an aqueous solution. This result indicates that the sulfhydryl moeity of peptide 1 bound on GO is crucial for the formation of the GO-P1 assembly. In addition, the absorbance maximum of the GO-P1 assembly was slightly blue-shifted from 210 to 200 nm when compared to that of the unassembled GO-peptide hybrid, GO-P2, which indicated the formation of an H-aggregate (Figure 3-23).[145] When the fluorescence of the GO-P1 assembly and GO-P2 was measured, we found that the fluorescence of GO-P1 assembly was significantly quenched (Figure 3-22b), whereas that of GO-P2 dispersion showed constant fluorescence intensity for 2 h without formation of any assembly (Figure 3-22c). It is evident that assembly of GO induced by cysteine-containing peptides allows the effective modulation of the self-quenching mechanism. Meanwhile, a slight red-shift was observed in the fluorescence emission of GO-P2 after 2 h of standing in solution. We speculate that this red-shift might be caused by a change in dielectric environment surrounding GO due to the conformational variation of the peptide on the surface of GO-P2 during incubation.[146, 147]

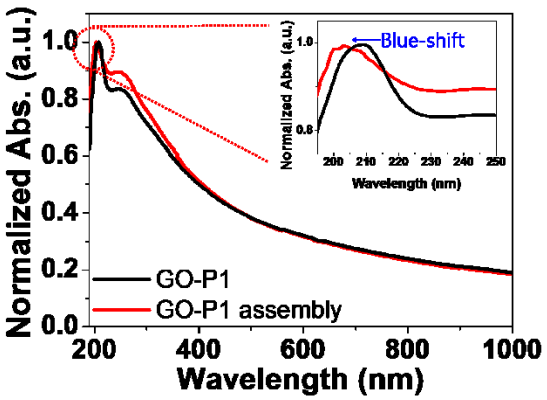

Figure 3-23. UV/Vis absorption spectra of GO-P1 (black line, 0.1 mg mL^{-1}) and GO-P1 assembly (red line, 0.1 mg mL^{-1}), showing absorption maxima at 210 and 200 nm, respectively.

We then evaluated the performance of the GO-P1 assembly in detecting MMP-2 activity. The self-quenched fluorescence of the GO-P1 assembly was gradually restored proportional to the MMP-2 concentration (Figures 3-24a and d), but not with chymotrypsin (Figure 3-25). This is a clear demonstration that the fluorescence restoration was caused specifically by MMP-2, which can be attributed to the proteolytic cleavage of the peptides in the GO-P1 assembly, resulting in its disassembly to the individually dispersed GO. On the other hand, the fluorescence of GO-P2, which is incapable of assembly owing to its absence of cysteine, did not respond noticeably to various concentrations of MMP-2 (Figures 3-24b and d). As an additional control, GO was functionalized with peptide 3 (GO-P3), which contained cysteine and had a non-specific peptide sequence for MMP-2. The GO-P3 spontaneously assembled, but its self-quenched fluorescence was not restored when MMP-2 was added to the GO-P3 assembly (Figures 3-24c and d), indicating that no enzymatic cleavage of the peptide 3 occurred by MMP-2 due to the absence of specific substrate peptide sequence. Taken together, these results show that the method based on GO assembly and disassembly is able to detect MMP-2 activity through its

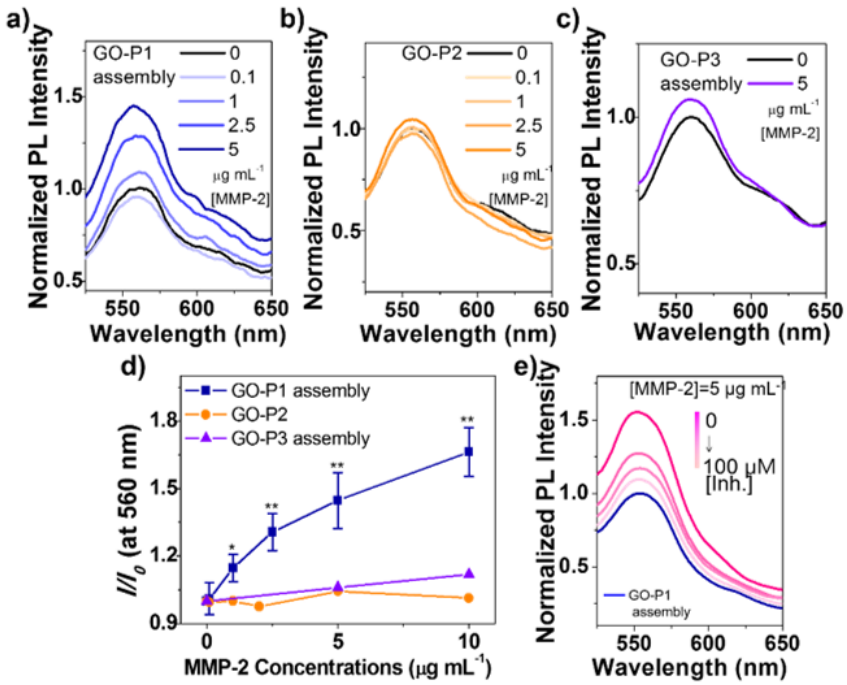

Figure 3-24. Turn-on fluorescence detection of MMP-2 with GO-peptide assemblies. Fluorescence responses of (a) GO-P1 assembly, (b) GO-P2 hybrid, and (c) GO-P3 assembly to MMP-2 at various concentrations. (d) Fluorescence recovery of GO-P1 assembly, GO-P2 hybrid, and GO-P3 assembly in response to various concentrations of MMP-2; I_0 and I are the intensities at 560 nm in the fluorescence spectra of the sensors before and after addition of MMP-2, respectively. *P<0.05; **P<0.001 (n=3) using one-way ANOVA. (e) Fluorescence response of GO-P1 assembly to MMP-2 (5 μg mL^{-1}) in the presence of various concentrations of MMP-2 inhibitor. All spectra were obtained under excitation at 400 nm.

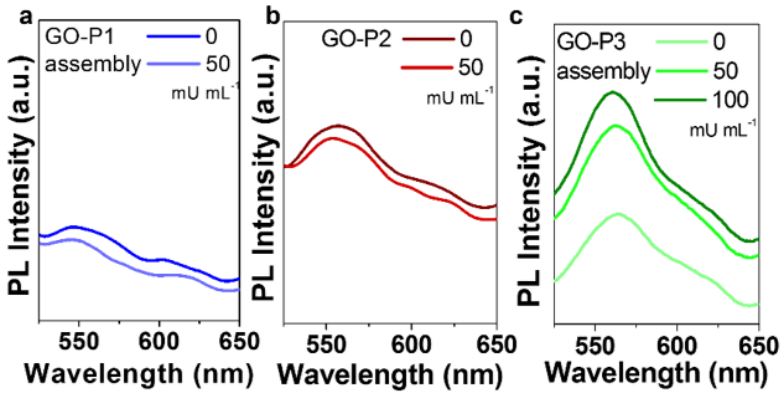

Figure 3-25. Fluorescence responses of (a) GO-P1 assembly, (b) GO-P2 hybrid, and (c) GO-P3 assembly in the presence of chymotrypsin. Fluorescence recovery was observed only for the GO-P3 assembly containing the chymotrypsin substrate peptide. All spectra were obtained under excitation at 400 nm.

turn-on fluorescence. Hence, the turn-on fluorescence mechanism of GO-P1 can be capitalized as an indicator to determine MMP-2 activity. When a MMP-2 inhibitor was added to the GO-P1 assembly, its turn-on fluorescence response gradually decreased according to the concentration of the inhibitor (Figure 3-24e). This indicates that the GO-P1 assembly platform can also be applied to the screening of protease inhibitors.

We carried out further analysis to confirm that the disassembly of the GO-P1 assembly was caused by MMP-2 specific proteolysis, which led to the restoration of its self-quenched fluorescence. A solution of the GO-P1 assembly was treated with MMP-2 and mass spectrometry (MS) analysis was performed after dithiothreitol (DTT) treatment for reducing disulfide bond to release the peptide fragments completely. A peak at m/z = 434.9 in the mass spectra (Figure 3-26a and 3-27a) is consistent with the mass of the peptide fragment (VRGC-NH_2, MW 434.5) hydrolyzed by MMP-2. The peptide fragment (VRGA-NH_2, MW 401.4) was also detected in the MS spectra of the GO-P2 treated with MMP-2 (Figure 3-27b, left panel). The MS data of GO-P1 assembly and GO-P2 treated with MMP-2 clearly indicate that the peptide substrate was cleaved by

MMP-2 regardless of the assembly. On the contrary, the MS spectra of a GO-P3 assembly treated with MMP-2 did not show any peak for the cleaved peptide fragment (Figures 3-26b and 3-27c, left panel), and no extra mass fragments were observed in the mass spectra of any samples that were not treated with MMP-2 (Figure 3-27, all right panels). These results provide strong evidence that the GO-P1 assembly was specifically disassembled by MMP-2-triggered peptide cleavage.

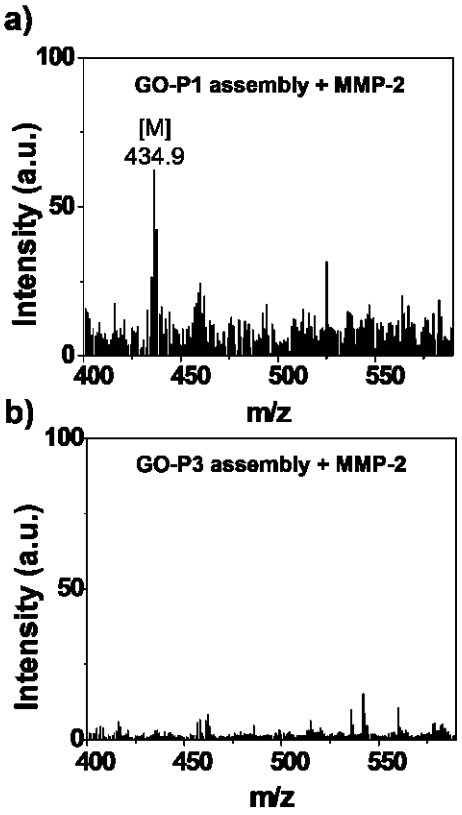

Figure 3-26. Mass spectrometry analysis of the GO-P1 assembly treated with MMP-2. (a) Mass spectra of the GO-P1 assembly solution after MMP-2 treatment, showing a peak at 434.9 m/z, attributed to the cleaved peptide fragment, VRGC; the calculated exact mass = 434.54 for $C_{16}H_{34}N_8O_4S$ [M]. (b) Mass spectra of a solution of GO-P3 assembly after MMP-2 treatment, showing no cleaved fragments.

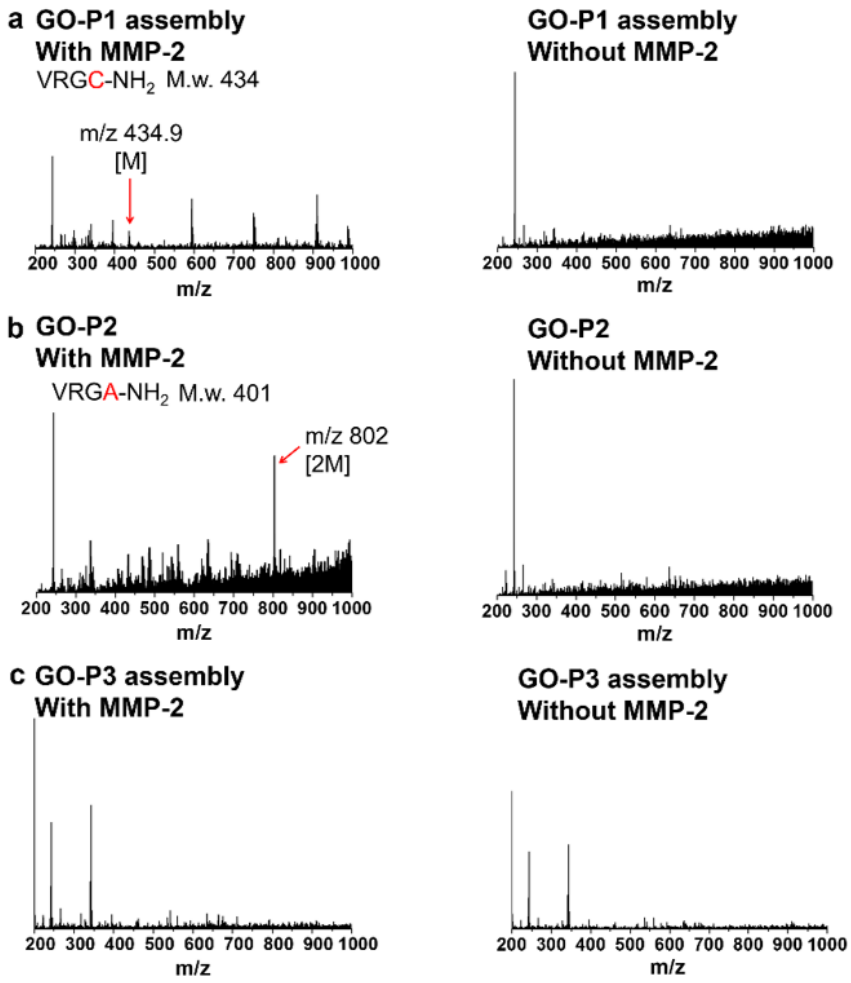

Figure 3-27. Mass spectroscopic analysis of proteolytic cleavage product of GO-peptide sensor by MMP-2. MS spectrum of (a) GO-P1 assembly, (b) GO-P2, and (c) GO-P3 assembly with (left panels) or without (right panels) MMP-2.

2.3 Kinetics of MMP-2 Detection by GO-P1 Assembly

The response kinetics of the GO-P1 assembly for MMP-2 detection was investigated. The turn-on fluorescence of the GO-P1 assembly increased in its intensity during incubation with MMP-2 and then reached 80% of its maxima within 10 min (Figure 3-28a). Based on this result, the rate of fluorescence increase was determined for different concentrations of the GO-P1 assembly, and the kinetic parameters such as Michaelis conatant (K_m) and a maximum rate (V_{max}) were calculated by Lineweaver-Burk plot (Figure 3-28b). The values of K_m and V_{max} were 0.072 μM and 0.056 min^{-1}, respectively, which were smaller than the previously reported ones.[74] The slower response kinetics of the GO-P1 assembly can be ascribed to the decreased accessibility of MMP-2 to the peptide substrate sandwiched by GO sheets causing steric hindrance. However, the response kinetics of the GO-P1 assembly is still within an acceptable range of hydrolysis rates when considering hydrolysis of various peptides by MMP-2.[1]

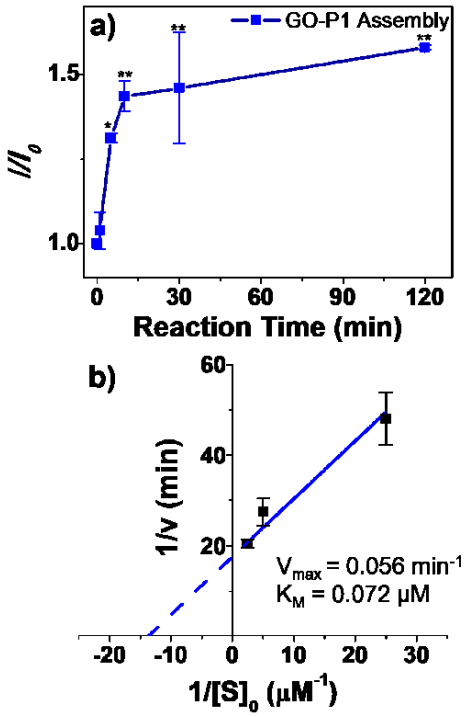

Figure 3-28. Kinetics of MMP-2 detection by GO-P1 assembly. (a) Turn-on fluorescence response of GO-P1 assembly in response to MMP-2 (5 μg mL^{-1}) versus reaction time. *P<0.05; **P<0.01 (n=3) using one-way ANOVA. (b) Lineweaver-Burk plot for the fluorescence response of the GO-P1 sensor to MMP-2 (5 μg mL^{-1}); $[S]_0$ is the concentration of GO-P1 assembly, and I_0 and I are the intensities of the fluorescence spectra of GO-P1 assembly at 560 nm before and after addition of MMP-2, respectively. All spectra were obtained under excitation at 400 nm; error bars represent standard deviation from the mean values (n = 3).

2.4 Detection of MMP-2 Secreted from Living Cells

The GO-P1 assembly was applied to the detection of MMP-2 secreted by HepG2, human liver hepatocellular carcinoma cells (Figure 3-29). It was reported that MMP-2 is predominantly expressed in HepG2 cells, and other MMPs such as MMP-1, 7, 9, and 10 are rarely produced.[148, 149] ELISA was used to quantify the amount of MMP-2 secreted by the cells as the incubation time was increased. The amount of human MMP-2 secreted from HepG2 cells increased from 2.2 ng mL^{-1} at 12 h of incubation time to 6.3 ng mL^{-1} at 36 h (Figure 3-30a). The fluorescence responses of the GO-P1 assembly were also measured at the same time intervals as the ELISA. The self-quenched fluorescence of the GO-P1 assembly was gradually restored when the MMP-2 concentration increased during the cell culture, indicating that this GO-P1-assembly sensor was able to detect MMP-2 secreted by the living cells (Figure 3-30, blue line and blue bar). The turn-on fluorescence response was well correlated with the MMP-2 concentration measured by ELISA. The limit of detection (LOD) of the GO-P1 assembly sensor for MMP-2 was 2.0 ng mL^{-1}. The sensitivity of GO-P1 assembly for MMP-2 detection is comparable with those of other

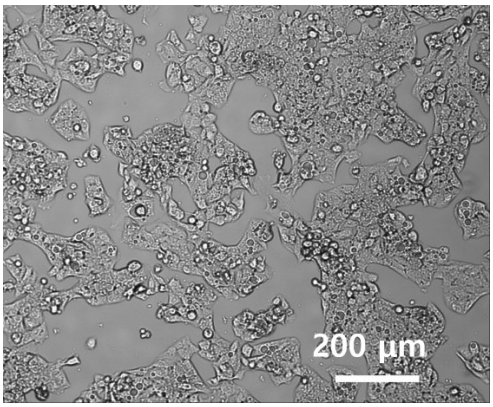

Figure 3-29. Optical image of HepG2 cells.

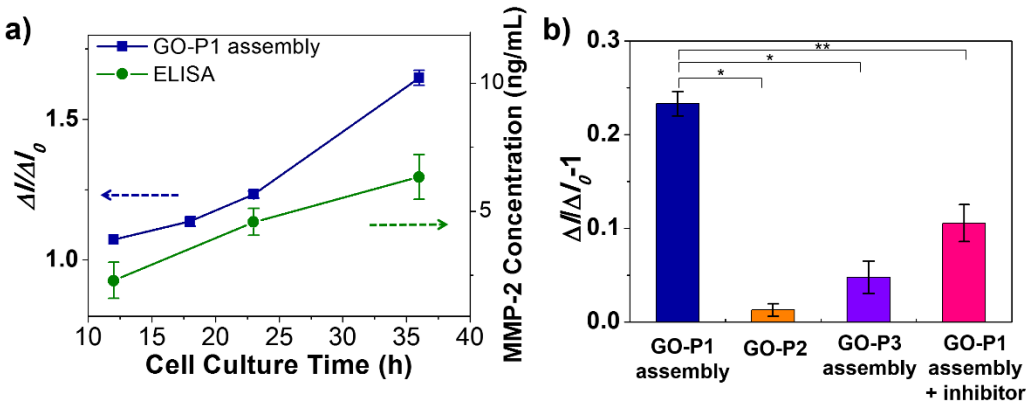

Figure 3-30. Detection of MMP-2 secreted by living cells with GO-P1 assembly. (a) Fluorescence response of GO-P1 assembly to cell-secreted MMP-2 (blue line) and ELISA-based quantification of the secreted MMP-2 versus cell culture time. (b) Fluorescence recovery of GO-P1 assembly (blue bar), GO-P2 (orange bar), GO-P3 assembly (purple bar), and GO-P1 assembly treated with 50 μM of MMP-2 inhibitor (pink bar) in 24 h cell-cultured media. ΔI_0 and ΔI indicate cell media background subtracted PL intensity after incubation of cell-free media and HepG2 cell-cultured media, respectively. *P<0.001; **P<0.01 (n=3) using one-way ANOVA. All error bars represent standard deviation from the mean.

FRET sensors.[74, 124, 129, 140] Moreover, GO-P1 assembly is much easier to be prepared since it does not require any quencher molecules that are essential in the FRET systems. In addition, the GO-P1 assembly sensor allows rapid and simple detection of MMP-2, requiring one step in much shorter time, when compared to ELISA, which takes 5 h with multiple steps. In particular, GO-P1 assembly is able to provide kinetic parameters for MMP-2 activity. Evidently from these results, GO-P1 assembly sensor is promising in rapid and simple monitoring of MMP-2 activity.

We performed additional control experiments to demonstrate the specificity of the GO-P1 assembly for MMP-2. No valid turn-on fluorescence response was observed when the GO-P2, which contained MMP-2 specific substrate peptide but did not assemble, was treated with the HepG2 cultured media containing MMP-2 (Figure 2-30b, orange bar). In addition, there was no significant recovery of the self-quenched fluorescence of the GO-P3 assembly, which did not bear the MMP-2 substrate sequence (Figure 3-30b, purple bar). Finally, HepG2 cultured media containing MMP-2 was preincubated with 50 μM of prinomastat hydrochloride, a MMP-2 inhibitor, and then added to the GO-P1 assembly. This gave a substantially decreased response relative to that of

GO-P1 without the inhibitor (Figure 3-30b, pink bar). These cellular experimental results demonstrate that the assembly-disassembly strategy using the peptide-functionalized GO is an effective way in designing biosensors for the selective detection of cell-secreted enzymes such as MMP-2. The application of GO assembly system could be expanded further for detecting biomolecules as well as high-throughput screening of protease inhibitors.

2.5 Summary

A spontaneous self-assembly and self-quenching based GO-peptide sensor have been developed without using additional quencher molecules for MMP-2 detection. The GO assembly and quenching strategy enabled to generate the fluorescence turn-on sensing platform which is highly selective and sensitive to MMP-2. This GO-peptide assembly sensor was able to report the kinetic parameters for MMP-2 activity as well. Finally, the GO-peptide assembly sensor was able to detect MMP-2 secreted by living cells faster and more effectively than the conventional assay method. The sensing principle can be expanded to detect and monitor other cell-secreted proteases, and to develop their inhibitors.

3. Fabrication of Cys-modified GO with Enhanced Fluorescence for Turn-on Fluorescence Detection of MMP-2

3.1 Preparation of Cys-GO

Despite of many advantages of GO as a fluorescent probe, PL properties of GO have rarely been utilized in biological labeling and sensing due to its low emission efficiency. Intensive efforts have been made in the exploration of new type of efficient carbon-based emitters such as carbon dots (CDs) and graphene quantum dots (GQDs). Especially, heteroatom doped CDs and GQDs significantly enhanced the quantum efficiency. Impressive progresses have been made on the bottom-up synthesis of CD derivatives. However, most of these synthetic methods suffer from shortcomings including expensive equipment, time-consuming procedures, slow, high cost, and harsh reaction conditions. More importantly, PL enhancement of GO itself via heteroatom doping have been rarely explored. Therefore, there is a still urgent need to develop a facile and efficient synthetic approach for the fabrication of heteroatom-doped GO with improved fluorescence signal.

Considering the above mentioned accounts, a facile and simple pathway to obtain N, S co-doped GO with highly enhanced PL is designed. Thus, Cys, broadly used heteroatom source in the CDs synthesis, was used to intoduce nitrogen and sulfur atoms to GO. Figure 3-31 shows the brief schematic illustration. Cys dissolved in acidic aqueous solution (1 mL, 1% HCl/DW) was added to 1 mL of GO/DMF solution (1 mg mL^{-1}). The mixture was sonicated by probe sonicator. During the reaction, the concentrations of Cys, sonication power, and reaction time were varied to figure out the optimal conditions for the effective doping of N and S into GO. Sonication power was adjusted to 10.5 W which is low enough to avoid the formation of another carbonaceous matters. As the reaction time increased from 1 to 12 h, fluorescence intensity of Cys-modified GO derivatives also increased (Figure 3-32a). However, at a much longer reaction time, the surface of GO was covered with unwanted carbonaceous substances, as shown in Figure 3-32a inset. Therefore, the reaction time was adjusted to 1 h. Next, the effect of Cys concentrations was explored. As the concentration of Cys increased from 40 to 120 mM, the fluorescence intensity was increased. At higher concentration than 120 mM, the fluoescence

emission was rather decreased (Figure 3-32b). With these results, the optimal reaction conditions were identified: 10.5 W sonication power, 1 h sonication time, and 120 mM of Cys.

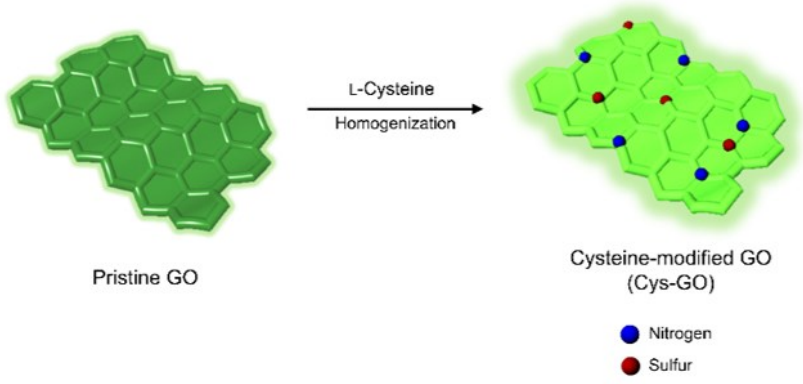

Figure 3-31. Schematic illustration of Cys-GO preparation.

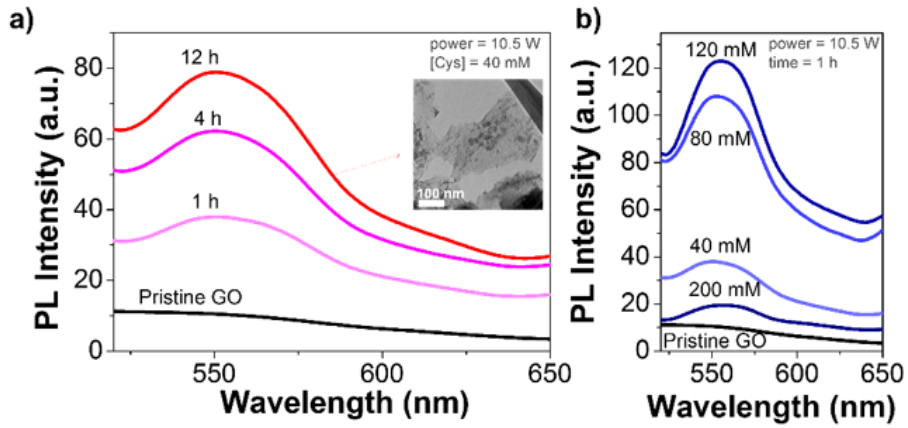

Figure 3-32. Optimization of reaction conditions. a) Fluorescence spectra of Cys-modified GO derivatives depending on the sonication times. Cys concentration was fixed as 40 mM. Inset: TEM image of Cys-GO (12 h reaction). b) Fluorescene spectra of Cys modified GO derivatives depending on the Cys concentrations. Reaction time was fixed as 1 h. All spectra were obtained under excitation at 400 nm.

3.2 Characterization of Cys-GO

TEM images of the obtained Cys-GO revealed that the morphology of Cys-GO did not significantly differ from that of pristine GO (Figure 3-33a, e), indicating that other carbonaceous substrance such as CDs were not generated. For better understanding of the elemental composition of Cys-GO, elemental mapping of Cys-GO and pristine GO sheets was conducted via electron energy loss spectroscopy (EELS). Carbon was detected in both sample areas of the TEM images (Figure 3-33b, f). In Cys-GO, nitrogen and sulfur were homogeneously distributed across the sheet (Figure 3-33g, h). On the contrary, nitrogen and sulfur was not detected in pristine GO (Figure 3-33c, d). In addition, the elemental analysis of Cys-GO showed an increase in nitrogen (10.4 wt%) and sulfur (23.3 wt%) contents compared to pristine GO (Table 3-3). The AFM images showed that the height of Cys-GO was between 3.3 and 3.5 nm, whereas pristine GO had a height of ~1.5 nm (Figure 3-33i, j). These height increase could be resulted from both the structural distortion due to the doping of heteroatom and conjugation of Cys to epoxy group of GO. These analytical results clearly demonstrate the successful introduction of nitrogen and sulfur atoms to GO.

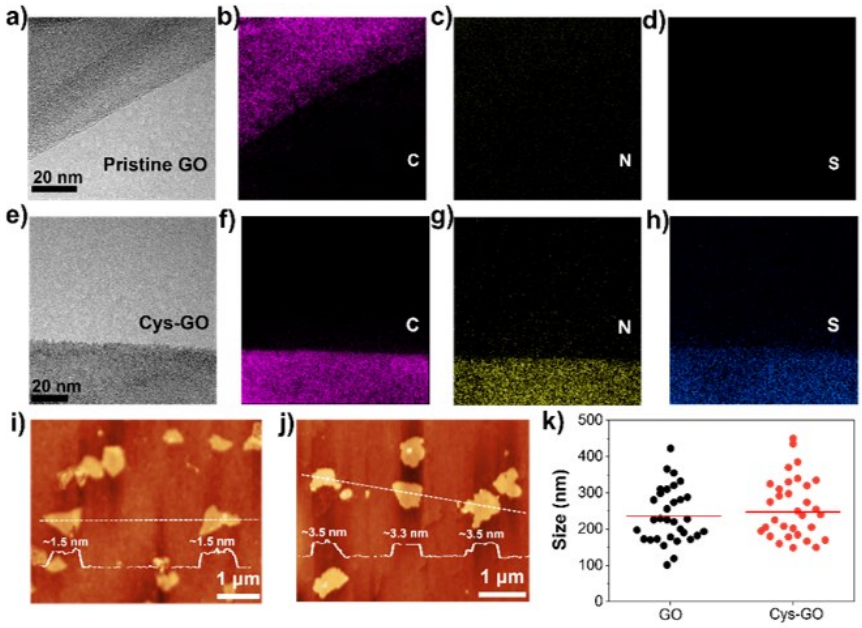

Figure 3-33. Characterization of Cys-GO. a) HR-TEM image of pristine GO and e) Cys-GO, and corresponding STEM-EDS elemental mapping of pristine (b-d) GO and (f-h) Cys-GO (b, f: carbon, c, g: nitrogen, d, h: sulfur). i) AFM images of pristine GO and j) Cys-GO, showing a height increase from 1.5 nm to ~3.5 nm as compared to pristine GO. k) Size distribution of pristine GO (black dot) and Cys-GO (red dot).

Table 3-3. Elemental Analysis of Cys-GO and Pristine GO

	C %	H %	N %	S %
Pristine GO	50.1	2.7	0.2	1.3
Cys-GO	30.6	4.8	10.4	23.3

To find out whether sonication process induced either size reduction or the formation of CDs, size distribution of single sheet of Cys-GO was compared with that of pristine GO. The size of GO sheets was defined as the average value of its largest and smallest transverse width. As shown in Figure 3-33k, there was no significant difference in sheet size between Cys-GO and pristine GO. These results support that the formation of CDs or chopping of pristine GO was not occurred under the reaction condition, which means that fluorescence enhancement of Cys-GO was originated from heteroatom introduction rather than size reduction.

3.3 Optical Properties of Cys-GO

The optical properties of Cys-GO were investigated. Figure 3-34a shows the UV/Vis absorption spectra of pristine GO and Cys-GO aqueous solution. Pristine GO showed absorption peaks at 230 and 303 nm due to π-π* and n-π* transitions, while these two peaks of Cys-GO were blue-shifted to 195 and 245 nm, respectively. The blue-shift may be attributed to the strong electronic affinity of N dopants[150, 151] or the decrease of planarity of GO due to heteroatom introduction to GO resulting in lesser conjugated system, which is in good agreement with the AFM results. When the fluorescence of Cys-GO and other amino acid treated GO was measured under 400 nm the excitation, we found that only the fluorescence of Cys-GO was significantly enhanced (Figure 3-34b, c). Except Cys-GO, fluorescence of other amino acid-modified GO showed marginal increase in the 0.5% HCl/DW-DMF solvent system. These results will be discussed in section 3.4 together with the structural analysis of Cys-GO. When Cys was covalently coupled to GO via amide bonding (Cys coupled GO), fluorescence intensity was not increased (Figure 3-34b, green line). In addition, Cys-GO showed lower zeta potential value than that of GO and Cys coupled GO (Table 3-4).

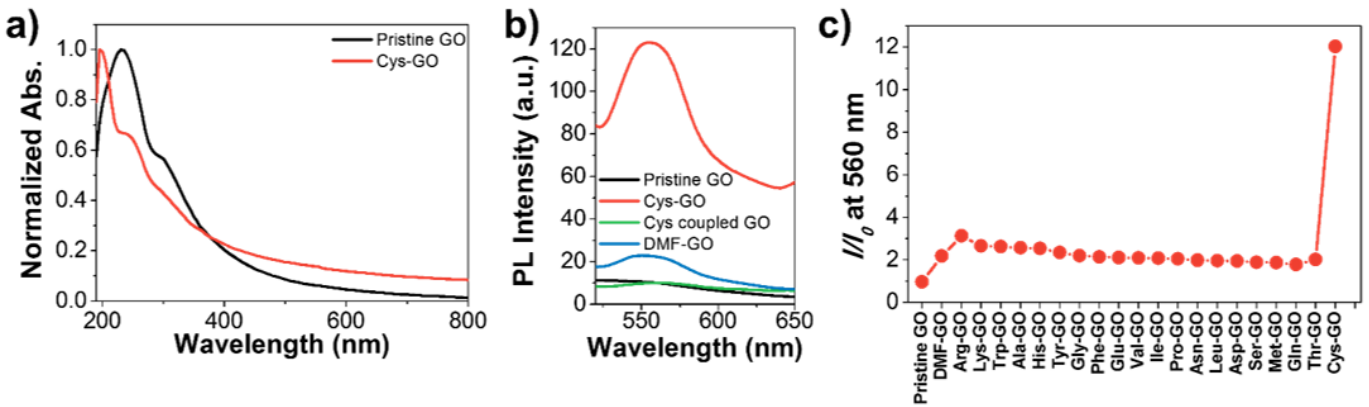

Figure 3-34. Optical properties of Cys-GO. a) UV/Vis absorption spectra of pristine GO (black line) and Cys-GO (red line). b) Fluorescence spectra of pristine GO (black line), Cys-GO (red line), Cys coupled GO (green line), and GO sonicated in 1% HCl/DW:DMF (1:1) (DMF-GO, blue line) at the same concentration (0.1 mg mL^{-1}). c) Effect of amino acid additives on fluorescence intensity.

Table 3-4. Zeta Potential of GO, Cys-GO, and Cys coupled GO

	Zeta potential (mV)
GO	-25.1 ± 1.1
Cys-GO	-35.4 ± 0.1
Cys coupled GO	-22.3 ± 1.1

These results indicate that Cys was introduced to GO as an electron-rich molecule rather than simple amino acid, and this distinctive infusion contributed to the fluorescence emission increase of Cys-GO.

Meanwhile, it is known that the excited state of GO undergoes relaxation process by interaction with solvent dipole during fluorescence emission.[152] If the solvation is weak due to strong interlayer interactions of GO in a solvent, the wavelength of emission peak is red-shifted. As shown in Figure 3-35a, the emission peak of GO was red-shifted depeding on the solvent polarity (red line, empty square). In addition, PL emission intensity was also influenced by the solvent polarity in the same manner as the emission peak shift (Figure 3-35a, black line, filled sqaure). The solvent polarity depending on the PL intensity may be due to the enhanced electron transfer between carbonyl group and sp^2 carbon by achieving a planar configuration from intra- or inter- hydrogen bonding of carboxyl group at the excited states.[153] DMF-GO also showed solvent-dependent PL emission profile. On the other hand, fluorescence emission of Cys-GO was not drastically influenced by the solvent polarity (Figure 3-35a, black line with filled circle and red line with empty circle). Furthermore, fluorescence from GO and DMF-GO is

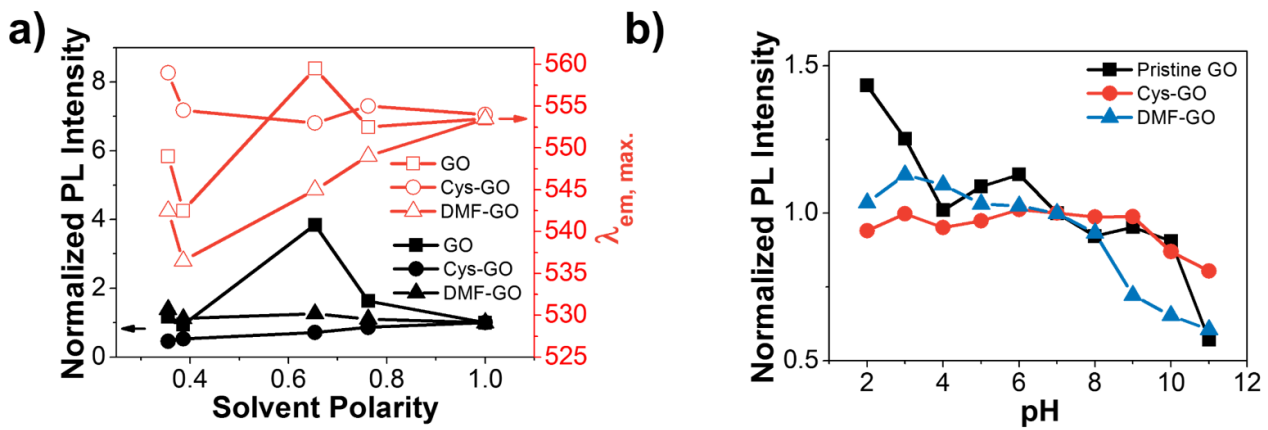

Figure 3-35. Fluorescence properties of Cys-GO. a) Normalized PL intensity of GO (black filled squares), DMF-GO (black filled triangle), and Cys-GO (black filled circle), and emission maximum of GO (red empty squares), DMF-GO (red empty triangle), and Cys-GO (red empty circle). b) Normalized PL intensity at 560 nm of pristine GO (black filled square) DMF-GO (blue filled triangle), and Cys-GO (red filled circle) as a function of pH.

strongly pH-dependent due to the protonation of carboxyl group at the excited state,[71, 154] whereas Cys-GO showed nearly constant emission throughout the pH range of 2 - 11 (Figure 3-35b). Taken together, these results suggest that fluorescence of GO and DMF-GO is evidently related to the behavior of an excited-state carbonyl groups, while increased fluorescence emission of Cys-GO is caused by the introduction of electron-rich heteroatom doping.

3.4 Structure of Cys-GO

The chemical composition of Cys-GO was characterized by XPS and FT-IR. Figure 3-36 displays the XPS profile of pristine GO, DMF-GO, and Cys-GO. The high resolution scan of C1s region of pristine GO showed that C components consist of C=C at 284.5 eV, C-O at 286.6 eV, and C=O at 288.8 eV (Figure 3-36 and 3-39).[155] There was no signal in the region of N1s and S2p. FT-IR spectrum of pristine GO also indicats the presence of C=O (1723.2 cm^{-1}), C=C (1627.6 cm^{-1}), C-OH (1231.5 cm^{-1}), and C-O (1070.5 cm^{-1}) (Figure 3-40a). Pristine GO is comprised of dominant sp^2 carbons and oxygen containing functional groups (Figure 3-41a). GO PL is known to occur by the electron transition between sp^2 carbon and oxygen containing functional groups. After sonication of GO without amino acid in 1% HCl/DW/DMF (DMF-GO), pyridinic N (398.3 eV) and pyrrolic N (400.5 eV) were introduced to GO affording DMF-GO (Figure 3-37b and 3-39). C1s spectra of DMF-GO was divided into four peaks at 284.5, 285.9, 286.8, 288.1 eV,[79, 155] which were attributed to C=C, C-N, C=N, and C=O groups, respectively (Figure 3-37a and 3-39). As shown in Figure 3-40b, FT-IR spectrum of DMF-GO also supported the evolution of nitrogen containing functional

groups, such as N-H (3430.1 cm^{-1}) and C-N (1394.6 cm^{-1}). Interestingly, C=C content was drastically increased in DMF-GO, which suggested that reactions between GO and DMF occurred during the sonication, followed by the formation of new sp^2 carbon with N doping (Figure 3-41b). Actually, DMF can be hydrolized into dimethylamine and formic acid under the acidic condition, and the hydrolized product, especially dimethylamine, can react with various functional groups in GO.[156] When dimethylamine instead of DMF was reacted with GO and Cys, the resulting product showed identical increase in PL as Cys-GO (Figure 3-42). These results suggest that DMF contributed to the N atom doping through the reaction between GO and dimethylamine hydrolized from DMF in acidic condition. These newly introduced conjugated C and N doping could contribute to the formation of new kind of surface state, by which excitated electrons are able to facilitate a high yield of radiative recombination.[79] Therefore, fluorescence emission of DMF-GO was slightly enhanced compared to GO (Figure 3-34b, blue line). On the other hand, the deconvoluted C1s spectrum of Cys-GO showed four peaks at 284.5, 286.1, 287.4, and 289.2 eV, corresponding to C=C, C-S, C-N, C=O, respectively, which indicates that the oxygen containing

functionalities are decreased with N and S doping onto GO (Figure 3-38 and 3-39).[155, 157] It should be noted that C=O contents were substantially decreased in Cys-GO. Carboxylic groups usually induce non-radiative recombination of localized electron-hole pairs, which leads to the non-emissive property of GO.[62, 63] Thererfore, the fluorescence signal of Cys-GO might be resulted from the decrease of non-emissive carboxylic acid groups. The N1s spectrum of Cys-GO showed the presence of two types of N atoms, pyridinic N (398.8 eV) and pyrrolic N (400.5 eV). In the deconvoluted S2p spectrum of Cys-GO, two types of S were observed at $S2p_{3/2}$ 162.9 eV and $S2p_{1/2}$ 164.0 eV for –SH, and $S2p_{3/2}$ 164.1 eV and $S2p_{1/2}$ 165.2 eV for -C-S-C-[158]. Furthermore, FT-IR spectrum of Cys-GO showed ovious changes in functionalities. Vibrational peaks of an pyridinic C=N (1619.8 cm^{-1}) and C=C (1587.3 cm^{-1}), aromatic C-N (1194.6 cm^{-1}), amide C-N (1405.9 cm^{-1}), and thiol (2588.1 cm^{-1}) were distinctly detected in IR spectrum (Figure 3-40c). On the basis of the XPS and IR results, we can conclude that the synthesized Cys-GO contained N and S elecments, and multiple functional groups (Figure 3-41c). Cys might participate in the reaction between GO and DMF via thiol functional groups which are able to react with epoxy or carboxyl

groups. The incorporated S atoms seem to be able to enhance the effect of N atoms on the properties of doped carbon materials through cooperative effects. In addition, passivation of edge carboxyl groups can also lead to the fluorescence enhancement. Therefore, Cys-GO showed a high enhancement of fluorescence.

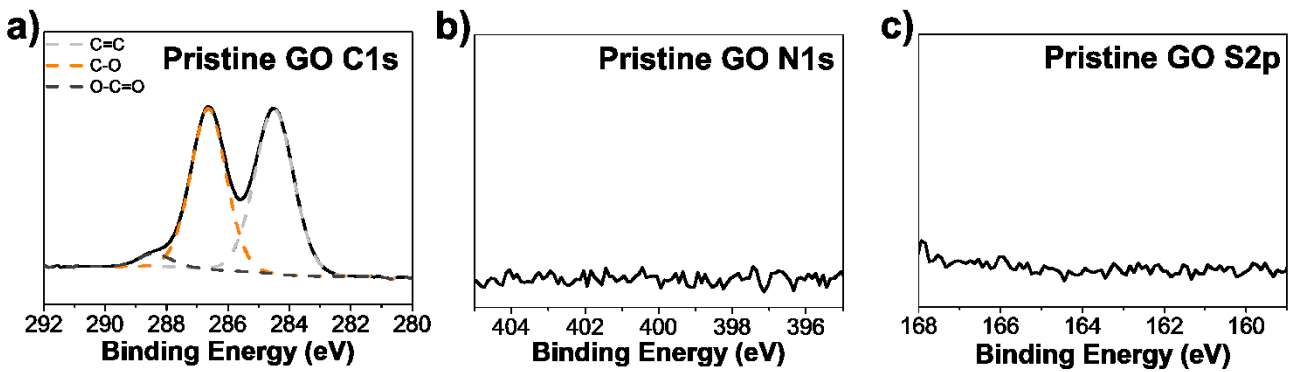

Figure 3-36. XPS spectra of pristine GO. a) C1s, b) N1s, and c) S2p XPS spectrum.

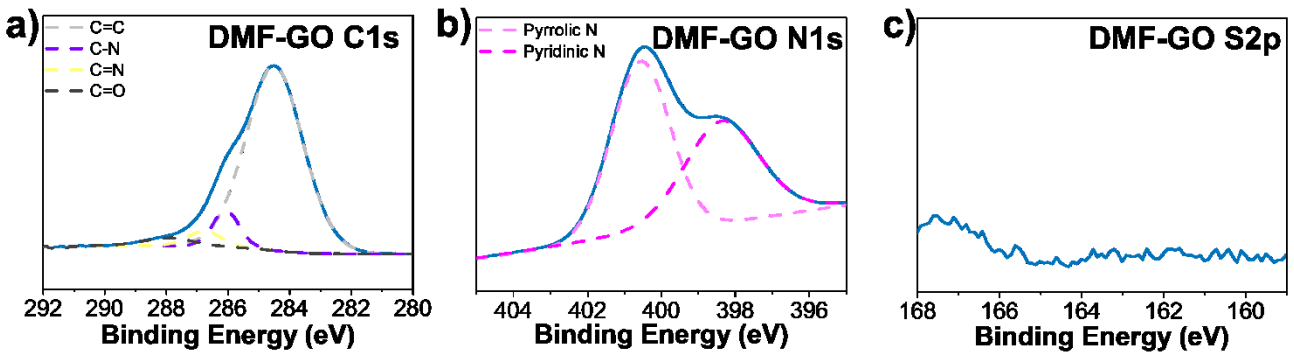

Figure 3-37. XPS spectra of DMF-GO. a) C1s, b) N1s, and c) S2p XPS spectrum.

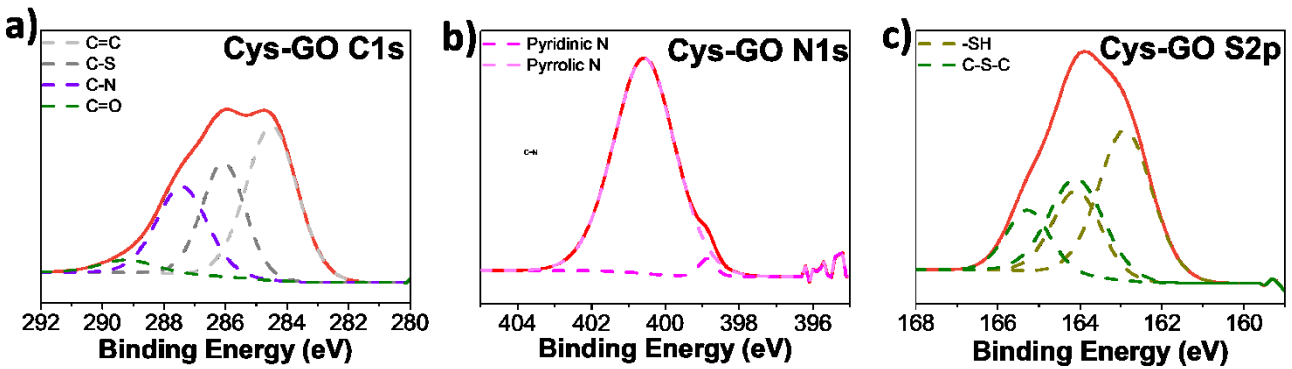

Figure 3-38. XPS spectra of Cys-GO. a) C1s, b) N1s, and c) S2p XPS spectrum.

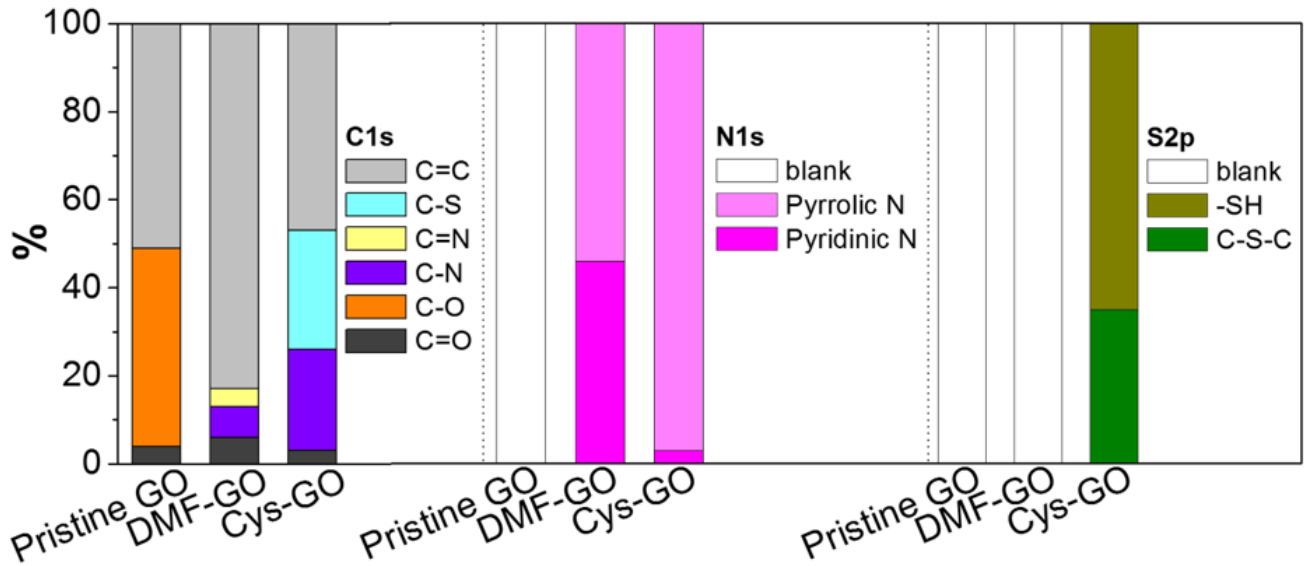

Figure 3-39. XPS envelope ratios of pristine GO, DMF-GO, and Cys-GO.

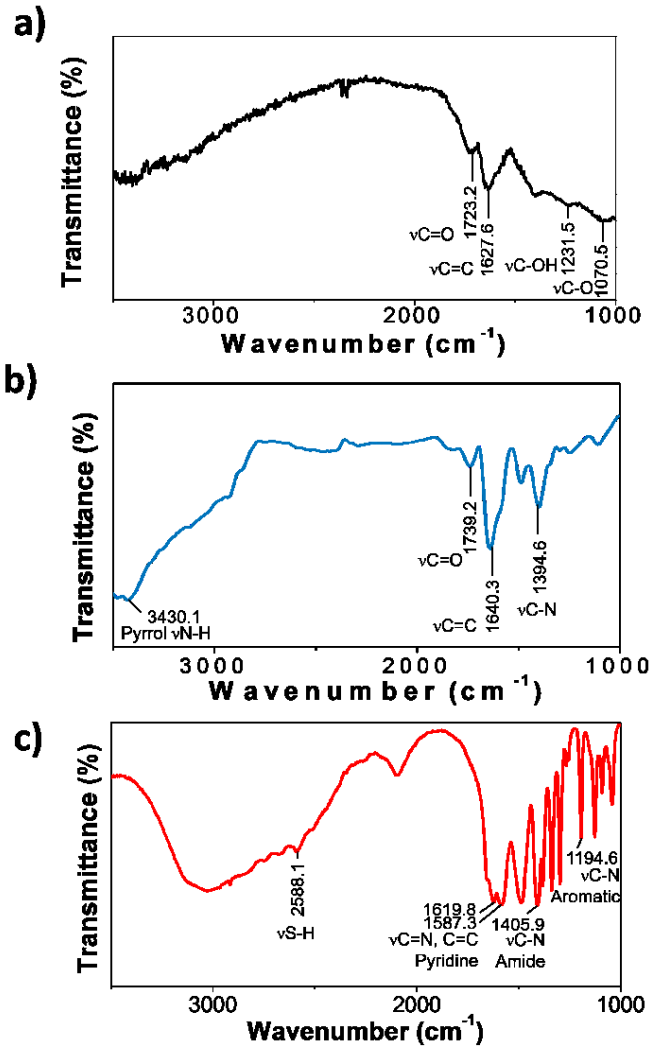

Figure 3-40. FT-IR spectra of pristine GO (a), DMF-GO (b), and Cys-GO (c).

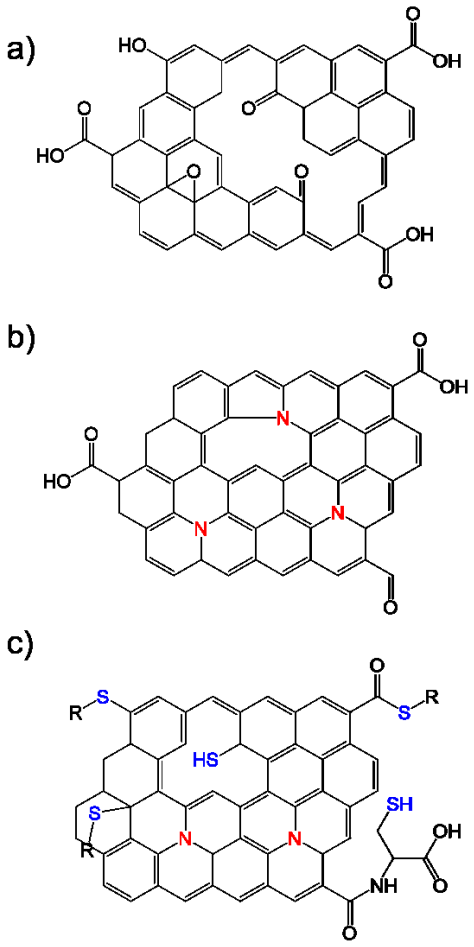

Figure 3-41. Proposed structure of pristine GO (a), DMF-GO (b), and Cys-GO (c).

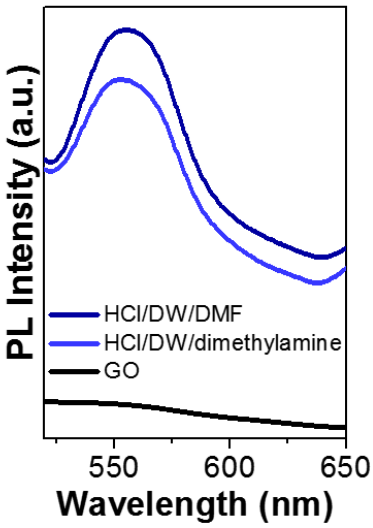

Figure 3-42. Fluorescence spectra of Cys-GO synthesized with dimethylamine instead of DMF.

3.5 Detection of MMP-2

We also applied Cys-GO for the detection of MMP-2. MMP-2 were detected by using the same method as before described in Chapter II; peptide-induced assembly and self quenching strategy. The Cys-GO assembly was triggered by the formation of disulfide bond between the peptides anchored on Cys-GO, and its disassembly induced the recovery of self-quenched PL of Cys-GO. Fluorescent Cys-GO was covalently linked with three kinds of peptides as depected in Table 3-5. Peptide 1 contained an maleimide troup at the N-terminus to allow its introduction to Cys-GO, a hydrophilic and stretchable spacer (KKPPPPK), a MMP-2 substrate peptide (GPLGVRG), and a sulfhydryl troup at the C-terminus for disulfide bond formation. Two additional peptides were synthesized for control experiments. Peptide 2 had the same MMP-2 substrate sequence as that of Peptide 1, but contained no Cys at the C-terminus. Due to the absence of Cys, peptide 2 was not expected to induce assembly of Cys-GO sheets via disulfide bond formation, and subsequent self-quenching of PL. Peptide 3 composed of a non-specific substrate peptide for MMP-2 (GGGG) with Cys at the C-terminus, and was consequently anticipated to induce Cys-GO assembly, but not its

Table 3-5. Peptide Sequences Coupled onto the Surface of Cys-GO for the Selective Detection of MMP-2

Entry	Target Enzyme	Sequence
Peptide 1	MMP-2	Maleimide-Lys-Lys-$(Pro)_4$-Lys-Gly-Pro-Leu-Gly[a]-Val-Arg-Gly-Cys[b]-$CONH_2$
Peptide 2	MMP-2	Maleimide-Lys-Lys-$(Pro)_4$-Lys-Gly-Pro-Leu-Gly[a]-Val-Arg-Gly-Ala-$CONH_2$
Peptide 3	-	Maleimide-Lys-Lys-$(Pro)_4$-Lys-Gly-Gly-Gly-Gly-Cys[b]-$CONH_2$

[a]MMP-2 recognition site.

[b]Cystein residue responsible for disulfide bonding.

disassembly by MMP-2. The only difference from the previous works was that conjugation between Cys-GO and the peptides was simply conducted via selective reaction between the inherently existed thiol groups in Cys-GO and maleimide moiety in the peptides. This means that conjugation was actually one step, whereas several GO modification steps were necessary to conjugate peptides in previous cases.

Cys-GO conjugated with Peptide 1 (Cys-GO-P1) were aseembled spontaneously when Cys-GO-P1 dispersion was dispersed in DMSO at RT. After disulfide bond formation in DMSO, Cys-GO-P1 and Cys-GO-P3 assembly showed significantly quenched fluorescence, whereas fluorescence of Cys-GO conjugated with Peptide 2 (Cys-GO-P2) remained almost the same (Figure 3-43). It is evident that the assembly of Cys-GO induced by Cys-containing peptides allowed the effective self-quenching. Then, MMP-2 detection capability of Cys-GO-P1 assembly was evaluated. As expected, the self-quenched fluorescence of Cys-GO-P1 assembly was gradually restored when MMP-2 was added in concentration dependent manner (Figure 3-44a). On the other hand, the fluorescence of Cys-GO-P2 neither quenched nor responded by the addition of MMP-2.

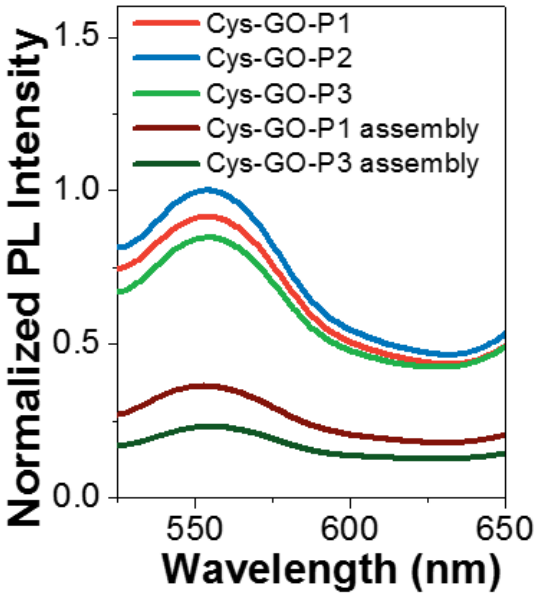

Figure 3-43. Fluorescence properties of Cys-GO-P1 assembly.

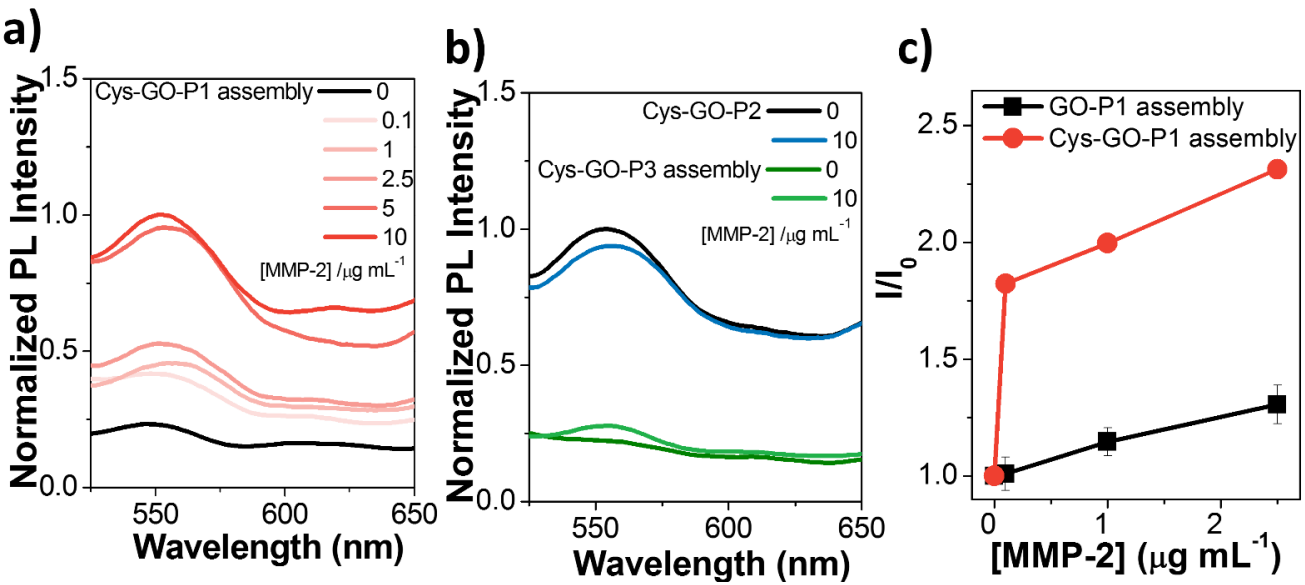

Figure 3-44. Detection of MMP-2 with Cys-GO-peptide assemblies by turn-on fluorescence. Fluorescence responses of (a) Cys-GO-P1 assembly, (b) Cys-GO-P2, and (c) Cys-GO-P3 assembly in the presence of MMP-2 at various concentrations. All spectra were obtained under excitation at 400 nm.

Furthermore, Peptide 3 conjugated Cys-GO (Cys-GO-P3), which can be assembled through disulfide bond but not cleavable by MMP-2, maintained quenched fluorescence upon the addition of MMP-2 (Figure 3-44b). It is clear that the fluorescence restoration was caused by MMP-2, resulting in disassembly of Cys-GO sheets to individually dispersed Cys-GO. It should be noted that Cys-GO-P1 assembly was able to detect MMP-2 more sensitively compared to GO-P1 assembly sensor (Figure 3-44c). This enhanced detection sensitivity might be originated from the increased fluorescence intensity of Cys-GO via N and S doping, which allowed better detection threshold. These experimental results suggest that Cys-GO is a promising probe in designing biosensors for highly sensitive detection of target enzymes, and further studies are needed to demonstrate its potential in various biomedical applications.

3.6 Summary

A simple and mild way to achieve heteroatom-doped GO have been developed to enhance fluorescence of GO. GO was homogenized with cysteine (Cys) as a N and S atom source in acidic DMF cosolvent system, resulting in Cys-modified GO (Cys-GO). Cys-GO is rich in N and S contents and exhibited highly bright fluorescene resulting from synergistic effect of N and S atoms. Finally, Cys-GO was used as a fluorescent probe for the detection of MMP-2 by means of peptide induced assembly/disassembly. Cys-GO-peptide assembly sensor was able to detect MMP-2 with significantly enhanced sensitivity. Cys-GO could potentially be used as an advanced fluorescence probe for the detection of various biological molecules.

4. Comparison of Sensing Performance

All GO-based optical biosensors developed in this thesis was able to detect MMP-2 via turn-on response of fluorescence signal. To compare the sensing performance of each sensors, detection sensitivity and response kinetics were evaluated (Table 3-6). Firstly, limit of detection (LOD) was calculated from fluorescence turn-on response depending on the MMP-2 concentrations. LOD value for the detection of MMP-2 in tube test was 5.7 and 2.7 μg mL^{-1} in GO-peptide-QXL and GO-Peptide assembly, respectively. In the case of cell-secreted MMP-2 detection, LOD value was 1.1 and 0.8 ng mL^{-1}. GO-Peptide assembly sensor was able to detect MMP-2 more sensitively compared to GO-peptide-QXL sensor. QXL quencher molecules of GO-peptide-QXL might disupt the fluorescence recovery after the release from the GO via proteolytic cleavage, and therefore, sensitivity of GO-peptide-QXL sensor could be lower. On the other hand, GO-Peptide assembly sensor was able to sensitively detect MMP-2 via fluorescence turn-on response without disturbance by quencher. In the case of Cys-GO-Peptide assembly sensor, fluorescece recovery upon the addition of MMP-2 was highly enhanced compared to that of GO-peptide-QXL ans GO-Peptide assembly.

Therefore, Cys-GO-Peptide assembly sensor can be applied to more sensitive detection of target biomolecules although LOD values were not calculated with current results.

Next, response kinetics were compared with kinetic constant which was calculated from Lineweaver-Burk plot. The values of K_m and V_{max} were 0.76 μM and 0.49 min^{-1}, and 0.072 μM and 0.056 min^{-1} for GO-peptide-QXL and GO-Peptide assembly, respectively. Slower response kinetics of the GO-Peptide assembly can be ascribed to the decreased accessibility of MMP-2 to the peptide substrate sandwiched by GO sheets causing steric hindrance. However, MMP-2 can easily contact with substrate peptide in GO-peptide-QXL.

A comparison of MMP-2 sensing performance between three sensors showed that GO-peptide-QXL exhibited more rapid sensing than GO-Peptide assembly, and GO-Peptide assembly exhibited more sensitive sensing than GO-peptide QXL. Although Cys-GO-Peptide assembly showed increased fluorescence recovery compared with GO-Peptide assembly, sensing performances should be compared accurately with LOD and kinetic parameters determined via further experiments. The performances of these biosensors in the present work can be further

developed and applied to the more sensitive and rapid sensing for the detection of target biomolecules.

Table 3-6. Comparison of MMP-2 Sensing Performance

	GO-Peptide-QXL	**GO-Peptide assembly**
Signal Transduction	FRET (GO-Quencher)	Self-quenching
LOD (Tube Test, μg mL^{-1})	5.7	2.7
LOD (*In Vitro* Cell Test, ng mL^{-1})	1.1	**0.8**
Response Kinetics	K_m = 0.76 μM V_{max} = **0.49 min^{-1}**	K_m = 0.072 μM V_{max} = 0.056 min^{-1}
Key Feature	**Rapid Detection**	**Sensitive Detection**

Chapter IV.
Conclusion

1. A new optical biosensor, which consist of fluorescent GO covalently linked with target-specific substrate peptide and quencher molecule, was developed for the detection of MMP-2.

2. Fluorescence quenching ability of various quencher molecules (metallo protoporphyrin derivatives and QXL_{570}) was screened. All quencher molecules could quenched fluorescence of GO, and QXL_{570} showed excellent quenching ability via FRET, especially.

3. GO-peptide-QXL complex was able to detect MMP-2 via fluorescence recovery resulting from the proteolytic cleavage and release of quencher molecules. In addition, cell-secreted MMP-2 was also selectively detected with high sensitivity via fluorescence turn-on response.

4. GO-peptide-QXL sensors showed outstanding storage stability, which is attributed to the covalent conjugation between GO and peptide-quencher and signal stability of GO in biological environment.

5. GO-peptide assembly sensor was designed to fabricate more simple sensing platform excluding the use of quencher molecules. GO was

conjugated with target specific substrate peptide bearing thiol functional groups to induce GO assembly via disulfide bond formation. Fluorescence signal of GO in GO-peptide assembly was efficiently quenched due to the self-quenching.

6. GO-peptide assembly sensor was successfully applied to the detection of MMP-2 by means of fluorescence turn-on response via proteolytic cleavage of peptide substrate and disassembly of GO-peptide assembled sensor.

7. N, S-doped Cys-GO was developed to enhance fluorescence signal of GO which showed inherently weak fluorescence. Cys-GO was synthesized under the mild reaction condition, and showed 10 fold enhanced fluorescence signal compared to GO.

8. In the formation of Cys-GO, DMF contribute to the doping of N via the reaction between oxygen containing functional groups in GO and dimethylamine which is formed by hydolysis of DMF molecules. In addition, Cys contribute to the doping of N and S atoms via the reaction

between functional groups of Cys and GO, resulting in the considerable decrease in carboxylic acid groups followed by decrease in non-radiative recombination process.

9. Highly enhanced PL of Cys-GO was attributed to both the formation of new surface state by N and S doping in basal plane of GO and passivation of non-radiative carboxyl functional groups.

10. Cys-GO was applied to the assembled sensor for the detection of MMP-2. Cys-GO assembled sensor showed improved turn-on response to the MMP-2 owing to the increased fluoresence signal, and coule be applied further for more sensitive detection of target biomolecules.

References

[1]. R. K. Saiki, S. Scharf, F. Faloona, K. B. Mullis, G. T. Horn, H. A. Erlich, N. Arnheim, Enzymatic amplification of b-globin genomic sequences and restriction site analysis for diagnosis of sickle cell anemia. *Science* **230**, 1350-1354 (1985).

[2]. K. Taniguchi, T. Kajiyama, H. Kambara, Quantitative analysis of gene expression in a single cell by qPCR. *Nature Methods* **6**, 503 (2009).

[3]. C.-K. Chiang, W.-T. Chen, H.-T. Chang, Nanoparticle-based mass spectrometry for the analysis of biomolecules. *Chemical Society Reviews* **40**, 1269-1281 (2011).

[4]. U. Resch-Genger, M. Grabolle, S. Cavaliere-Jaricot, R. Nitschke, T. Nann, Quantum dots versus organic dyes as fluorescent labels. *Nature Methods* **5**, 763-775 (2008).

[5]. W. Zhong, Nanomaterials in fluorescence-based biosensing. *Analytical and Bioanalytical Chemistry* **394**, 47-59 (2009).

[6]. J. Yao, M. Yang, Y. Duan, Chemistry, biology, and medicine of fluorescent nanomaterials and related systems: new insights into biosensing, bioimaging, genomics, diagnostics, and therapy. *Chemical Reviews* **114**, 6130-6178 (2014).

[7]. A. M. Smith, S. Nie, Chemical analysis and cellular imaging with quantum dots. *Analyst* **129**, 672-677 (2004).

[8]. G. Ruan, A. Agrawal, A. M. Smith, X. Gao, S. Nie, in *Reviews in Fluorescence 2006*. (Springer, 2006), pp. 181-193.

[9]. J. M. Klostranec, W. C. Chan, Quantum dots in biological and biomedical research: recent progress and present challenges. *Advanced Materials* **18**, 1953-1964 (2006).

[10]. I. L. Medintz, H. T. Uyeda, E. R. Goldman, H. Mattoussi, Quantum dot bioconjugates for imaging, labelling and sensing. *Nature Materials* **4**, 435-446 (2005).

[11]. X. Gao, L. Yang, J. A. Petros, F. F. Marshall, J. W. Simons, S. Nie, In vivo molecular and cellular imaging with quantum dots. *Current Opinion in Biotechnology* **16**, 63-72 (2005).

[12]. S. E. Skrabalak, J. Chen, Y. Sun, X. Lu, L. Au, C. M. Cobley, Y. Xia, Gold nanocages: synthesis, properties, and applications. *Accounts of Chemical Research* **41**, 1587-1595 (2008).

[13]. C. L. Haynes, R. P. Van Duyne, Nanosphere lithography: a versatile nanofabrication tool for studies of size-dependent nanoparticle optics. *The Journal of Physical Chemistry B* **105**, 5599-5611 (2001).

[14]. M. A. El-Sayed, Some interesting properties of metals confined in time and nanometer space of different shapes. *Accounts of Chemical Research* **34**, 257-264 (2001).

[15]. P. Mulvaney, Surface plasmon spectroscopy of nanosized metal particles. *Langmuir* **12**, 788-800 (1996).

[16]. K. Kuningas, H. Päkkilä, T. Ukonaho, T. Rantanen, T. Lövgren, T. Soukka, Upconversion fluorescence enables homogeneous immunoassay in whole blood. *Clinical Chemistry* **53**, 145-146 (2007).

[17]. Z. Chen, H. Chen, H. Hu, M. Yu, F. Li, Q. Zhang, Z. Zhou, T. Yi, C. Huang, Versatile synthesis strategy for carboxylic acid-functionalized upconverting nanophosphors as biological labels. *Journal of the American Chemical Society* **130**, 3023-3029 (2008).

[18]. T. Rantanen, M. L. Järvenpää, J. Vuojola, K. Kuningas, T. Soukka, Fluorescence-Quenching-Based Enzyme-Activity Assay by Using Photon Upconversion. *Angewandte Chemie International Edition* **47**, 3811-3813 (2008).

[19]. F. Wang, X. Liu, Recent advances in the chemistry of lanthanide-doped upconversion nanocrystals. *Chemical Society Reviews* **38**, 976-989 (2009).

[20]. J. Shen, L.-D. Sun, C.-H. Yan, Luminescent rare earth nanomaterials for bioprobe applications. *Dalton Transactions*, 5687-5697 (2008).

[21]. M. Zhang, L. Bai, W. Shang, W. Xie, H. Ma, Y. Fu, D. Fang, H. Sun, L. Fan, M. Han, Facile synthesis of water-soluble, highly fluorescent graphene quantum dots as a robust biological label for stem cells. *Journal of Materials Chemistry* **22**, 7461-7467 (2012).

[22]. S.-T. Yang, X. Wang, H. Wang, F. Lu, P. G. Luo, L. Cao, M. J. Meziani, J.-H. Liu, Y. Liu, M. Chen, Carbon dots as nontoxic and

high-performance fluorescence imaging agents. *The Journal of Physical Chemistry C* **113**, 18110-18114 (2009).

[23]. A. Zhu, Q. Qu, X. Shao, B. Kong, Y. Tian, Carbon-dot-based dual-emission nanohybrid produces a ratiometric fluorescent sensor for in vivo imaging of cellular copper ions. *Angewandte Chemie International Edition* **51**, 7185-7189 (2012).

[24]. Y. Song, X. Wang, C. Zhao, K. Qu, J. Ren, X. Qu, Label-Free Colorimetric Detection of Single Nucleotide Polymorphism by Using Single-Walled Carbon Nanotube Intrinsic Peroxidase-Like Activity. *Chemistry–A European Journal* **16**, 3617-3621 (2010).

[25]. P. W. Barone, R. S. Parker, M. S. Strano, In vivo fluorescence detection of glucose using a single-walled carbon nanotube optical sensor: design, fluorophore properties, advantages, and disadvantages. *Analytical Chemistry* **77**, 7556-7562 (2005).

[26]. Z. Liu, S. Tabakman, K. Welsher, H. Dai, Carbon nanotubes in biology and medicine: in vitro and in vivo detection, imaging and drug delivery. *Nano Research* **2**, 85-120 (2009).

[27]. L. Zhou, Y. Lin, Z. Huang, J. Ren, X. Qu, Carbon nanodots as fluorescence probes for rapid, sensitive, and label-free detection of Hg 2+ and biothiols in complex matrices. *Chemical Communications* **48**, 1147-1149 (2012).

[28]. C. H. Lu, H. H. Yang, C. L. Zhu, X. Chen, G. N. Chen, A graphene platform for sensing biomolecules. *Angewandte Chemie International Edition* **48**, 4785-4787 (2009).

[29]. S. He, B. Song, D. Li, C. Zhu, W. Qi, Y. Wen, L. Wang, S. Song, H. Fang, C. Fan, A graphene nanoprobe for rapid, sensitive, and multicolor fluorescent DNA analysis. *Advanced Functional Materials* **20**, 453-459 (2010).

[30]. H. Chang, L. Tang, Y. Wang, J. Jiang, J. Li, Graphene fluorescence resonance energy transfer aptasensor for the thrombin detection. *Analytical Chemistry* **82**, 2341-2346 (2010).

[31]. C. Yu, X. Li, F. Zeng, F. Zheng, S. Wu, Carbon-dot-based ratiometric fluorescent sensor for detecting hydrogen sulfide in aqueous media and inside live cells. *Chemical Communications* **49**, 403-405 (2013).

[32]. S. Zhu, Q. Meng, L. Wang, J. Zhang, Y. Song, H. Jin, K. Zhang, H. Sun, H. Wang, B. Yang, Highly photoluminescent carbon dots for multicolor patterning, sensors, and bioimaging. *Angewandte Chemie International Edition* **52**, 3953-3957 (2013).

[33]. J. Shen, Y. Zhu, X. Yang, C. Li, Graphene quantum dots: emergent nanolights for bioimaging, sensors, catalysis and photovoltaic devices. *Chemical Communications* **48**, 3686-3699 (2012).

[34]. T. Förster, Zwischenmolekulare energiewanderung und fluoreszenz. *Annalen Der Physik* **437**, 55-75 (1948).

[35]. T. Clegg. Fluorescence resonance energy transfer. in *Fluorescence Imaging Spectroscopy and Microscopy 1996* (John Wiely & Sons, 1996), pp. 179-251.

[36]. J. R. Lakowicz, *Principles of fluorescence spectroscopy*. (Springer, 2006).

[37]. K. E. Sapsford, L. Berti, I. L. Medintz, Materials for fluorescence resonance energy transfer analysis: beyond traditional donor–acceptor combinations. *Angewandte Chemie International Edition* **45**, 4562-4589 (2006).

[38]. I. L. Medintz, A. R. Clapp, H. Mattoussi, E. R. Goldman, B. Fisher, J. M. Mauro, Self-assembled nanoscale biosensors based on quantum dot FRET donors. *Nature Materials* **2**, 630-638 (2003).

[39]. D. M. Willard, A. Van Orden, Quantum dots: resonant energy-transfer sensor. *Nature Materials* **2**, 575-576 (2003).

[40]. Y. Wang, Z. Tang, S. Tan, N. A. Kotov, Biological assembly of nanocircuit prototypes from protein-modified CdTe nanowires. *Nano Letters* **5**, 243-248 (2005).

[41]. D. M. Willard, L. L. Carillo, J. Jung, A. Van Orden, CdSe-ZnS quantum dots as resonance energy transfer donors in a model protein-protein binding assay. *Nano Letters* **1**, 469-474 (2001).

[42]. A. Shamirian, A. Ghai, P. T. Snee, QD-Based FRET probes at a glance. *Sensors* **15**, 13028-13051 (2015).

[43]. S. Jiang, Y. Zhang, Upconversion nanoparticle-based FRET system for study of siRNA in live cells. *Langmuir* **26**, 6689-6694 (2010).

[44]. L. Wang, R. Yan, Z. Huo, L. Wang, J. Zeng, J. Bao, X. Wang, Q. Peng, Y. Li, Fluorescence Resonant Energy Transfer Biosensor Based

on Upconversion-Luminescent Nanoparticles. *Angewandte Chemie International Edition* **44**, 6054-6057 (2005).

[45]. J. Tang, B. Kong, H. Wu, M. Xu, Y. Wang, Y. Wang, D. Zhao, G. Zheng, Carbon nanodots featuring efficient FRET for real-time monitoring of drug delivery and two-photon imaging. *Advanced Materials* **25**, 6569-6574 (2013).

[46]. H. Dai, Y. Shi, Y. Wang, Y. Sun, J. Hu, P. Ni, Z. Li, A carbon dot based biosensor for melamine detection by fluorescence resonance energy transfer. *Sensors and Actuators B: Chemical* **202**, 201-208 (2014).

[47]. J. Shi, C. Chan, Y. Pang, W. Ye, F. Tian, J. Lyu, Y. Zhang, M. Yang, A fluorescence resonance energy transfer (FRET) biosensor based on graphene quantum dots (GQDs) and gold nanoparticles (AuNPs) for the detection of mecA gene sequence of Staphylococcus aureus. *Biosensors and Bioelectronics* **67**, 595-600 (2015).

[48]. N. L. Rosi, C. A. Mirkin, Nanostructures in biodiagnostics. *Chemical Reviews* **105**, 1547-1562 (2005).

[49]. S. I. Lim, C.-J. Zhong, Molecularly mediated processing and assembly of nanoparticles: exploring the interparticle interactions and structures. *Accounts of Chemical Research* **42**, 798-808 (2009).

[50]. I. U. Arachchige, S. L. Brock, Sol–gel methods for the assembly of metal chalcogenide quantum dots. *Accounts of Chemical Research* **40**, 801-809 (2007).

[51]. D. Vanmaekelbergh, P. Liljeroth, Electron-conducting quantum dot solids: novel materials based on colloidal semiconductor nanocrystals. *Chemical Society Reviews* **34**, 299-312 (2005).

[52]. T. Kim, M. Noh, H. Lee, S.-W. Joo, S. Y. Lee, K. Lee, Fluorescence-based detection of point mutation in DNA sequences by CdS quantum dot aggregation. *The Journal of Physical Chemistry B* **113**, 14487-14490 (2009).

[53]. W. Wu, T. Zhou, A. Berliner, P. Banerjee, S. Zhou, Glucose-Mediated Assembly of Phenylboronic Acid Modified CdTe/ZnTe/ZnS Quantum Dots for Intracellular Glucose Probing. *Angewandte Chemie International Edition* **49**, 6554-6558 (2010).

[54]. K. Mizusawa, Y. Ishida, Y. Takaoka, M. Miyagawa, S. Tsukiji, I. Hamachi, Disassembly-driven turn-on fluorescent nanoprobes for selective protein detection. *Journal of the American Chemical Society* **132**, 7291-7293 (2010).

[55]. J. Liu, X. Yang, K. Wang, R. Yang, H. Ji, L. Yang, C. Wu, A switchable fluorescent quantum dot probe based on aggregation/disaggregation mechanism. *Chemical Communications* **47**, 935-937 (2011).

[56]. Y. Liu, K.-R. Wang, D.-S. Guo, B.-P. Jiang, Supramolecular assembly of perylene bisimide with b-cyclodextrin grafts as a solid-state fluorescence sensor for vapor detection. *Advanced Functional Materials* **19**, 2230 (2009).

[57]. Y. Hama, Y. Urano, Y. Koyama, A. J. Gunn, P. L. Choyke, H. Kobayashi, A self-quenched galactosamine-serum albumin-rhodamineX conjugate: a “smart” fluorescent molecular imaging probe synthesized with clinically applicable material for detecting peritoneal ovarian cancer metastases. *Clinical Cancer Research* **13**, 6335-6343 (2007).

[58]. Y. Hama, Y. Urano, Y. Koyama, M. Kamiya, M. Bernardo, R. S. Paik, I. S. Shin, C. H. Paik, P. L. Choyke, H. Kobayashi, A target cell–specific activatable fluorescence probe for in vivo molecular imaging of cancer based on a self-quenched avidin-rhodamine conjugate. *Cancer Research* **67**, 2791-2799 (2007).

[59]. H. Kobayashi, M. Ogawa, R. Alford, P. L. Choyke, Y. Urano, New strategies for fluorescent probe design in medical diagnostic imaging. *Chemical Reviews* **110**, 2620-2640 (2009).

[60]. W. S. Hummers Jr, R. E. Offeman, Preparation of graphitic oxide. *Journal of the American Chemical Society* **80**, 1339-1339 (1958).

[61]. Q. Mei, K. Zhang, G. Guan, B. Liu, S. Wang, Z. Zhang, Highly efficient photoluminescent graphene oxide with tunable surface properties. *Chemical Communications* **46**, 7319-7321 (2010).

[62]. G. Eda, Y. Y. Lin, C. Mattevi, H. Yamaguchi, H. A. Chen, I. Chen, C. W. Chen, M. Chhowalla, Blue photoluminescence from chemically derived graphene oxide. *Advanced Materials* **22**, 505-509 (2010).

[63]. Z. Luo, P. M. Vora, E. J. Mele, A. C. Johnson, J. M. Kikkawa, Photoluminescence and band gap modulation in graphene oxide. *Applied Physics Letters* **94**, 111909 (2009).

[64]. K. P. Loh, Q. Bao, G. Eda, M. Chhowalla, Graphene oxide as a chemically tunable platform for optical applications. *Nature Chemistry* **2**, 1015-1024 (2010).

[65]. T. Gokus, R. Nair, A. Bonetti, M. Bohmler, A. Lombardo, K. Novoselov, A. Geim, A. Ferrari, A. Hartschuh, Making graphene luminescent by oxygen plasma treatment. *ACS Nano* **3**, 3963-3968 (2009).

[66]. W. Cai, R. D. Piner, F. J. Stadermann, S. Park, M. A. Shaibat, Y. Ishii, D. Yang, A. Velamakanni, S. J. An, M. Stoller, Synthesis and solid-state NMR structural characterization of 13C-labeled graphite oxide. *Science* **321**, 1815-1817 (2008).

[67]. D. Yang, A. Velamakanni, G. Bozoklu, S. Park, M. Stoller, R. D. Piner, S. Stankovich, I. Jung, D. A. Field, C. A. Ventrice, Chemical analysis of graphene oxide films after heat and chemical treatments by X-ray photoelectron and Micro-Raman spectroscopy. *Carbon* **47**, 145-152 (2009).

[68]. C. T. Chien, S. S. Li, W. J. Lai, Y. C. Yeh, H. A. Chen, I. Chen, L. C. Chen, K. H. Chen, T. Nemoto, S. Isoda, Tunable photoluminescence from graphene oxide. *Angewandte Chemie International Edition* **51**, 6662-6666 (2012).

[69]. L. Cao, M. J. Meziani, S. Sahu, Y.-P. Sun, Photoluminescence properties of graphene versus other carbon nanomaterials. *Accounts of Chemical Research* **46**, 171-180 (2012).

[70]. J. Shang, L. Ma, J. Li, W. Ai, T. Yu, G. G. Gurzadyan, The origin of fluorescence from graphene oxide. *Scientific Reports* **2**, 792 (2012).

[71]. C. Galande, A. D. Mohite, A. V. Naumov, W. Gao, L. Ci, A. Ajayan, H. Gao, A. Srivastava, R. B. Weisman, P. M. Ajayan, Quasi-molecular fluorescence from graphene oxide. *Scientific Reports* **1**, 85 (2011).

[72]. S. H. Jin, D. H. Kim, G. H. Jun, S. H. Hong, S. Jeon, Tuning the photoluminescence of graphene quantum dots through the charge transfer effect of functional groups. *Acs Nano* **7**, 1239-1245 (2013).

[73]. M. Li, S. K. Cushing, X. Zhou, S. Guo, N. Wu, Fingerprinting photoluminescence of functional groups in graphene oxide. *Journal of Materials Chemistry* **22**, 23374-23379 (2012).

[74]. S. Y. Kwak, J. K. Yang, S. J. Jeon, H. I. Kim, J. Yim, H. Kang, S. Kyeong, Y. S. Lee, J. H. Kim, Luminescent Graphene Oxide with a Peptide-Quencher Complex for Optical Detection of Cell-Secreted Proteases by a Turn-On Response. *Advanced Functional Materials* **24**, 5119-5128 (2014).

[75]. Y. Sun, C. Shen, J. Wang, Y. Lu, Facile synthesis of biocompatible N, S-doped carbon dots for cell imaging and ion detecting. *RSC Advances* **5**, 16368-16375 (2015).

[76]. F. Arcudi, L. Đorđević, M. Prato, Synthesis, Separation, and Characterization of Small and Highly Fluorescent Nitrogen-Doped Carbon NanoDots. *Angewandte Chemie International Edition* **55**, 2107-2112 (2016).

[77]. X. Zhai, P. Zhang, C. Liu, T. Bai, W. Li, L. Dai, W. Liu, Highly luminescent carbon nanodots by microwave-assisted pyrolysis. *Chemical Communications* **48**, 7955-7957 (2012).

[78]. C.-Y. Teng, T.-F. Yeh, K.-I. Lin, S.-J. Chen, M. Yoshimura, H. Teng, Synthesis of graphene oxide dots for excitation-wavelength independent photoluminescence at high quantum yields. *Journal of Materials Chemistry C* **3**, 4553-4562 (2015).

[79]. Y. Dong, H. Pang, H. B. Yang, C. Guo, J. Shao, Y. Chi, C. M. Li, T. Yu, Carbon-Based Dots Co-doped with Nitrogen and Sulfur for High Quantum Yield and Excitation-Independent Emission. *Angewandte Chemie International Edition* **52**, 7800-7804 (2013).

[80]. L. Lin, M. Rong, S. Lu, X. Song, Y. Zhong, J. Yan, Y. Wang, X. Chen, A facile synthesis of highly luminescent nitrogen-doped graphene quantum dots for the detection of 2, 4, 6-trinitrophenol in aqueous solution. *Nanoscale* **7**, 1872-1878 (2015).

[81]. H. Ding, J.-S. Wei, H.-M. Xiong, Nitrogen and sulfur co-doped carbon dots with strong blue luminescence. *Nanoscale* **6**, 13817-13823 (2014).

[82]. Y. Song, S. Zhu, S. Zhang, Y. Fu, L. Wang, X. Zhao, B. Yang, Investigation from chemical structure to photoluminescent

mechanism: a type of carbon dots from the pyrolysis of citric acid and an amine. *Journal of Materials Chemistry C* **3**, 5976-5984 (2015).

[83]. H. Ding, S.-B. Yu, J.-S. Wei, H.-M. Xiong, Full-color light-emitting carbon dots with a surface-state-controlled luminescence mechanism. *ACS Nano* **10**, 484-491 (2015).

[84]. T. Ogi, K. Aishima, F. A. Permatasari, F. Iskandar, E. Tanabe, K. Okuyama, Kinetics of nitrogen-doped carbon dot formation via hydrothermal synthesis. *New Journal of Chemistry* **40**, 5555-5561 (2016).

[85]. S. Li, Y. Li, J. Cao, J. Zhu, L. Fan, X. Li, Sulfur-doped graphene quantum dots as a novel fluorescent probe for highly selective and sensitive detection of Fe3+. *Analytical Chemistry* **86**, 10201-10207 (2014).

[86]. W. Wang, Y. Li, L. Cheng, Z. Cao, W. Liu, Water-soluble and phosphorus-containing carbon dots with strong green fluorescence for cell labeling. *Journal of Materials Chemistry B* **2**, 46-48 (2014).

[87]. J. Zhou, X. Shan, J. Ma, Y. Gu, Z. Qian, J. Chen, H. Feng, Facile synthesis of P-doped carbon quantum dots with highly efficient photoluminescence. *RSC Advances* **4**, 5465-5468 (2014).

[88]. W. Ai, Z. Luo, J. Jiang, J. Zhu, Z. Du, Z. Fan, L. Xie, H. Zhang, W. Huang, T. Yu, Nitrogen and sulfur codoped graphene: multifunctional electrode materials for high-performance Li-ion batteries and oxygen reduction reaction. *Advanced Materials* **26**, 6186-6192 (2014).

[89]. Z.-H. Sheng, L. Shao, J.-J. Chen, W.-J. Bao, F.-B. Wang, X.-H. Xia, Catalyst-free synthesis of nitrogen-doped graphene via thermal annealing graphite oxide with melamine and its excellent electrocatalysis. *ACS Nano* **5**, 4350-4358 (2011).

[90]. V. Urbanová, K. Holá, A. B. Bourlinos, K. Čépe, A. Ambrosi, A. H. Loo, M. Pumera, F. Karlický, M. Otyepka, R. Zbořil, Thiofluorographene–Hydrophilic Graphene Derivative with Semiconducting and Genosensing Properties. *Advanced Materials* **27**, 2305-2310 (2015).

[91]. C. Hu, C. Yu, M. Li, X. Wang, Q. Dong, G. Wang, J. Qiu, Nitrogen-doped carbon dots decorated on graphene: a novel all-carbon hybrid electrocatalyst for enhanced oxygen reduction reaction. *Chemical Communications* **51**, 3419-3422 (2015).

[92]. D. Guo, R. Shibuya, C. Akiba, S. Saji, T. Kondo, J. Nakamura, Active sites of nitrogen-doped carbon materials for oxygen reduction reaction clarified using model catalysts. *Science* **351**, 361-365 (2016).

[93]. D. Wei, Y. Liu, Y. Wang, H. Zhang, L. Huang, G. Yu, Synthesis of N-doped graphene by chemical vapor deposition and its electrical properties. *Nano Letters* **9**, 1752-1758 (2009).

[94]. C.-J. Shih, S. Lin, R. Sharma, M. S. Strano, D. Blankschtein, Understanding the pH-dependent behavior of graphene oxide aqueous solutions: a comparative experimental and molecular dynamics simulation study. *Langmuir* **28**, 235-241 (2011).

[95]. D. Pan, J. Zhang, Z. Li, C. Wu, X. Yan, M. Wu, Observation of pH-, solvent-, spin-, and excitation-dependent blue photoluminescence from carbon nanoparticles. *Chemical Communications* **46**, 3681-3683 (2010).

[96]. E. Morales-Narváez, A. Merkoçi, Graphene oxide as an optical biosensing platform. *Advanced Materials* **24**, 3298-3308 (2012).

[97]. S. Zhu, J. Zhang, C. Qiao, S. Tang, Y. Li, W. Yuan, B. Li, L. Tian, F. Liu, R. Hu, Strongly green-photoluminescent graphene quantum dots for bioimaging applications. *Chemical Communications* **47**, 6858-6860 (2011).

[98]. F. Liu, J. Y. Choi, T. S. Seo, Graphene oxide arrays for detecting specific DNA hybridization by fluorescence resonance energy transfer. *Biosensors and Bioelectronics* **25**, 2361-2365 (2010).

[99]. X. Sun, Z. Liu, K. Welsher, J. T. Robinson, A. Goodwin, S. Zaric, H. Dai, Nano-graphene oxide for cellular imaging and drug delivery. *Nano Research* **1**, 203-212 (2008).

[100]. J. H. Jung, D. S. Cheon, F. Liu, K. B. Lee, T. S. Seo, A graphene oxide based immuno-biosensor for pathogen detection. *Angewandte Chemie International Edition* **49**, 5708-5711 (2010).

[101]. H. Dong, W. Gao, F. Yan, H. Ji, H. Ju, Fluorescence resonance energy transfer between quantum dots and graphene oxide for sensing biomolecules. *Analytical Chemistry* **82**, 5511-5517 (2010).

[102]. J. Balapanuru, J. X. Yang, S. Xiao, Q. Bao, M. Jahan, L. Polavarapu, J. Wei, Q. H. Xu, K. P. Loh, A Graphene Oxide–Organic Dye Ionic Complex with DNA-Sensing and Optical-Limiting Properties. *Angewandte Chemie International Edition* **49**, 6549-6553 (2010).

[103]. H. Jang, Y. K. Kim, H. M. Kwon, W. S. Yeo, D. E. Kim, D. H. Min, A Graphene-Based Platform for the Assay of Duplex-DNA Unwinding by Helicase. *Angewandte Chemie International Edition* **49**, 5703-5707 (2010).

[104]. M. Zhang, B.-C. Yin, W. Tan, B.-C. Ye, A versatile graphene-based fluorescence "on/off" switch for multiplex detection of various targets. *Biosensors and Bioelectronics* **26**, 3260-3265 (2011).

[105]. Y. Wen, C. Peng, D. Li, L. Zhuo, S. He, L. Wang, Q. Huang, Q.-H. Xu, C. Fan, Metal ion-modulated graphene-DNAzyme interactions: design of a nanoprobe for fluorescent detection of lead (II) ions with high sensitivity, selectivity and tunable dynamic range. *Chemical Communications* **47**, 6278-6280 (2011).

[106]. X.-H. Zhao, R.-M. Kong, X.-B. Zhang, H.-M. Meng, W.-N. Liu, W. Tan, G.-L. Shen, R.-Q. Yu, Graphene–DNAzyme based biosensor for amplified fluorescence "turn-on" detection of Pb2+ with a high selectivity. *Analytical Chemistry* **83**, 5062-5066 (2011).

[107]. Y. Piao, F. Liu, T. S. Seo, The photoluminescent graphene oxide serves as an acceptor rather than a donor in the fluorescence resonance energy transfer pair of Cy3. 5–graphene oxide. *Chemical Communications* **47**, 12149-12151 (2011).

[108]. T. Feng, D. Feng, W. Shi, X. Li, H. Ma, A graphene oxide-peptide fluorescence sensor for proteolytically active prostate-specific antigen. *Molecular BioSystems* **8**, 1441-1445 (2012).

[109]. S.-R. Ryoo, J. Lee, J. Yeo, H.-K. Na, Y.-K. Kim, H. Jang, J. H. Lee, S. W. Han, Y. Lee, V. N. Kim, Quantitative and multiplexed microRNA sensing in living cells based on peptide nucleic acid and nano graphene oxide (PANGO). *ACS Nano* **7**, 5882-5891 (2013).

[110]. C. Chung, Y.-K. Kim, D. Shin, S.-R. Ryoo, B. H. Hong, D.-H. Min, Biomedical applications of graphene and graphene oxide. *Accounts of Chemical Research* **46**, 2211-2224 (2013).

[111]. H. Jang, J. Lee, D.-H. Min, Graphene oxide for fluorescence-mediated enzymatic activity assays. *Journal of Materials Chemistry B* **2**, 2452-2460 (2014).

[112]. H. Jang, S. R. Ryoo, Y. K. Kim, S. Yoon, H. Kim, S. W. Han, B. S. Choi, D. E. Kim, D. H. Min, Discovery of Hepatitis C Virus NS3 Helicase Inhibitors by a Multiplexed, High-Throughput Helicase Activity Assay Based on Graphene Oxide. *Angewandte Chemie International Edition* **52**, 2340-2344 (2013).

[113]. L. Cao, L. Cheng, Z. Zhang, Y. Wang, X. Zhang, H. Chen, B. Liu, S. Zhang, J. Kong, Visual and high-throughput detection of cancer cells using a graphene oxide-based FRET aptasensing microfluidic chip. *Lab on a Chip* **12**, 4864-4869 (2012).

[114]. H. Wang, Q. Zhang, X. Chu, T. Chen, J. Ge, R. Yu, Graphene oxide–peptide conjugate as an intracellular protease sensor for

caspase-3 activation imaging in live cells. *Angewandte Chemie International Edition* **50**, 7065-7069 (2011).

[115]. M. Zhang, B.-C. Yin, X.-F. Wang, B.-C. Ye, Interaction of peptides with graphene oxide and its application for real-time monitoring of protease activity. *Chemical Communications* **47**, 2399-2401 (2011).

[116]. M. J. Bissell, D. Radisky, Putting tumours in context. *Nature Reviews Cancer* **1**, 46-54 (2001).

[117]. M. Egeblad, Z. Werb, New functions for the matrix metalloproteinases in cancer progression. *Nature Reviews Cancer* **2**, 161-174 (2002).

[118]. M. Nakajima, K. Morikawa, A. Fabra, C. D. Bucana, I. J. Fidler, Influence of organ environment on extracellular matrix degradative activity and metastasis of human colon carcinoma cells. *Journal of the National Cancer Institute* **82**, 1890-1898 (1990).

[119]. H. Kawamata, S. Kameyama, K. Kawai, Y. Tanaka, L. Nan, D. H. Barch, W. G. Stetler-Stevenson, R. Oyasu, Marked acceleration of the metastatic phenotype of a rat bladder carcinoma cell line by the expression of human gelatinase A. *International Journal of Cancer* **63**, 568-575 (1995).

[120]. G. La Rocca, I. Pucci-Minafra, A. Marrazzo, P. Taormina, S. Minafra, Zymographic detection and clinical correlations of MMP-2 and MMP-9 in breast cancer sera. *British Journal of Cancer* **90**, 1414-1421 (2004).

[121]. T. Freestone, R. J. Turner, A. Coady, D. J. Higman, R. M. Greenhalgh, J. T. Powell, Inflammation and matrix metalloproteinases in the enlarging abdominal aortic aneurysm. *Arteriosclerosis, Thrombosis, and Vascular Biology* **15**, 1145-1151 (1995).

[122]. C. Lombard, J. Saulnier, J. Wallach, Assays of matrix metalloproteinases (MMPs) activities: a review. *Biochimie* **87**, 265-272 (2005).

[123]. U. Pieper-Fürst, U. Kleuser, W. F. Stöcklein, A. Warsinke, F. W. Scheller, Detection of subpicomolar concentrations of human matrix metalloproteinase-2 by an optical biosensor. *Analytical Biochemistry* **332**, 160-167 (2004).

[124]. D. Feng, Y. Zhang, T. Feng, W. Shi, X. Li, H. Ma, A graphene oxide–peptide fluorescence sensor tailor-made for simple and sensitive detection of matrix metalloproteinase 2. *Chemical Communications* **47**, 10680-10682 (2011).

[125]. W. J. Akers, B. Xu, H. Lee, G. P. Sudlow, G. B. Fields, S. Achilefu, W. B. Edwards, Detection of MMP-2 and MMP-9 activity in vivo with a triple-helical peptide optical probe. *Bioconjugate Chemistry* **23**, 656-663 (2012).

[126]. G. Yang, L. Li, R. K. Rana, J.-J. Zhu, Assembled gold nanoparticles on nitrogen-doped graphene for ultrasensitive electrochemical detection of matrix metalloproteinase-2. *Carbon* **61**, 357-366 (2013).

[127]. J. O. McIntyre, B. Fingleton, K. S. Wells, W. David, C. C. Lynch, S. Gautam, L. M. Matrisian, Development of a novel fluorogenic proteolytic beacon for in vivo detection and imaging of tumour-associated matrix metalloproteinase-7 activity. *Biochemical Journal* **377**, 617-628 (2004).

[128]. S. Lee, E. J. Cha, K. Park, S. Y. Lee, J. K. Hong, I. C. Sun, S. Y. Kim, K. Choi, I. C. Kwon, K. Kim, A Near-Infrared-Fluorescence-Quenched Gold-Nanoparticle Imaging Probe for In Vivo Drug Screening and Protease Activity Determination. *Angewandte Chemie International Edition* **47**, 2804-2807 (2008).

[129]. H. Yao, Y. Zhang, F. Xiao, Z. Xia, J. Rao, Quantum dot/bioluminescence resonance energy transfer based highly sensitive detection of proteases. *Angewandte Chemie International Edition* **46**, 4346-4349 (2007).

[130]. J.-K. Yang, S.-Y. Kwak, S.-J. Jeon, E. Lee, J.-M. Ju, H.-I. Kim, Y.-S. Lee, J.-H. Kim, Proteolytic disassembly of peptide-mediated graphene oxide assemblies for turn-on fluorescence sensing of proteases. *Nanoscale* **8**, 12271-12282 (2016).

[131]. K. A. Mkhoyan, A. W. Contryman, J. Silcox, D. A. Stewart, G. Eda, C. Mattevi, S. Miller, M. Chhowalla, Atomic and electronic structure of graphene-oxide. *Nano Letters* **9**, 1058-1063 (2009).

[132]. M. B. M. Krishna, N. Venkatramaiah, R. Venkatesan, D. N. Rao, Synthesis and structural, spectroscopic and nonlinear optical measurements of graphene oxide and its composites with metal and

metal free porphyrins. *Journal of Materials Chemistry* **22**, 3059-3068 (2012).

[133]. J. J. Brege, C. Gallaway, A. R. Barron, Fluorescence quenching of single-walled carbon nanotubes in SDBS surfactant suspension by metal ions: Quenching efficiency as a function of metal and nanotube identity. *The Journal of Physical Chemistry C* **111**, 17812-17820 (2007).

[134]. J. M. Freije, M. Balbín, A. M. Pendas, L. M. Sánchez, X. S. Puente, C. López-Otín, in *New Trends in Cancer for the 21st Century*. (Springer, 2003), pp. 91-107.

[135]. K. Kessenbrock, V. Plaks, Z. Werb, Matrix metalloproteinases: regulators of the tumor microenvironment. *Cell* **141**, 52-67 (2010).

[136]. E. I. Deryugina, J. P. Quigley, Matrix metalloproteinases and tumor metastasis. *Cancer and Metastasis Reviews* **25**, 9-34 (2006).

[137]. J. Seltzer, K. Akers, H. Weingarten, G. Grant, D. McCourt, A. Eisen, Cleavage specificity of human skin type IV collagenase (gelatinase). Identification of cleavage sites in type I gelatin, with confirmation using synthetic peptides. *Journal of Biological Chemistry* **265**, 20409-20413 (1990).

[138]. Z. Liu, J. T. Robinson, X. Sun, H. Dai, PEGylated nanographene oxide for delivery of water-insoluble cancer drugs. *Journal of the American Chemical Society* **130**, 10876-10877 (2008).

[139]. Z. Xia, Y. Xing, M.-K. So, A. L. Koh, R. Sinclair, J. Rao, Multiplex detection of protease activity with quantum dot nanosensors prepared by intein-mediated specific bioconjugation. *Analytical Chemistry* **80**, 8649-8655 (2008).

[140]. E. Song, D. Cheng, Y. Song, M. Jiang, J. Yu, Y. Wang, A graphene oxide-based FRET sensor for rapid and sensitive detection of matrix metalloproteinase 2 in human serum sample. *Biosensors and Bioelectronics* **47**, 445-450 (2013).

[141]. I. L. Medintz, A. R. Clapp, F. M. Brunel, T. Tiefenbrunn, H. T. Uyeda, E. L. Chang, J. R. Deschamps, P. E. Dawson, H. Mattoussi, Proteolytic activity monitored by fluorescence resonance energy transfer through quantum-dot–peptide conjugates. *Nature Materials* **5**, 581-589 (2006).

[142]. Y. Wang, P. Shen, C. Li, Y. Wang, Z. Liu, Upconversion fluorescence resonance energy transfer based biosensor for ultrasensitive detection of matrix metalloproteinase-2 in blood. *Analytical Chemistry* **84**, 1466-1473 (2012).

[143]. C. Wei, M. Chen, J. Tao, X. Wu, M. Khan, D. Liu, N. Huang, L. Li, CdS nanorods assisted thermal oxidation of polythiol segments of PS-b-polythiols to produce core cross-linking micellar clusters. *Polymer Chemistry* **5**, 7034-7041 (2014).

[144]. A. L. Vance, T. M. Willey, A. J. Nelson, T. Van Buuren, C. Bostedt, L. J. Terminello, G. A. Fox, M. Engelhard, D. Baer, XAS and XPS characterization of monolayers derived from a dithiol and structurally

related disulfide-containing polyamides. *Langmuir* **18**, 8123-8128 (2002).

[145]. M. Şinoforoğlu, B. Gür, M. Arık, Y. Onganer, K. Meral, Graphene oxide sheets as a template for dye assembly: graphene oxide sheets induce H-aggregates of pyronin (Y) dye. *RSC Advances* **3**, 11832-11838 (2013).

[146]. D. A. Heller, E. S. Jeng, T.-K. Yeung, B. M. Martinez, A. E. Moll, J. B. Gastala, M. S. Strano, Optical detection of DNA conformational polymorphism on single-walled carbon nanotubes. *Science* **311**, 508-511 (2006).

[147]. G. Bisker, J. Dong, H. D. Park, N. M. Iverson, J. Ahn, J. T. Nelson, M. P. Landry, S. Kruss, M. S. Strano, Protein-targeted corona phase molecular recognition. *Nature Communications* **7**, DOI:10.1038/ncomms10241 (2016).

[148]. A. Monvoisin, C. Bisson, K. Si-Tayeb, C. Balabaud, A. Desmoulière, J. Rosenbaum, Involvement of matrix metalloproteinase type-3 in hepatocyte growth factor-induced invasion of human hepatocellular carcinoma cells. *International Journal of Cancer* **97**, 157-162 (2002).

[149]. T.-W. Chung, S.-K. Moon, Y.-C. Lee, J.-G. Kim, J.-H. Ko, C.-H. Kim, Enhanced expression of matrix metalloproteinase-9 by hepatitis B virus infection in liver cells. *Archives of Biochemistry and Biophysics* **408**, 147-154 (2002).

[150]. Y. Li, Y. Zhao, H. Cheng, Y. Hu, G. Shi, L. Dai, L. Qu, Nitrogen-doped graphene quantum dots with oxygen-rich functional groups. *Journal of the American Chemical Society* **134**, 15-18 (2011).

[151]. M. Li, W. Wu, W. Ren, H.-M. Cheng, N. Tang, W. Zhong, Y. Du, Synthesis and upconversion luminescence of N-doped graphene quantum dots. *Applied Physics Letters* **101**, 103107 (2012).

[152]. S. K. Cushing, M. Li, F. Huang, N. Wu, Origin of strong excitation wavelength dependent fluorescence of graphene oxide. *ACS Nano* **8**, 1002-1013 (2013).

[153]. T. Werner, D. M. Hercules, Fluorescence of 9-anthroic acid and its esters. Environmental effects on excited-state behavior. *The Journal of Physical Chemistry* **73**, 2005-2011 (1969).

[154]. S. K. Cushing, M. Li, F. Q. Huang, N. Q. Wu, Origin of Strong Excitation Wavelength Dependent Fluorescence of Graphene Oxide. *Acs Nano* **8**, 1002-1013 (2014).

[155]. S.-A. Wohlgemuth, R. J. White, M.-G. Willinger, M.-M. Titirici, M. Antonietti, A one-pot hydrothermal synthesis of sulfur and nitrogen doped carbon aerogels with enhanced electrocatalytic activity in the oxygen reduction reaction. *Green Chemistry* **14**, 1515-1523 (2012).

[156]. W.-W. Wang, J.-S. Dang, X. Zhao, S. Nagase, Formation Mechanisms of Graphitic-N: Oxygen Reduction and Nitrogen Doping of Graphene Oxides. *The Journal of Physical Chemistry C* **120**, 5673-5681 (2016).

[157]. H. Kang, S. Jeong, Y. Park, J. Yim, B. H. Jun, S. Kyeong, J. K. Yang, G. Kim, S. Hong, L. P. Lee, Near-Infrared SERS Nanoprobes with Plasmonic Au/Ag Hollow-Shell Assemblies for In Vivo Multiplex Detection. *Advanced Functional Materials* **23**, 3719-3727 (2013).

[158]. Y. Yan, Y.-X. Yin, S. Xin, Y.-G. Guo, L.-J. Wan, Ionothermal synthesis of sulfur-doped porous carbons hybridized with graphene as superior anode materials for lithium-ion batteries. *Chemical Communications* **48**, 10663-10665 (2012).

국문 초록

넓은 영역의 파장대에서 형광 특성을 보이는 산화 그라핀 (Graphene Oxide, GO)은 체내 환경에서 광학적 성질이 안정할 뿐 아니라, 생체 분자들과 상호작용을 잘 하기 때문에 광학적 바이오센서 개발을 위한 신호 매개체로 상당한 이목을 끌고 있다. 그러나 기존의 GO 기반 바이오센서는 GO의 형광 억제 현상을 이용하고, 체내 환경에서 낮은 안정성을 보이는 유기 염료의 사용에 한계가 존재하였다. 따라서, 본 연구에서는 GO를 형광체로 이용하여 광학적 바이오센서를 개발하고, 다양한 방법으로 GO을 개질하여 센서 작동 기작을 다양하게 하거나 민감도를 향상시키고자 하였다.

첫번째로, GO와 기질 펩타이드, GO의 형광에 대한 퀜처 분자가 공유 결합으로 이어진 광학적 바이오센서를 합성하고, 매트릭스 메탈로프로테이나아제-2 (MMP-2)의 민감하고 간편한 검출로 응용하였다. GO 형광의 억제에 적합한 퀜처 분자를 찾기 위하여 메탈로포피린 유도체들과 QXL_{570}의 GO 형광 억제 기작을 관찰하여, GO로부터 QXL_{570}으로의 형광 공명 에너지 전이에 의한 형광 억제가 가장 효율적임을 확인하였다.

고안된 GO-펩타이드-QXL 센서는 억제 되었던 MMP-2에 의한 기질 펩타이드 가수분해의 결과로 GO의 형광이 회복됨을 통해 민감하고 선택적으로 MMP-2를 검출할 수 있었으며, 세포에서 분비된 MMP-2도 검출해 내었다.

다음으로, 퀜처의 사용을 배제하는 간편한 바이오센서 제작을 위하여 GO 조립체 합성에 의한 자가 형광 억제를 이용한 MMP-2의 검출에 응용하였다. GO를 티올기를 포함하는 기질 펩타이드로 개질한 후, 다이설파이드 결합을 유도하여 GO-펩타이드 조립체를 합성하고, GO의 자가 형광 억제를 유도하였다. 고안된 GO-펩타이드 조립체는 MMP-2의 존재하에 기질 가수분해에 의한 조립체 분해를 통해 자가 억제되었던 형광을 회복하였으며, 이를 통해 MMP-2를 선택적으로 검출하였다. 또한 세포에서 분비된 MMP-2 역시 선택적이고 민감하게 검출해 내었다.

세번째로, GO 형광 신호 향상을 위하여 질소, 황이 도입된 시스테인-GO (Cys-GO)을 합성하고, 좀 더 민감한 목표물 검출에 응용하였다. 산이 포함된 물/디메틸포름아마이드 용액에 GO와 시스테인을 분산시키고, 온화한 조건 하에 균질기를 이용하여 Cys-GO를 합성하였다. Cys-GO는 매우 높은

함량의 질소와 황을 포함하였으며, GO에 비해 10배 이상 증가된 형광 신호를 나타내었다. 신호 증가 기작을 탐색하기 위하여 표면 분석과 광학적 성질을 평가하였으며, 질소와 황의 동시 도입이 큰 역할을 함을 확인하였다. 또한, Cys-GO를 앞의 조립체 센서로 응용하여 MMP-2 검출을 시도하였으며, 증가된 형광 신호를 통해 향상된 민감도를 나타냄을 확인하였다.

본 연구를 통해 새롭게 개발된 GO 형광 기반의 광학적 바이오센서는 높은 검출 감도를 지니는 진단 도구로서 향후 다양한 의·약학 및 산업 분야에 널리 쓰일 수 있을 것으로 기대된다.

주요어: 산화 그라핀, 형광 나노재료, 광학적 바이오센서, 형광 공명 에너지 전이, 매트릭스 메탈로프로테이나아제-2, 분자 유도 조립체, 자가 형광 억제, 질소/황 도핑 산화 그라핀

학 번: 2011-21046